System Study and CO_2 Emissions Analysis of a Waste Energy Recovery System for Natural Gas Letdown Station Application

By

Adegboyega Babasola

A thesis submitted to the Department of Chemical Engineering
in conformity with the requirements for the degree of
Masters of Applied Science

Queen's University
Kingston, Ontario, Canada
August, 2010

Abstract

A CO_2 emission analysis and system investigation of a direct fuel cell waste energy recovery and power generation system (DFC-ERG) for pressure letdown stations was undertaken. The hybrid system developed by FuelCell Energy Inc. is an integrated turboexpander and a direct internal reforming molten carbonate fuel cell system in a combined circle.

At pressure letdown stations, popularly called city gates, the pressure of natural gas transported on long pipelines is reduced by traditional pressure regulating systems. Energy is lost as a result of pressure reduction. Pressure reduction also results in severe cooling of the gas due to the Joule Thompson effect, thus, requiring preheating of the natural gas using traditional gas fired-burners. The thermal energy generated results in the emission of green house gases. The DFC-ERG system is a novel waste energy recovery and green house gas mitigation system that can replace traditional pressure regulating systems on city gates.

A DFC-ERG system has been simulated using UniSim^{TM} Design process simulation software. A case study using data from Utilities Kingston's city gate at Glenburnie was analysed. The waste energy recovery system was modelled using the design specifications of the FuelCell Energy Inc's DFC 300 system and turboexpander design characteristics of Cryostar TG120. The Fuel Cell system sizing was based on the required thermal output, electrical power output, available configuration and cost. The predicted performance of the fuel cell system was simulated at a current density of 140mA/cm^2, steam to carbon ratio of 3, fuel utilization of 75% and oxygen utilization of 30%. The power output of the turboexpander was found to strongly depend on the high pressure natural gas flowrate, temperature and pressure. The simulated DFC-ERG system was found to reduce CO_2 emissions when the electrical power generated by the DFC-ERG system replaced electrical power generated by a coal fired plant.

Acknowledgements

I will like to express my profound gratitude to my supervisor Dr. Brant Peppley. His patience, guidance and support for this research were invaluable.

This research would not have been possible without the financial support of Ontario Fuel Cell Research and Innovation network (OFCRIN) and Queen's Graduate Award.

Many thanks also go to our industrial contacts, David Teichroeb and Stephen Pogorski of Enbridge Gas for providing the necessary information and access to their facility. A big thank you also goes to Chris Phippine of Utilities Kingston for providing the data for this research. I would also like to thank Dr. Kunal Karan, Dr John Pharoah and Dr. Chris Thurgood of the Royal Military College for their technical guidance.

I wish to thank my colleagues and friends in the Fuel Cell Research Centre for their advice and support when I most needed it.

Last but not the least I most express my heartfelt appreciation to my family; Oladunni, Favour and Flourish. Your love, patience, encouragement and moral support gave me the necessary motivation to complete this thesis.

Table of Contents

List of Figures

List of Tables

Nomenclature

$N^{i}_{CO(a)}$ ……...……Molar flowrate of CO at the anode inlet (kgmol/hr)

$N^{i}_{CO2(a)}$ ……..……Molar flowrate of CO_2 at the anode inlet (kgmol/hr)

$N^{i}_{H2O(a)}$ ……..……...Molar flowrate of H_2O at the anode inlet (kgmol/hr)

$N^{i}_{CH4(a)}$ ……..……Molar flowrate of CH_4 at the anode inlet (kgmol/hr)

$N^{i}_{H2(a)}$ ……..……Molar flowrate of H_2 at the anode inlet (kgmol/hr)

$N^{e}_{CO(a)}$……..……Molar flowrate of CO at the anode exit (kgmol/hr)

$N^{e}_{CO2(a)}$ ……..……Molar flowrate of CO_2 at the anode exit (kgmol/hr)

$N^{e}_{H2O(a)}$ ……..……Molar flowrate of H_2O at the anode exit (kgmol/hr)

$N^{e}_{CH4(a)}$ ……Molar flowrate of CH_4 at the anode exit (kgmol/hr)

$N^{e}_{H2(a)}$ ……..….Molar flowrate of H_2 at the anode exit (kgmol/hr)

$N^{i}_{O2(c)}$ ……..Molar flowrate of O_2 at the cathode inlet (kgmol/hr)

$N^{i}_{CO2(c)}$ ……..……Molar flowrate of CO_2 at the cathode inlet (kgmol/hr)

$N^{e}_{CO2(c)}$ ……..……Molar flowrate of CO_2 at the cathode exit (kgmol/hr)

$N^{e}_{O2(c)}$ ……..……..Molar flowrate of O_2 at the cathode exit (kgmol/hr)

R_1…….Rate of steam reforming reaction (kgmol/hr)

R_2……Rate of water gas shift reaction (kgmol/hr)

R_3……..Rate of electrochemical reaction (kgmol/hr)

m_f ……..……...Mass flowrate of fuel (kg/hr)

J……..……Current density (mA/cm^2)

n……Number of cell in stack

A……Geometric cell area (cm^2)

F…….……Faraday's constant (Coulomb)

K_{WGS}…….……Equilibrium constant for the shift reaction

T……...Cell operating temperature (^{o}C)

Q_A^i……..…….Thermal power at anode inlet (kW)

Q_A^O……..…….Thermal power at anode inlet (kW)

Q_c^i…….……...Thermal power at cathode inlet (kW)

Q_C^O……..……Thermal power at cathode outlet (kW)

Q_E ……...Electrical power (kW)

Q_{gen} ……Thermal power generated in the cell (kW)

Q_{loss}…….……...Thermal losses (kW)

Q_u…….……...Useful thermal power (kW)

W_{el} …….……Electrical work of fuel cell (kW)

f……...Useful heat fraction

Δh_{WGS}…….…….. ……..Reaction heat of water gas shift reaction (kJ/mol)

Δh_{el}… ……..……...Reaction heat of electrochemical reaction (kJ/mol)

h_1……..Turboexpander preheat enthalpy (kJ/mol)

h_2…….....……..Turboexpander outlet enthalpy (kJ/mol)

h_{2s} ……..……Turboexpander isentropic outlet enthalpy (kJ/mol)

h_f … ...……Enthalpy of fuel (kJ/mol)

R_i……....Internal resistance (Ohm cm^2)

R_{tot} ……..…Total cell reaction resistance (ohm cm^2)

V…….……Cell output voltage (V)

E …….……....Open circuit voltage (V)

η_{ne} ……..Nernst lost (V)

ΔG……..……Change in Gibbs free energy (kJ/mol)

R……..…….Universal Gas constant (8.314kJ/kmol K)

$P_{H2,an}$…….……..Partial pressure of H_2 at the anode (bar)

$P_{H2O,an}$ ……Partial pressure of H_2O at the anode (bar)

$P_{CO2,an}$……..Partial pressure of CO_2 at the anode (bar)

$P_{O2,ca}$……...…….……....Partial Pressure of O_2 at the cathode (bar)

$P_{CO2,ca}$…….……...Partial pressure of CO_2 at the cathode (bar)

η_{el}……..…….....Electrical efficiency of cell

η_{en}…….……Fuel cell energy efficiency

η_g…….……Global efficiency

η_{te} ……Turboexpander efficiency

Chapter 1

Introduction

1.1 Problem Statement

Long distance natural gas transportation is done by pipeline companies through high pressure pipelines usually in the range of 400 to 700 psi while local utilities networks operate at lower pressure (50 to 100 psi) that is more appropriate for the consumer. At the pressure letdown stations, usually called the city gates, energy is lost as pressure is reduced using pressure regulating or control valve systems. Reducing the gas pressure with traditional pressure reduction systems also result in severe cooling of the gas due to Joule-Thomson effect [1]. The cold gas can create frost and cause other operational concerns. Typically some of the natural gas is used by combustion burners to pre-heat the high pressure gas resulting in further energy cost and green house gas emission to the atmosphere.

There is a growing interest in the gas and pipeline industries to recapture the waste energy using an energy recovery system in place of the traditional pressure reducing systems. Expansion Turbines have been demonstrated as a replacement system for recovering energy. In this application, an axial or radial flow turbine is placed between the high pressure and low pressure pipelines. As natural gas flows through the turbo expander, the energy of compression drives a generator producing electricity. The exhaust from the turboexpander, thus, flows into the municipal distribution pipeline system at the required lower pressure.

To maximize the electricity generated by the turboexpander and to ensure that the temperature of the low-pressure exhaust does not cause frost heaving, the high-pressure inlet gas must be preheated to a higher temperature [2, 3]. This means some gas must be consumed resulting in greenhouse gases

being generated and some parasitic loss of natural gas. An innovative method of offsetting the impact of consuming gas to preheat the turboexpander input is the use of a natural gas fuelled molten carbonate fuel cell system. The waste heat from the system can be used to preheat the gas while at the same time additional electrical power, which can be sold to the electrical grid, is produced.

The goal of this project is to validate the benefits of the application of a hybrid power plant consisting of a Direct Internal Reforming Molten Carbonate Fuel Cell also called Direct Fuel Cell and a Turboexpander system (DFC-ERG^{TM}) for waste energy recovery, green house gas mitigation and coal fired plant substitute in Ontario. The reference hybrid energy recovery system for this work is the world's first Direct Fuel Cell Energy Recovery Generation power plant that has been installed and is currently operating at the Enbridge Gas facility in Toronto, Ontario. The system design and integration is the result of a joint development effort by Enbridge Inc, a gas distribution company with head office in Calgary, Alberta and Fuel Cell Energy Inc. based in Danbury, Connecticut [4]. This $10 Million project produces a combined 2.2MW of ultra-clean electricity; enough to power about 1700 residences.

The principal goal of this work is to carry out a system analysis of the Enbridge DFC-ERG power plant to assess the viability and benefits of installing such a hybrid system in small to medium sized municipalities for recapturing compression energy and mitigating greenhouse gas emission and also, by extension, to reduce or eliminate the use of coal-fired power plants in Ontario.

This thesis is organized into six chapters; Introduction, Literature Review, Modeling of 1.2MW Direct Fuel Cell, Simulation and System Analysis, Results and Discussions, Conclusion and Recommendation. The Introduction provides an overview of the pressure letdown stations in the Ontario gas distribution network, current challenges with regards to the use of fired-heaters to preheat the high pressure gas and the waste recovery power plant installed at the Enbridge Gas Inc. pressure letdown station in Toronto, Ontario. The Literature Review gives a review of previous and ongoing work on the design of molten carbonate fuel cell systems for distributed generation applications. The

chapter also reviews waste energy recapturing systems installations in other locations around the world. The Modelling of Direct Fuel Cell chapter presents the mathematical model developed to simulate the performance of a 1.2MW molten carbonate fuel cell system. The System Analysis chapter will describe the balance of plant for the energy recovery system and the design of an energy recovery system for Utilities Kingston's pressure letdown station. The Results and Discussions presents an analysis of the system performance, energy recovery and green house gas mitigation. The Conclusions and Recommendations chapter summarizes the principal findings of the thesis results and suggests areas for future work.

1.2 Natural Gas Pipeline System

Natural gas is the major fuel for all sectors of the economy (except transportation) in Ontario. It is the primary fuel used in residential, commercial and industrial space heating [5]. As shown in Fig 1.1 natural gas accounts for about 16% of Ontario's energy supply [6].

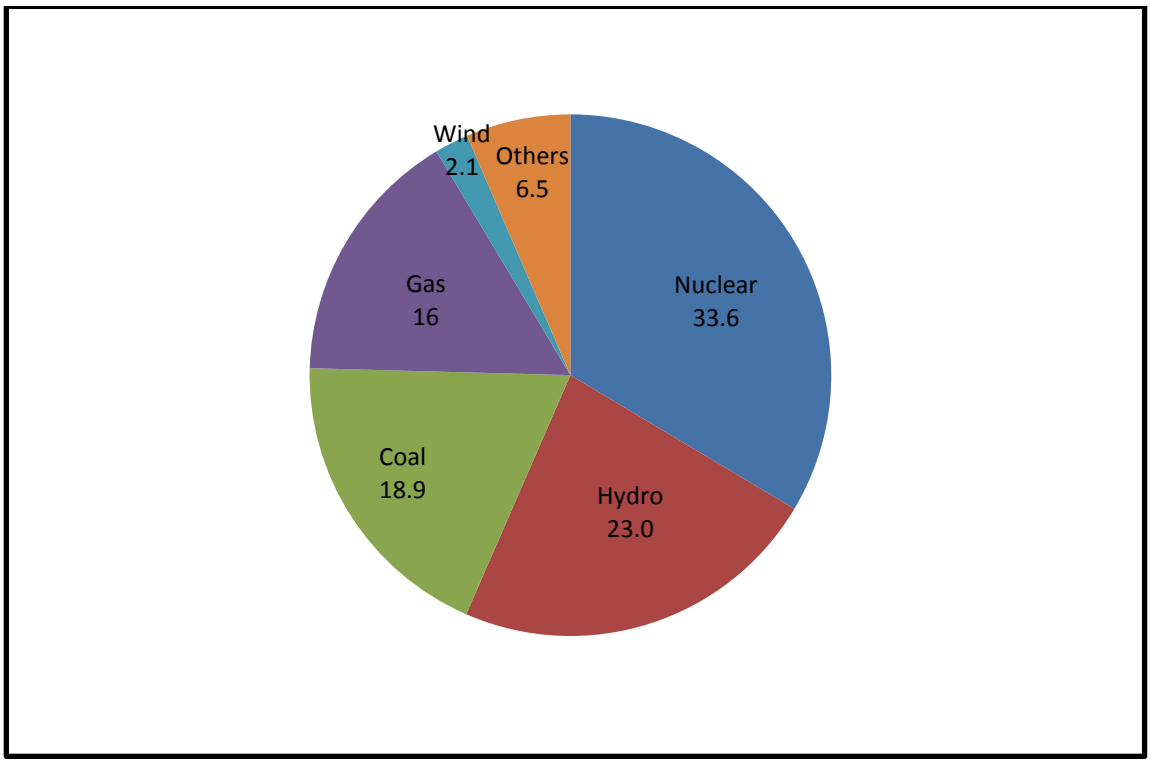

Figure1.1 Ontario Installed Electricity Generation by Fuel Type [(IESO [6])

Natural Gas (NG) is produced and processed in Alberta and Saskatchewan in Canada. The gas is transported by the pipeline companies to Ontario municipalities through high pressure pipelines to the local distribution stations called the city gates. In many cases, natural gas produced in a well will require long distance transportation to its point of consumption. Pipelines serve as the highways for natural gas transport. Canada is a major supplier of natural gas to the United States of America through pipeline transportation. Table 1.1 shows the amount of Canada's natural gas transported to US through transmission pipeline from November 2008 to April 2009 [7].

Table1.1 US Natural Gas Import by Countries [7]

Type - Area	Nov-08	Dec-08	Jan-09	Feb-09	Mar-09	Apr-09
Import Volumes						
Total	322,469	367,733	360,145	322,127	324,433	312,020
Pipeline	299,667	337,024	333,213	294,262	292,848	255,979
Canada	293,642	329,860	327,585	293,843	292,342	255,777
Mexico	6,025	7,164	5,629	419	506	202
LNG	22,802	30,708	26,932	27,865	31,585	56,041
Algeria	0	0	0	0	0	0
Australia	0	0	0	0	0	0
Brunei	0	0	0	0	0	0
Egypt	9,181	8,663	5,142	5,846	11,627	21,898
Equatorial Guinea	0	0	0	0	0	0
Indonesia	0	0	0	0	0	0
Malaysia	0	0	0	0	0	0
Nigeria	0	0	0	0	0	8,050
Norway	0	3,067	2,965	6,000	2,894	5,880
Oman	0	0	0	0	0	0
Qatar	0	0	0	0	0	0
Trinidad	13,621	18,978	18,825	16,019	17,064	20,212
United Arab Emirates	0	0	0	0	0	0
Other	0	0	0	0	0	0

Pipeline provides a cheap means of transporting natural gas up to 2,500km [8]. In order to get maximum efficiency and volume through the pipelines, the gas is highly pressurized (2500-7000 kPa). There are three main gas pipeline transportation companies in Ontario, Enbridge Pipeline Inc., Union Gas Inc. and NRG Energy Inc. These natural gas distribution companies are regulated by the Ontario Energy Board (OEB). The board reviews and approves the rate proposed to be charged to customers by the distribution companies.

Table 1.2 is the number of NG customers in Ontario per regulated gas distribution companies in 2007 [9]. There are a total of 3,208,500 natural gas customers in Ontario. These customers are serviced mainly through pipelines implying a huge network of natural gas pipelines in Ontario.

Table1.2 Ontario Regulated Natural Gas Distribution Customers in 2007 (OEB 2007 Year Book [9])

SYSTEM GAS CUSTOMERS	**ENBRIDGE**	**UNION**	**NRG** (2006)	TOTAL
Low Volume (less than 50 cubic meter/yr)	1,148,358	822,220	6398	1,976,976
Large Volume (more than 50 cubic meter/yr)	209	3,454	16	3679
Total number of Customers (including customers of retailers)	**1,902,000**	**1,300,000**	**6,500**	**3,208,500**

The pipeline network, as shown in Figure 1.2 [10], has many letdown stations where gas pressure must be reduced. The traditional method of reducing pressure at the distribution stations is through the

use of pressure regulating systems. As was mentioned earlier, energy is wasted as pressure is reduced. This energy could be captured and converted to useful energy through waste energy recovery systems. There are 42 pressure letdown stations and 2200 districts stations in the Greater Toronto Area (GTA) alone. Estimated maximum electricity generation from these stations using waste energy recovery system is about 150MW, enough to reduce the use of coal-fired power plants that currently account for 18.9% of Ontario total power capacity. Furthermore, because the variation in the use of NG and electricity tend to follow the same daily cyclic pattern, this additional electricity is available when the demand for electricity increases.

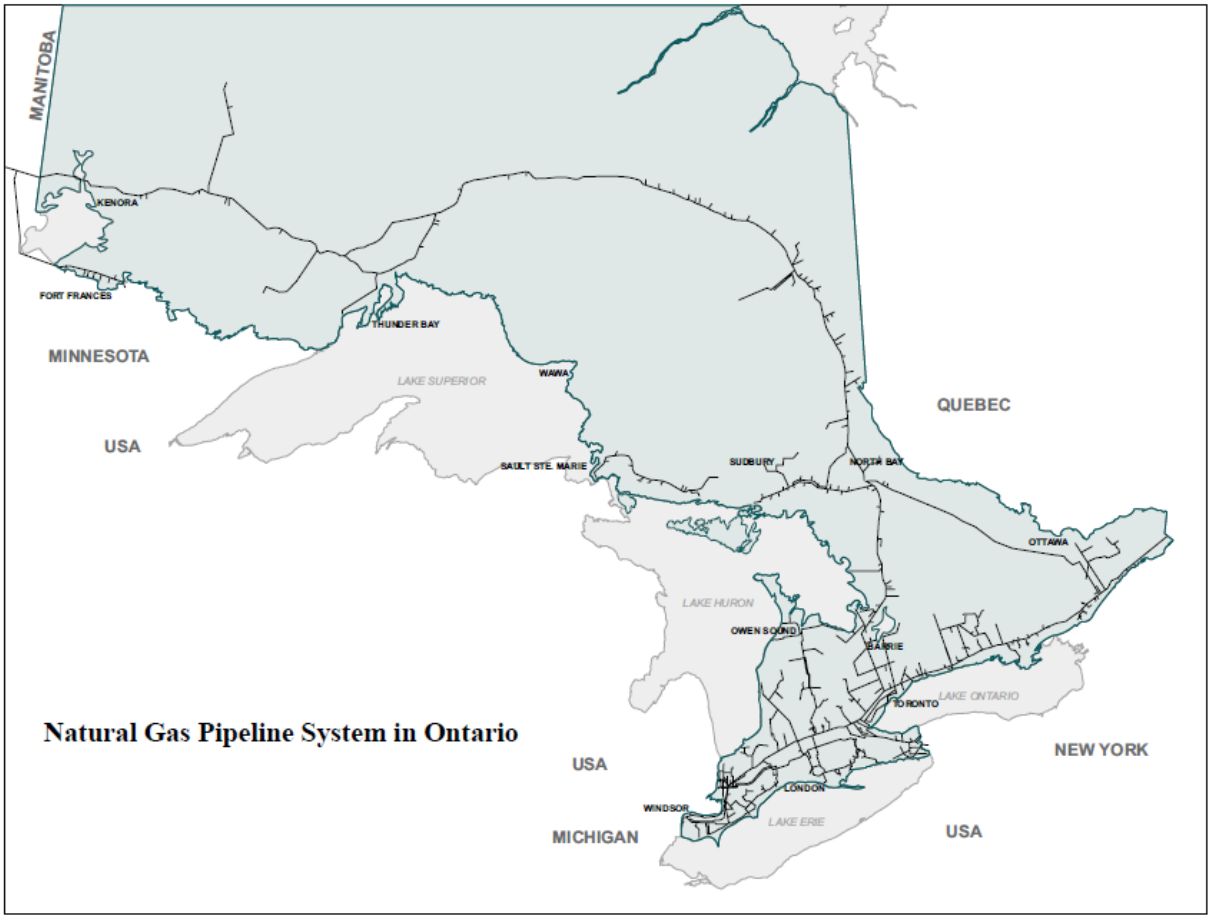

Figure1.2 Natural Gas Pipeline Systems in Ontario (OEB, [10])

1.3 Direct Fuel Cell Hybrid System Background

Burning fossil fuel for power generation is a major source of green house gas emitted to the atmosphere causing such effects as global warming and acid rain. There has been increased global interest in reducing emission of these gases through better use of fossil fuel and also through the use of clean sources of energy such as wind, solar, biomass, and geothermal. The fuel cell can provide a beneficial solution as a low emission power generation system. Fuel cells directly convert chemical energy to electrical energy and heat energy at high efficiency with low environmental impact.

Table1.3 Evolution of Molten Carbonate Fuel Cell Components (Fuel Cell Handbook [11])

Component	Catalyst (1965)	Catalyst (1975)	Current Status
Anode	Pt, Pd, or Ni	Ni-10 wt% Cr	▪ Ni-Cr/Ni-Al ▪ 3-6µm pore size ▪ 45-70% initial porosity ▪ 0.2-1.5mm thickness ▪ 0.1-1m^2/g
Cathode	Ag_2O or lithiated NiO	Lithiated NiO	▪ Lithiated NiO ▪ 7-15µm pore size ▪ 70-80% initial porosity ▪ 60-65% porosity after lithiation and oxidation ▪ 0.5-1mm thickness ▪ 0.5 m^2/g
Electrolyte Support	MgO	Mixture of α-,β-, and γ- $LiAlO_2$ 10-20 m^2/g	▪ α-$LiAlO_2$, γ- $LiAlO_2$ ▪ 0.1-12 m^2/g ▪ 0.5-1 mm thickness

The molten carbonate fuel cell (MCFC) is a high temperature electrochemical power system that operates at temperatures greater than 600^{o}C. The high temperature is needed to achieve sufficient conductivity of its carbonate electrolyte, which is a liquid solution of lithium, sodium and/ or potassium carbonate soaked in a ceramic matrix of $LiAlO_2$ as shown in Table 1.3 [11].

High temperature also favours the strong endothermic steam reforming reaction (equation 1.1). The technology has reached commercialization stage and is attracting the attention of local utilities for distributed combined heat and power applications. By utilizing the heat generated by the MCFC system for process and/or space heating, total efficiency of over 85% can be achieved.

Three main configurations have been of interest to designers; the external reforming molten carbonate fuel cell (ER-MCFC), the indirect internal reforming molten carbonate fuel cell (IIR-MCFC) and the direct internal reforming molten carbonate fuel cell (DIR-MCFC). FuelCell Energy Inc. has designed the IIR-DIR-MCFC configuration as shown in figure 1.3 [12].

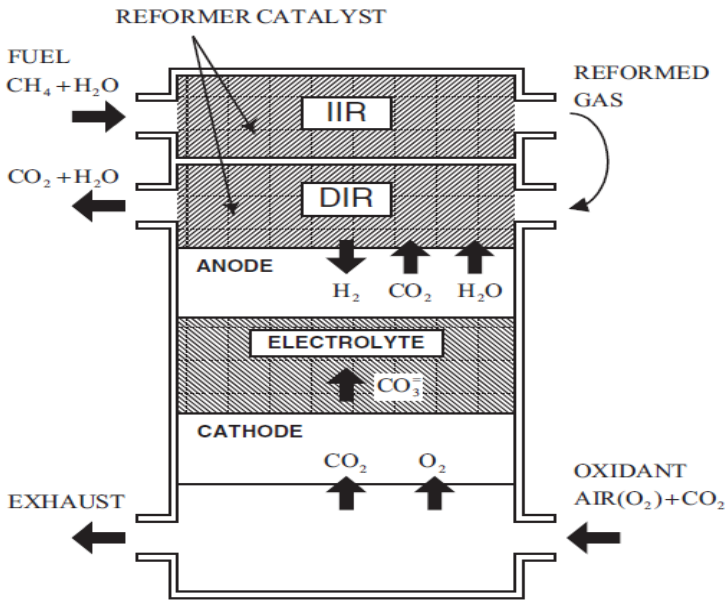

Figure1.3 FuelCell Energy Inc. Direct Fuel Cell Configuration (Lucas M.D. *et al.*, 2005 [12])

In this novel design, the steam reforming and the water gas shift reaction (equation 1.2) occur in the IIR and the DIR compartments ensuring higher conversion of methane to form hydrogen for the non-combustion electrochemical reaction, equation 1.5, which is the result of the anode and cathode half cell reactions, equations 1.3 and 1.4 respectively.

There is currently considerable interest in the integration of MCFC with turbines (both gas turbines and expansion turbines) for distributed generation of electric power [13]. The benefits of the hybrid system are generation of ultra-clean electricity, very low environmental impact, very high efficiency, use of the high temperature of the fuel cell exhaust in a Brayton cycle [14].

$$CH_4 + H_2O \leftrightarrow CO + 3H_2 \quad (1.1)$$

$$CO + H_2O \leftrightarrow CO_2 + H_2 \quad (1.2)$$

$$Anode: H_2 + CO_3^{2-} \rightarrow H_2O + CO_2 + 2e^- \quad (1.3)$$

$$Cathode: \frac{1}{2}O_2 + CO_2 + 2e- \rightarrow CO_3^{2-} \quad (1.4)$$

$$Cell: H_2 + \frac{1}{2}O_2 + CO_2 \rightarrow H_2O + CO_2 \quad (1.5)$$

Since the expansion turbine operates more efficiently when the inlet temperature is high, the molten carbonate fuel cell system exhaust can provide the heat to raise the temperature of the turbine inlet stream. Because of the indirect heat transfer to the turboexpander and absence of a combustor, NO_x is not generated [15].

The hybrid system (DFC-ERG) is suitable over a range of applications from sub-MW industrial to medium scale MW distributed generation to large central station plants. This is because of the independent operating pressures of the molten carbonate fuel cell and the turboexpander.

The MCFC can readily use natural gas as feed which makes its application in the natural gas pipeline transportation very attractive. The pipeline infrastructure is already available, thus, gas distribution companies would only require some upgrade of their facilities to incorporate the DFC-ERG power system for waste energy recovery and power generation.

1.3.1 Enbridge Direct Fuel Cell Energy Recovery Generation System (DFC-ERG)

The world's first DFC-ERG system was installed at an Enbridge pressure letdown station in Toronto, Ontario. The 2.2MW (1.2MW DFC+1MW Turboexpander) hybrid power plant was developed by FuelCell Energy Inc. This $10 million collaborative power project was supported by the Canadian Federal government ($2.3 million) through National Resources Canada and the Ontario provincial government ($500,000) through the Ministry of Research and Innovation. The City of Toronto also provided some support for this project by enacting a by-law allowing residents and businesses to export clean electrical energy to the grid [16].

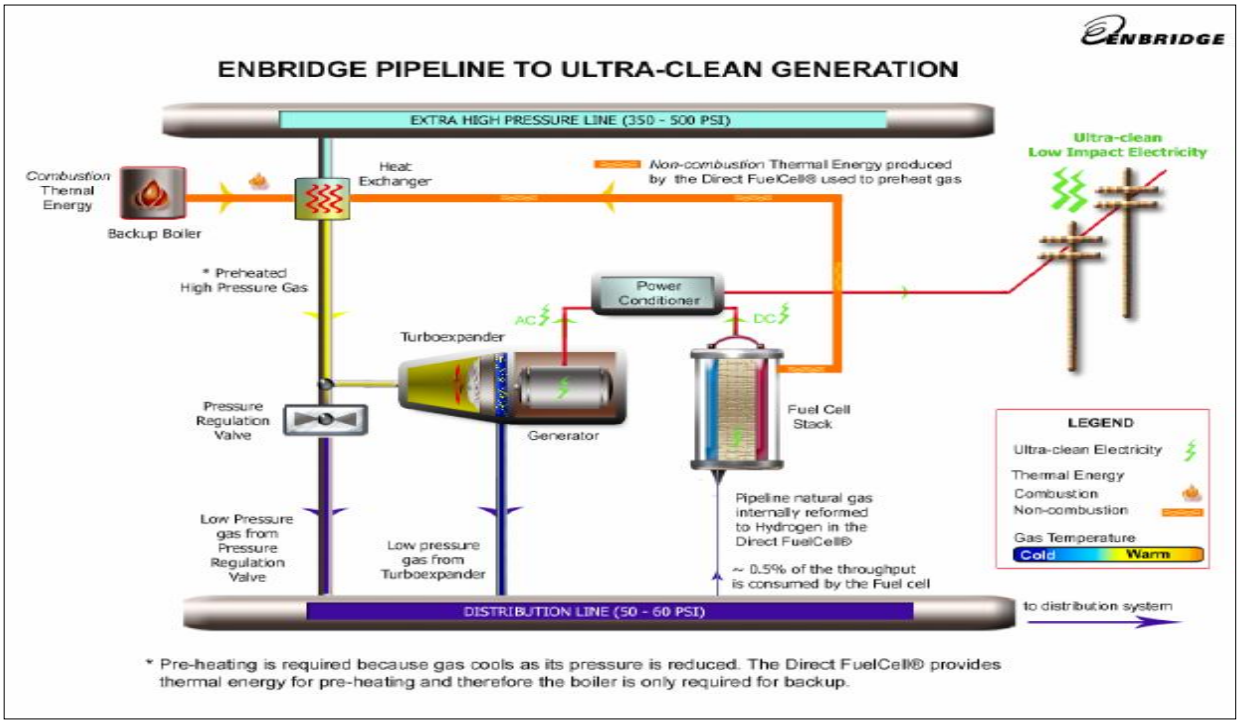

Figure1.4 Enbridge Inc. DFC-ERG System (David Teichroeb, Enbridge Gas Inc. [17])

The DFC-ERG system is located inside the urban centre in Toronto where it is mostly needed thus reducing electric grid congestion and system losses.

Figure 1.4 is the Process flow diagram of the Enbridge Inc. DFC-ERG system [17]. Natural gas is transported from Calgary to Toronto through the high pressure pipeline at about 350-500 psi. The gas is preheated using the non-combustion exhaust heat of the fuel cell. A conventional boiler unit only serves as a back-up system for preheating.

Preheated gas passes through the expansion turbine and exits as low pressure gas for distribution. A small portion of the low pressure natural gas is internally reformed in the direct fuel cell to form hydrogen that is used in the fuel cell to generate DC electrical power and heat. The expansion turbine is connected to a generator which produces AC electrical power. A power conditioner unit conditions the electrical power produced by the DFC and turboexpander to produce utility quality power for the grid. The entire plant operates without combustion, so emissions of pollutants (NOx and SOx) are negligible.

1.4 Importance of Greenhouse Gas Mitigation Analysis and Objective of Thesis

Green house gases (GHG) are gases in the atmosphere that absorb and emit radiation within the thermal infrared range. Some GHGs are necessary in order to keep the temperature at a level suitable to support life. Without GHGs the earth's surface would be covered in ice. However, when excess GHGs are emitted to the atmosphere such as those due to human activities CO_2, water vapour, CH_4, N_2O and O_3 can absorb too much radiation and result in the atmospheric temperature rising to a point such that various species are unable to survive. The main focus of this project is to determine the amount of Carbon dioxide (CO_2) that the DFC-ERG could avoid under various operating scenarios. In particular the gas usage pattern for the City of Kingston was used as a sample operating scenario.

Most of the anthropogenic CO_2 emissions (about 80%) are from fossil fuel combustion. Fossil fuels include, coal, conventional oil, natural gas and bitumen / synthetic crude oil. The main sectors where these fuels are utilized are transportation, electricity generation and heating.

Canada's CO_2 equivalent emission was about 721 megatonnes in 2006 [18] and Ontario's emissions account for about 30% of the total GHG emission.

The target of the Ontario government is to reduce the province's GHG emission to 6% below the 1990 emission (177 mega tonnes) by 2014 and 15 percent below 1990 by 2020. As a step towards achieving this target, all the coal-fired power plants would be shut down which will result in approximately half the required reduction. Low environmental impact power generating systems would replace the coal fired power plants in order to meet the electricity demand of the province.

The waste energy recovery generation power plant is being proposed as a substitute to the use of coal. This project intends to evaluate the GHG reduction that DFC-ERG systems could achieve if they were used at pressure reduction stations in Ontario. The analysis will be based partly on determining the reduction in the need to operate coal fired plants during peak demand periods, thus helping the Provincial Government to achieve its goals of reducing GHG emissions.

Chapter 2

Literature Review

This chapter reviews previous studies done on modeling and system analysis of molten carbonate fuel cell systems for combined heat and power generation. Review of relevant work on waste energy recovery systems and green house gas emission evaluation on natural gas distribution network were also outlined.

The review is structured into four parts: Waste energy recovery systems, design/ modeling of MCFC, system analysis of MCFC and GHG reduction systems.

2.1 Waste Energy Recovery Systems

This section reviews previous study on waste energy recovery power plants. Various examples of waste energy recovery systems exist but the papers reviewed here are directly related to natural gas pipeline pressure letdown stations. There are very few published works on natural gas pipeline energy recovery systems.

Madalloni *et al.,* 2007 [1] quantified the exergy that can be extracted from various letdown stations using an expander coupled with an electric generator. In this study two orientations where considered; preheating of turbine inlet gas orientation and purification of turbine inlet gas orientation. In the preheating orientation, an heat source is used to raise the temperature of the turbine inlet gas stream thus preventing hydrate formation due to the cooling effect of the turbo expander. The purification oriented system reduces the water content of the natural gas before going through the expansion process preventing hydrate formation at the expander outlet. Water removal using a molecular sieve was considered. A mathematical model was developed and used to calculate the electrical work

produced by the turbine at different turbine inlet conditions; temperature, pressure and flow rate. The model accommodates the seasonal variable nature of gas flow rate and pressure entering letdown stations. Data from Terasen Gas pressure reduction station in British Columbia was used to test this model. It was concluded that for a pressure ratio of 4:1, a preheating system has a potential of generating electrical work of 140KW per kg/s of natural gas while a purification system has a potential of generating electrical work of 110KW per kg/s of natural gas.

Daneshi, *et al.*, 2008 [8] completed a review of energy recovery projects in North America and around the world. In their work, the way waste energy is converted into electricity, as well as the advantages and disadvantages of using waste energy conversion technologies were analysed. They observed that gas pipeline transportation is only economical up to 2500 km and not economical beyond 4000 km based on cost of transportation. They also observed that temperature drop in natural gas at pressure reducing stations using control valve is about 4.5 degrees centigrade per 1MPa of pressure drop while temperature drop using a turbine is 15-20 degrees centigrade depending on gas composition and state. Existing energy recovery plants in North America were reviewed: WOWGen renewable energy power plant in Abilene, Texas for Dyess Air force base that produce 6 MW of electrical power using the heat exiting municipal solid waste collected from the Dyess Air force base and the city of Abilene; LNG liquefaction plant in Sacramento California, a project developed by the US Department of Energy (DOE), the Idaho National Engineering and Environmental Laboratories (INEEL), and Pacific Gas and Electric (PG&E); the Enbridge Inc./ Fuel Cell Energy Inc. 2.2 MW hybrid electric power energy recovery system, which is the reference power plant for the current work. Other waste energy recovery systems around the world were also reviewed: Electrabel 2.6 MWe energy recovery system on the public distribution network in Belgium; the Karsto expansion project (using GE's Turbo expander-Compressor system), a collaborative project between Statoil and M.W Kellogg Limited on behalf of Gassco (a Norwegian gas transport company); Badak LNG liquefaction project in Indonesia; and the

5MWe Salizone plant in Italy. The paper concluded that energy recovery systems can be used effectively in many applications.

Hedman, 2008 [19] completed a report on energy recovery opportunities for interstate natural gas pipelines. The report summarizes the analysis of three energy recovery opportunities for interstate natural gas pipeline systems in United States: power generation using heat recovered from a compressor; power generation from turboexpander on city gates; power generation from gas turbine exhaust with inlet-cooling system (TIC). The objective of Hedman's report was to evaluate the technical applicability of each option. It was observed that pipeline companies can expect revenue of about $0.005/KWh from waste energy provided for power generation which would equal approximately $165,000 per annum for a 5 MW energy recovery power generation system at 75% load factor as shown in Fig 2.1

The study concluded that there are opportunities where heat recovery to power systems can be and are being economically applied to the pipeline system. A Turboexpander with turbine inlet air cooling system, however, was considered not commercially viable for interstate natural gas pipelines except for areas where the power purchase price include some incentives for clean energy, like states where waste heat recovery projects qualify as an option under renewable energy portfolio standard and where compressor capacity and load factor are above certain minimums; total gas turbine station capacity of at least 15,000kWh and operated at or more than 5250 hours per year (60%load factor) over the previous 12 months.

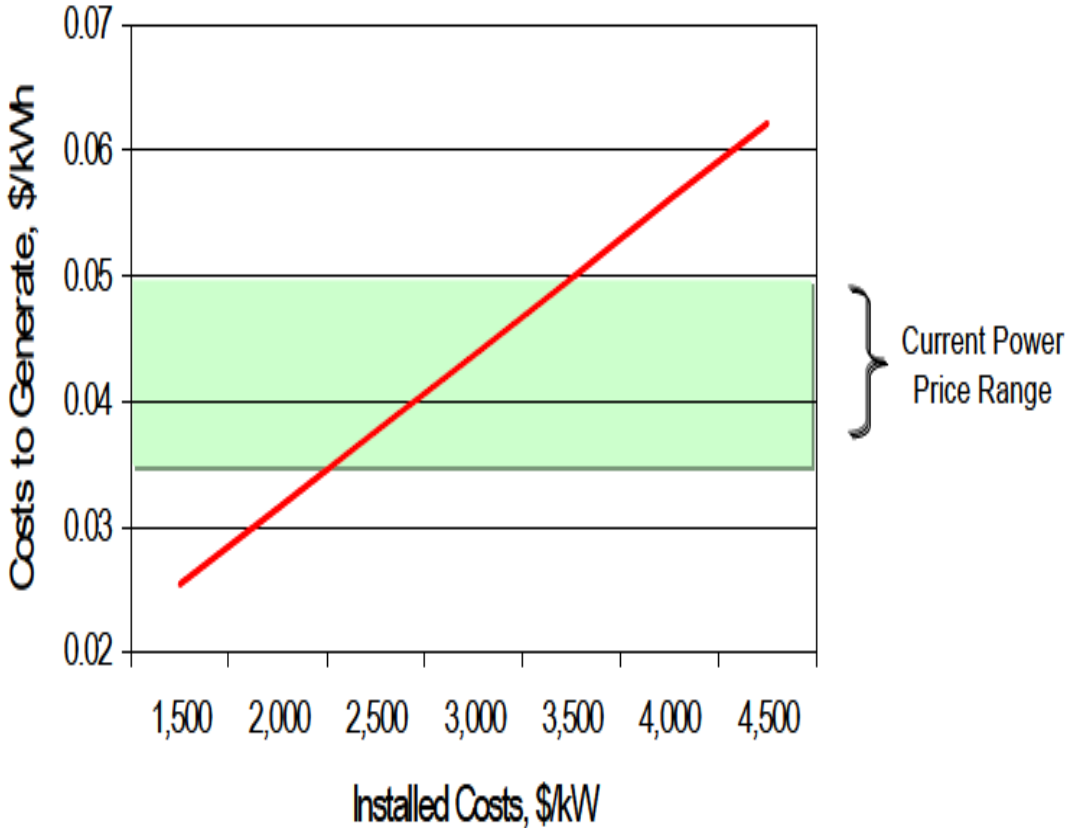

Figure 2.1 Cost to Generate Power as a Function of Capital Cost (Hedman B.A., 2008 [19])

Jaroslav, 2004 [2] analysed the performance of expansion turbine in natural gas pressure reduction stations. He showed that through the use of expansion turbines at city gates it is possible to produce clean, green electricity utilizing the potential energy of natural gas being delivered under high pressure. General flow sheet simulator HYSYS was used for this analysis. For computation of state variables, Peng-Robinson's variant of the Redlich-Kwong equation was used.

Parameters of natural gas in a gas transmission station at Velke Nemcice was used as input data for his calculation (Table 2.1)

Table 2.1 Natural Gas Transmission Station Parameters (Jaroslav P, 2004 [2])

Gas Properties at Inlet:								
Column number		1	2	3	4	5	6	7
Flow rate	Nm^3/h	60000	60000	60000	60000	60000	60000	60000
Temperature	^oC	3	3	3	3	3	3	3
Pressure	MPa	5.5	6.3	4.5	5.5	5.5	5.5	5.5
Gas Properties at outlet:								
Temperature	^oC	3	3	3	3	3	-7	13
Pressure	MPa	1.8	1.8	1.8	1.4	2.3	1.8	1.8
Results:								
Temperature at Turbine Inlet	^oC	71.3	80.2	58.3	86.1	56.7	60.2	82.3
Heat Energy Requirement	kW	1939	2242	1525	2356	1530	1617	2261
Power Generation	kW	1367	1547	1107	1719	1036	1309	1424
Thermal Efficiency	%	70.5	69.0	72.6	73.0	67.7	81.0	63.0
Total Thermal efficiency	%	98.3	98.3	98.4	98.3	98.4	98.4	98.4

He concluded that 80% waste energy was recovered from the letdown station and pressure ratio is an important parameter that greatly influences both power output and requirements on preheating. His model also calculated the influence of turbine's isentropic efficiency on power output, heat consumption and temperature at expander inlet.

2.2 Design and Modeling of Molten Carbonate Fuel Cell

In this section, MCFC model development and validation is discussed. Some works on stack design were also reviewed. Numerous studies have been done on both steady state and dynamic model for the MCFC.

Ghezel-Ayagh *et al.,* 2005 [15] studied the state of direct fuel cell/ turbine systems development. In their paper, the effort of FuelCell Energy Inc. in developing fuel cell/ turbine hybrid systems for clean electrical power with very high efficiency was highlighted. A proof of concept test of the DFC/T system in the sub-MW power plant facility was completed. They found that the gas turbine extended the high efficiency of the fuel cell without the need for additional fuel. The key features of the DFC/T hybrid system were electrical efficiency of 75% on natural gas and 60% on coal gas, system emissions were minimal, carbon dioxide released to the atmosphere was reduced, the design is simple and it has potential cost competitiveness with existing combined cycle power plants. Thermal management of the system was confirmed and the control strategies refined.

In a paper by Freni *et al.*, 1997 [20], comparison between the DIR-MCFC and the indirect IIR-MCFC configurations was done. The advantages and disadvantages of the two models in terms of mass transfer, thermal balance and efficiencies were made. Freni *et al.* found that the effect of operating pressure on methane conversion is substantial mainly in the IIR configuration. They also observed that there was a decrease in outlet methane content with current density. Furthermore, comparison also showed a higher cell voltage in the DIR configuration than the IIR configuration at fixed current density and cell temperature. It was also observed that power density increased with cell pressure and temperature. They also observed that significant differences exist between the two configurations at 1atm and 923K; 129 mW/cm^2 for the DIR case and 117 mW/cm^2 for the IIR case.

Baranak *et al.,* 2007 [21] developed a model for analysing the performance of the MCFC. A simple mathematical model based on reaction kinetics and mass transfer was developed to predict polarization characteristics, the effect of temperature, gas flow rates, fuel utilization and electrolyte type on cell performance. Two types of electrolytes were studied: $LiNaCO_3$ and $LiKCO_3$. The parallel and cross flow patterns were also analysed.

It was found that MCFCs with $LiNaCO_3$ electrolyte have better performance than those with $LiKCO_3$ electrolyte and the performance of the cell with cross flow is slightly higher than the performance of the cell with co-flow. It was also found that cell potential increases with temperature up to 625^oC. Above this temperature, it was observed that the cell potential maintained a steady and asymptotic pattern with no considerable changes. The model results showed strong dependence of cell potential on the operating pressure for both the MCFC with $LiKCO_3$ and the MCFC with $LiNaCO_3$ electrolytes. The results suggest a stronger dependency of the cell potential on the pressure in comparison with that described by the Nernst equation. According to the Nernst equation, an eight fold increase in pressure results in an increase of 41.6mV in the reversible cell potential at 650^oC, while an increase of approximately 60mV was calculated in the study for both MCFCs. This stems from the fact that the real variation in the cell potential is higher than that calculated from the Nernst equation due to the decreased overpotentials consisting of anode, cathode and internal losses.

A lumped-parameter, first principle based non-linear dynamic model for a MCFC system has been developed by Lukas *et al.,* 2005 [12]. Physical arguments and time scale separation were used to derive simpler, reduced-order, model structures that are useful for control analysis and design. The assumptions made in the fuel cell stack model are finite dimensional dynamics, separate reactor models for describing anode and cathode mass balance and a single thermal balance for the stack temperature profile. The stack dynamic model was validated by comparing the dynamic response of the model with that of a 20kW, 30 cell stack, $7800cm^2$ active area laboratory test unit which was referred to as the

plant. The transient test occurred after 3000 hours of test unit operation. The first test was conducted using a sudden perturbation in load current at 25kW under constant oxidant and fuel flow. The second test was conducted by a sudden change in load current at 16kW also at constant oxidant and fuel flow. The lumped-parameter fuel cell stack dynamic model was validated using the results obtained from the laboratory test unit. Physical arguments were used to simplify the equation set. The model was also extended to include the fuel cell balance of plant (BOP).

A transient mathematical model for a counter flow MCFC has been developed by Heidebrecht *et al.*, 2003 [22]. The model is based on the description of physical phenomena related to the concentration in anode and cathode chambers, temperature in gas and solid phases as well as potential field in the electrode/ electrolyte interface. For the electrode kinetics, a pore model which combines Tafel microkinetics with mass transport kinetics was applied. Assumptions such as constant pressure in the gas phase, plug flow and lumped solid phase for energy balance were made. It was said that using this model, it is possible to simulate steady state as well as dynamic behaviour of the cell over a wide range of parameters. It was concluded that the model can easily be extended to describe complete cells with several channels in Cross-flow constellation which enables direct comparison of the effectiveness of different operating strategies for MCFCs.

Roberts *et al.*, 2006 [23] analysed the performance of a hybrid carbonate fuel cell/gas turbine. In their work, two models developed in two different laboratories; National Fuel Cell Research Center (NFCRC) and National Energy Technology Laboratory (NETL), were compared.

The two models were developed to have similar features and have the configuration of the Fuel Cell Energy Inc. Direct FuelCell/Turbine (DFC/T^{TM}) sub-MW system. The models are modification of previous work by Roberts *et al.* [24.] The significant change in the models is the addition of internal reforming simulation capabilities. The parameters used in their model are shown in Table 2.2. The anode gas of the MCFC was modeled to enter a reformation channel in counter-flow with the internal

cathode and anode gas flows. It was found that by creating this counter flow with reformation beginning where the anode and cathode gases exits, the temperature profile in the fuel cell was more uniform.

Table 2.2 Fuel Cell Parameters for Roberts *et al.* models [23]

Parameter	Unit	Value
Number of Channels;	-	216
Cell Active Area;	m^2	1.08
Anode Specification:		
Inlet Temperature;	K	923
Inlet Pressure;	kPa	104.4
Exit Pressure;	kPa	104.4
Channel Width;	mm	3.1
Channel height;	mm	1.3
Inlet CH_4; mole fraction	-	0.2798
Inlet CO; mole fraction	-	0.005
Inlet CO_2; mole fraction	-	0.0346
Inlet H_2; mole fraction	-	0.1168
Inlet H_2O; mole fraction	-	0.5662
Cathode Specification:		
Inlet Temperature;	K	923
Inlet Pressure;	kPa	104.4
Exit Pressure;	kPa	104.4
Inlet CO_2; mole fraction	-	0.1553
Inlet H_2O; mole fraction	-	0.1553
Inlet N_2; mole fraction	-	0.559
Inlet O_2; mole fraction	-	0.1294
Channel Width;	mm	3.1
Channel height;	mm	3.2
Exchange Current Density;	amp/m^2	50
Diff. Limiting Current Density;	amp/m^2	4000
Transfer Coefficient;	-	0.75
Cell Specification:		
Thickness;	cm	1.0
Heat Capacity;	J/kg K	800
Density;	Kg/m^3	1500
Net Resistance;	Ohm m^2	$-6.667x10^{-7}$ (T-273) + $4.7833X10^{-4}$ / A_{cell}
Separator Specification:		
Thickness;	Mm	1.0
Heat Capacity;	J/kg K	611
Density;	Kg/m^3	7900

The gas turbine model developed was a single stage radial compressor and expander connected on the same shaft to a generator. It was concluded that the model can be a valuable tool when applied to study a large number of complex perturbations and control strategies.

2.3 System Analysis

This section reviews published work on simulation and system analysis of MCFC systems. Factors such as endurance, performance, efficiency and economics are discussed.

A study completed by Matelli *et al.*, 2005 [25] used a simulation of a high temperature natural gas-fueled fuel cell system for onsite or cogeneration power plants. The performance of solid oxide fuel cell and molten carbonate fuel cell systems were compared in this analysis. Internal steam reforming of natural gas was considered in their work. The method of element potentials (MEP) was used to find the equilibrium composition of the reforming reaction. The natural gas steam reforming process was simulated using the chemical equilibrium solver STANJAN. It was found that for the reforming reaction, high yield of H_2 is obtained at 700^{o}C which is closer to the operating temperature of the MCFC than at 900 ^{O}C for SOFC. The MCFC reformation process was said to release less carbon dioxide than the SOFC. Matelli and Bazzo observed from their simulation results that the MCFC thermodynamic efficiency is greater than that of the SOFC but the SOFC achieves a greater operating efficiency than the MCFC. They also observed that the theoretical efficiencies of both fuel cells were equal and relatively high.

A steady state simulation of a molten carbonate fuel cell power plant was presented by Simon *et al.*, 2003 [26]. In their work, a numerical model of fuel cell performance was developed and integrated as a custom block in Aspen Plus^{TM} for the simulation. The model considered local temperature, pressure

and composition changes along the gas path in the ducts of the MCFC. Four equations were solved simultaneously similar to the semi-empirical model of Bosio *et al.*, 1999 [27]. Finite difference and relaxation methods were implemented in Fortran 90 for the numerical solution. Factors affecting global efficiency of the power plant were studied through a sensitivity analysis by initially simulating a base case using preliminary input specification; cell temperature (650 ^{o}C), fuel utilization (75%), oxygen utilization (30%), pressure (3.5 bar), steam/methane ratio (3:1), steam temperature (170 ^{o}C). Their result showed that global efficiency can be kept over 50-55% derived from about 60% of fuel cell stack efficiency and 12% bottoming efficiency of hybridizing the MCFC with a gas turbine. Co-generative efficiency in the simulation was in the range of 75%.

They concluded that there is still room for improvement in efficiency by increasing the steam to methane ratio, pressurizing the system and decreasing the air feed rate.

Marra and Bosio, 2007 [28] completed a system analysis of a 1 MW hybrid Molten Carbonate Fuel Cell/ Turbine power plant.

In their work, an initial study of a reference 500KW MCFC hybrid plant based on the Ansaldo Fuel Cells (AFCo) conceptual design was carried out using Aspen Plus simulation software. Results of the simulation of the reference 500kW plant are presented in Table 2.3. The reference plant was later used to investigate the performance of three configurations of the plant scheme. The first configuration consisted of coupling two 500KW units that use a common compressor, gas turbine and cogeneration system; the second configuration considered a single reformer, burner and air blower while in the third configuration, a complete water recovery system on the second configuration was considered.

Table 2.3 Comparison of Solutions of Three Analysed Configurations in Respect to Reference 1MW System (Marra and Bosio, 2007 [28])

	Load: 100%	75%	50%	25%
Fuel:				
Q (kg/h)	347	266	184	97
T (^oC)	191	191	191	191
P (atm)	3.6	3.6	3.6	3.6
Air:				
Q (kg/h)	2750	2120	1530	885
T (^oC)	203	203	230	230
P (atm)	3.6	3.6	3.6	3.6
Fuel Cell:				
J (A/cm^2)	1547	1160	773	386
T max (^oC)	686	682	685	679
Power (KW_{el})	504	395	273	141
Turbine:				
Net Power (KW_{el})	59	44	32	17
Thermal Recovery:				
Power KW_t)	412	314	226	125
Efficiency:				
Reduction of η_{EL} Plant respect to 100% load	-	0.0	3.0	7.5
Net Power:				
Net electrical power (KW_{el})	522	403	268	134
Net thermal power (KW_t)	197	149	112	65

The water recovery scheme utilizes a heat exchanger to condense excess water by cooling the hot gases coming from the reformer. The water recovered is preheated by the help of a second heat exchanger and used for the methane steam reforming reaction. Their results as seen in figure 2.2 show that this third plant scheme had the best global plant performance.

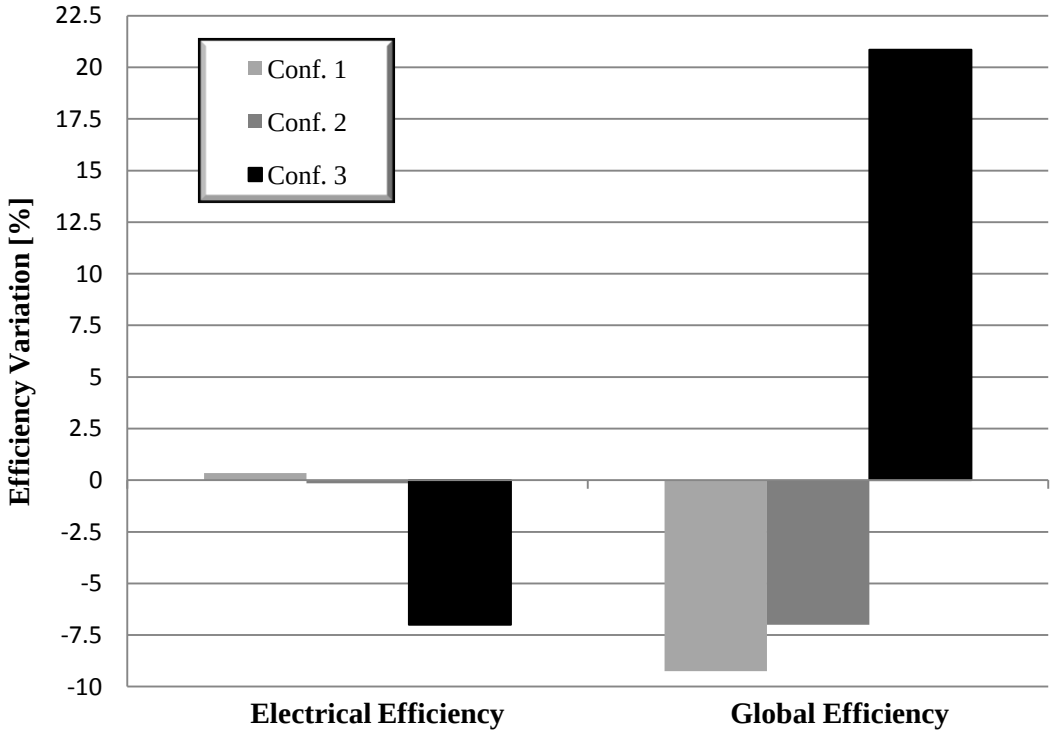

Figure 2.2 Simulation Result of 500kW MCFC Hybrid Plant (Marra and Bosio, 2007[28])

The effect of system configuration and operating conditions on the efficiency of a 100kW MCFC system has been studied by Kang *et al.*, 2002 [29]. A model was developed for the MCFC system to analyze the effect of various parameters on system efficiency. The model was validated using experimental data obtained from a 25kW MCFC system. The simulation software, CYCLE-TEMPO^{TM} (version 4.02) was used to set up a process model for the 25kW system. A gross efficiency of 12.3% was obtained for this system. Kang claimed that the reason for the lower efficiency was the lack of thermal integration between the fuel processor and the fuel cell heat. The size of the stack also accounted for the low efficiency. The fuel cell stack for the 100kW system consists of 170 unit cells with a total active area of 6000cm^2, operating at a current density of 150mA cm^{-2}, with fuel and oxidant utilizations of 80% and 30% respectively. The steam to carbon ratio was maintained at 3. They concluded that the efficiency of the MCFC system is strongly affected by system configuration, with the highest efficiency obtained from a system that used a turbo-charger to provide additional power. Their result also confirmed that the optimal fuel utilization for a MCFC system is above 60% and the optimal oxidant utilization should be above 30%.

Sugiura and Naruse, 2002 [30] completed a system study on the application of co-generation system using a direct internal reforming molten carbonate fuel cell (DIR-MCFC) for residential use. Heat and material balances among system components were used to construct the system structure that maintains cell temperature of 650^{o}C without additional heat supply. The heat balance of the DIR-MCFC cell derived by Sugiura and Naruse based on cell reaction, reforming reaction, inflow heat flux, outflow heat flux, output electric power and heat loss from the cell is written as:

$$(Q_{cell} - Q_E) - Q_{ref} + (Q_{AI} - Q_{AO}) + (Q_{CI} - Q_{CO}) - Q_{loss} = 0 \quad (2.1)$$

Q_E and Q_{ref}, are the electrical power of the cell and the heat flux of the reformer unit respectively. Q_{AI} and Q_{CI} represent the inlet heat flux of anode and cathode respectively while Q_{AO} and Q_{CO} are respectively the heat flux of anode and cathode outlets.

The heat flux of the cell reaction was calculated using:

$$Q_{cell} - Q_E = \Delta H_{H2O} Y_{H2} - Q_E \quad (2.2)$$

Where ΔH_{H2O} is the enthalpy of formation of steam in joules/mole and Y_{H_2} is the molar flow rate of hydrogen in moles/second.

The heat loss Q_{loss} from the DIR-MCFC was estimated to be 10% of the total heat flux of the cell.

In their work, the scale of the co-generation DIR-MCFC system was selected based on a model family's heat and power needs. The model family was developed from the results of a survey conducted on room layout, the family size and number of electrical appliances and consumption of electricity based on social aspects of residents of Osaka, Japan. Two fuel types where considered: city

gas and propane. They observed that the electric power generated when using propane was lower than when city gas was used, due to the need for a super heater for the propane system. They concluded that using city gas to meet the model family energy needs, the optimum system scale was 3kW while the optimum scale using propane for the same model family was 6kW. They also observed that the excess energy available for storage and for generating hot-water were much more for propane fed DIR-MCFC system than the city gas fed system due to the larger scale of the propane fed system. They further concluded that the co-generation system using city gas is a viable choice for domestic use, especially on single units while the propane gas model is best suited for apartment houses.

In another study, Lunghi *et al.*, 2003 [31] presented a system analysis and optimization of a hybrid MCFC/ gas turbine plant. The performance of a hybrid MCFC indirect heated gas turbine system as a function of the fuel cell stack size and the fuel utilization was studied. They showed that a fuel cell stack optimized for stand alone operation is not necessarily optimal for integration in a hybrid cycle and that lower fuel utilization could increase the plant efficiency since the turbine section utilizes the unconverted fuel to provide heat for the turbine inlet stream.

An optimization study of the plant design as a function of the fuel cell design parameters was conducted while maintaining the operating characteristics of a GE-Nuovo Pignone commercial gas turbine constants with an electric output of 2000kW, efficiency of 26.3%, inlet and outlet temperatures of 1100^{o}C and 550^{o}C respectively, with an overall gas flowrate of 11kg/s and an air flowrate for refrigeration of 0.6195kg/s respectively. A numerical simulation using Aspen Plus was conducted to determine the operating parameters and stack size that matches the gas turbine operating parameters. A proprietary code which was developed by Lunghi *et al.* and presented in a previous work [32] was used to evaluate the performance of the MCFC. The code allows for the evaluation of gas flow rate, cell voltage, power produced and active surface of the stack for any values of fuel utilization coefficient, current density, inlet gas stream composition and flow rate. Their analysis showed that when the fuel utilization coefficient is greater than 0.7, maximum fuel efficiency is obtained. They

also observed that the power produced by the fuel cell at this condition was very high (10522kW) compared to that of the gas turbine (2391.4kW) and since capital cost of MCFC is assumed to be higher than gas turbine, the cost of electricity produced will be very high for this operating condition. They also observed that when the fuel utilization coefficient is less than 0.6, the efficiency obtained was too low. Thus, only cases of fuel utilization coefficient of 0.6 and 0.7 were considered in their analysis. The maximum plant efficiencies they obtained from their simulation results for fuel utilization of 0.6 and 0.7 are, respectively, 57% and 58.3% and fuel cell power of 7576kW and 10522kW, respectively. From the perspective of capital cost, operating condition with utilization coefficient of 0.6 will provide a more acceptable cost of electrical power.

2.5 CO_2 Emission Mitigation Initiative

There is increased effort in reducing green house gas emission caused by energy production, power generation and utilization. The approaches to mitigation of greenhouse gas receiving the greatest interest are; energy conservation, renewable sources of energy, highly efficient systems and CO_2 sequestration. The mitigation initiatives considered in this review concern highly efficient system designs.

A model and experimental investigation of the use of MCFC to capture CO_2 from gas turbine exhaust gases was completed by Amorelli *et al.,* 2004 [33]. A conceptual design of a hybrid 1.6MW MCFC integrated with a typical natural gas fired, small industrial gas turbine with power output of 4.6MW was studied for CO_2 mitigation. The gas turbine operating at standard conditions (15^oC and nominal pressure at sea level) was said to generate over 3 tonnes of CO_2 per hour, that is, over 25,000 tonnes of CO_2 per annum. The hybrid system designed by Amorelli *et al.,* was modeled using Ansaldo Fuel Cell (AFCo) MCFC design specifications. The gas turbine was designed so that the exhaust contained about 4% vol. CO_2. In the scheme considered, the turbine exhaust is fed to the cathode. The anode

outlet is fed to a CO_2 separator, thus separating out steam and CO_2; the separated CO_2 is stored and can be sequestered or used in a green house while the steam could be used in the steam methane reaction process. The residual gas from the separator (mainly CO, H_2 and CH_4) is then recombined with the cathode off-gas at the catalytic burner before being released to the atmosphere. In their model, Amorelli *et al.* observed that the CO_2 content of the reformate at the anode increased from about 25% at the inlet to about 55% at the outlet corresponding to a concentration of about 85%wt dry basis. They also observed that CO_2 content in the turbine exhaust stream was reduced by 50% across the fuel cell.

The experimental investigation carried out to validate their model result showed that for a stand-alone MCFC, a CO_2 concentration at the cathode inlet of about 7% vol. corresponded to a power output of about 1.6MW and above this concentration only limited power increase was observed. At lower (sub-optimal|) concentrations (<7%) which is typical of gas turbine exhaust streams, the power density of the system was observed to decline. At 4% vol. CO_2 concentration, the output power was reported to be 1.47MW for the MCFC system and at 3% vol. the system output power was about1.3MW. They concluded that their results confirmed that the CO_2 level in gas turbine exhaust is adequate for the MCFC cathode reaction system. They further concluded that under the above conditions, it would be possible to reduce the CO_2 emission per kWh produced by 45% at 4% vol. CO_2 and 50% at 3%vol. CO_2 concentration in the gas turbine exhaust stream.

In another study, carbon emission and mitigation cost comparisons between fossil fuel, nuclear and renewable energy resources for electricity generation was completed by Sims *et al.*, 2003 [34]. Their work presented typical CO_2 emissions and cost/kWh from conventional pulverized coal-fired power generation plants and compared them with alternative types of generation and also with greenhouse gas mitigation technologies expected to be firmly in operation by 2020. These technologies includes, natural gas fired combined cycle gas turbine (CCGT), CO_2 capture and storage, nuclear power, hydro power, wind, biomass, PV and solar thermal.

Data used for their analysis were obtained from the Organization of Economic Co-operation and Development (OECD, 1998) and US DOE/EIA (2000). Cost and carbon emissions of the coal baseline system were taken from the average of several coal-fired projects under construction at the time of their work. They assumed that a maximum of 20% of proposed coal baseline capacity at the time of their studies would be replaced by gas, nuclear and renewable technologies during 2006-2010 and 50% during 2011-2020. These assumptions allowed for a 5-year lead time for decisions on the alternatives to be made and construction to be undertaken. They also assumed that for CO_2 capture and storage, pilot plants first developed in developed countries (referred to as Annex I Countries) could be operational in 2010 and the annual mitigation potential would be between 2 and 10 million tons of Carbon equivalent each for coal and for gas technologies. Sims *et al.* thus estimated the mitigation potential for CO_2 capture and storage technology at between 40 and 200 Mt C split between coal and gas and between annex I and non-annex I (consist of 19 developing countries which includes Brazil, Russia, India and China) countries.

From the results of their analysis, they estimated the maximum mitigation that could be achieved in 2010 and 2020 as respectively 140Mt C and 660 Mt C based on the assumption of maximum displacement of new coal power stations. Also, from the results of their mitigation analysis, they predicted that carbon dioxide capture and storage options would enable significant reductions in emissions from coal-fired generation but the cost would be between $100 and $150 per ton carbon depending on the technology used. They further stated that gas-fired combined cycle gas turbine (CCGT) with CO_2 capture and storage appeared more attractive where natural gas production and delivery infrastructure exist and nuclear power mitigation costs are in the range of $50 to $100 per ton carbon versus coal but between $125 to $300 per ton carbon versus natural gas. They concluded that the choice in terms of cost savings and carbon emissions reduction benefits for innovative technologies to displace new coal power plants is very site specific and the lowest cost option, in terms of dollars per ton of carbon avoided, will differ from case to case. They further concluded that compared with business as usual, the global electricity sector has the potential to lower its carbon

emission reductions by between 1.5 to 4.7% by 2010 and 8.7 and 18.7% by 2020 based on the data and assumptions used in their analysis.

Chapter 3

Methodology and Model Development of Direct Fuel Cell

This chapter describes the tools and methods used in the system analysis of the DFC-ERG system. It further explains the process employed for the CO_2 mitigation analysis carried out to access carbon reduction potential of the system and the potential to reduce the dependence on coal-fired plants in Ontario. Model development of a 1.2 MW direct fuel cell is outlined in this section.

3.1 Methodology

The system study completed in this thesis was performed with UniSim ^{TM} Design process simulation flowsheet software. UniSim (formerly HYSYS) is a program that can be used to design chemical plants. It is built around a library of the physical properties of a large number of chemical species, a set of subroutines to estimate the behaviour of many types of plant equipment (heat exchangers, reactors, etc.) and a graphical user interface to accept specifications for the case, and display results. The user describes the process in terms of pieces of equipment interconnected by process streams, and the program solves all the mass, energy and equilibrium equations, taking into consideration the specified design parameters for the units. It is an intuitive, interactive and very complex system that enables steady state and transient models for plant design, performance monitoring, troubleshooting, operational improvement/ optimization, business planning and asset management. Through the completely interactive interface, process variables and unit operation topology can easily be manipulated. Simulation can also be customized using UniSim's customization and extensibility capabilities.

The equation of state (EOS) selected for calculating fluid properties in UniSim is the Soave-Redlich-Kwong (SRK) equation of state. SRK equation takes into account the temperature dependencies of

molecular attraction term. It is a cubic model with two empirical constants used to correlate fluid properties and phase equilibria in the process industry.

A 1.2 MW Direct Fuel Cell/ 1.0 MW Turboexpander system was modeled in UniSim to simulate the performance of a reference 2.2 MW DFC-ERG power generating system installed at the Enbridge pressure letdown station in Toronto, Ontario. On the basis of these results, an energy recovery/ power generation system design was developed for Utilities Kingston's pressure letdown station at Glenburnie. Like most chemical simulation programs, electrochemical reaction unit models are not available in UniSim. Thus, a user defined model for the molten carbonate fuel cell unit was built using a spreadsheet sub-unit in UniSim which was integrated to the thermodynamic and unit model library of the program.

The DIR-MCFC was modeled using a material balance, an energy balance and the electrochemical reactions of the cell. Thus, the fuel cell performance was modelled to represent the FuelCell Energy, Inc. DFC300 system in terms of the electrical efficiency, the fuel and oxidant utilization, the steam to carbon ratio, the cell operating voltage, operating temperature, operating pressure and current density of the cell. The balance of plant (BOP) was modeled, fixing the output of the fuel cell and ensuring that it provides the required heat for the turboexpander inlet natural gas stream, such that the temperature of the gas after expansion was acceptable. The electrical output of the turboexpander varies with the inlet natural gas flow rate and pressure. These parameters vary seasonally and with time of the day. The efficiency of the expander was, therefore, varied according to the fluctuation of gas flow. Other units considered in the balance of plant are: the anode exhaust oxidizer, the pre-reforming unit, the reformer, the pumps, and the exchangers.

System analysis was conducted to assess the amount of CO_2 emissions per kWh of electricity generated by the waste energy recovery model. Comparisons were made with the emission intensity of

coal powered plants to determine the relative reduction in CO_2 compared to coal powered plants for power generation. Mitigation analysis was also done to determine the amount of carbon emissions avoided by using the MCFC to preheat the turboexpander inlet stream rather than combusting natural gas when regulating valve system is used to reduce pressure at letdown stations.

Data used for the system analysis were obtained from the Utilities Kingston's city gate at Glenburnie which currently uses a regulating valve systems to reduce the high pressure natural gas (usually between 600psi and 925psi) in a six inch TransCanada transmission pipeline to a pressure of about 325psi in an eight inch distribution pipeline. The principal sources of data for the emission intensity comparison and CO_2 mitigation analysis are published data of the Independent Electricity System Operator, (IESO), Ontario Power Generation (OPG) and the Ontario Ministry of Environment. The IESO provides real time data on power generation per hour for different energy systems; mainly Nuclear, Coal, Hydro, Gas, and Wind. IESO also provides an 18-month forecast on electricity consumption in Ontario every five minutes on their website. Their data were helpful in determining the emission intensity of coal powered plants based on generation output and amount per kWh of carbon emissions.

3.2 Fuel Cell Model Development

This section gives a detailed analysis of the DIR-MCFC model development that was used for the waste energy recovery system simulated in UniSim. As was stated earlier, UniSim design does not have a predefined electrochemical model, thus the fuel cell model was developed using energy and material balance based on the reaction stoichiometry and thermodynamics. The main reactions considered are the steam methane reforming reaction (equation 1.1), water gas shift reaction (equation 1.2) and the electrochemical reaction (equation 1.5). The assumptions made in developing the model follows those made by Gilbert Commonwealth Inc. for the development of a novel model named

USRMC0, an external reforming MCFC, as reported by Williams *et al.*, 1993 [35]. The assumptions are as follows:

1. Uniform temperature in cell;
2. The water gas shift reaction is considered to reach equilibrium at pre-reforming and direct internal reforming outlets;
3. No steam reforming reaction occurs within the anode compartment of the fuel cell;
4. Transport process are fast in comparison to the rate of the electrochemical reactions;
5. The fuel for which the fuel utilization is based consists of only hydrogen;
6. No solids and impurities are present in the inlet and outlet stream;
7. Gas distribution among cells in the stack is uniform;
8. All gases are ideal.

Although the model Gilbert Commonwealth Inc. developed assumed that the fuel contained both of carbon monoxide (CO) and hydrogen, based on the work done by Weber *et al.*, 2002 [36] which showed that electrochemical oxidation of CO in the cell is insignificant, the CO was not included in the fuel utilisation calculation.

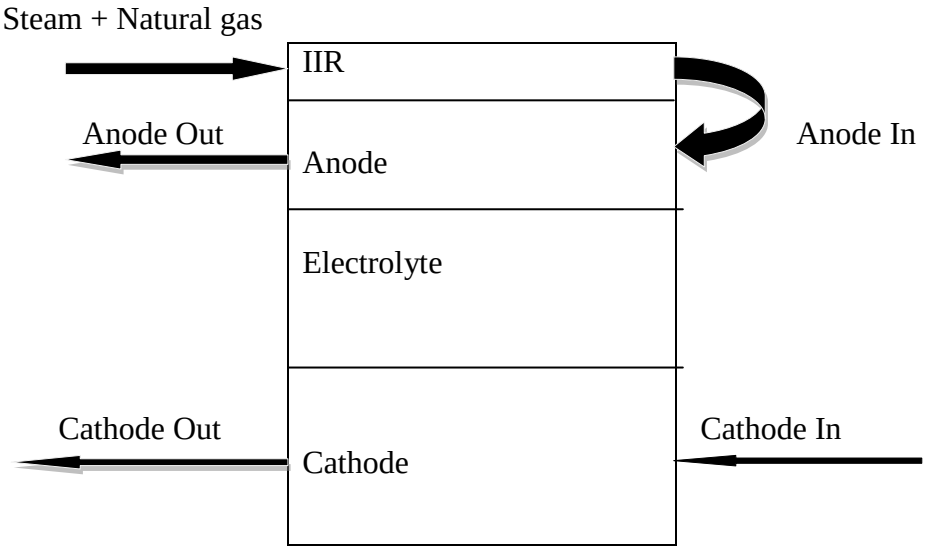

Figure 3.1 Schematic of Internal Reforming Molten Carbonate Fuel Cell

3.2.1 Material Balance

Natural gas and steam enters the indirect internal reforming (IIR) section as shown in Figure 3.1. Steam reforming (SR) and water gas shift (WGS) reactions occur in this compartment with the aid of catalysts generating carbon monoxide, carbon dioxide, hydrogen with some unreacted steam, methane, ethane, propane and nitrogen still present at the outlet of the IIR compartment. This stream is re-introduced into the fuel cell through the anode compartment where further production of hydrogen is done using reforming catalyst incorporated within the pores of the anode. Oxidation also occurs within the pores.

The assumption that no steam reforming reaction occur in the anode compartment implies that the rate of steam reforming at the direct internal reforming section is zero.

A Gibb's reactor subroutine in UniSim was used to model the IIR compartment and the reactor outlet stream became the anode inlet. The material balance equations at the anode section are given as follows:

$$N^{e}_{CO(a)} = N^{i}_{CO(a)} - R_2 \quad (3.1)$$

$$N^{e}_{CO2\,(a)} = N^{i}_{CO2\,(a)} + R_2 + R_3 \quad (3.2)$$

$$N^{e}_{H2O(a)} = N^{i}_{H2O(a)} - R_2 + R_3 \quad (3.3)$$

$$N^{e}_{H2(a)} = N^{i}_{H2(a)} + R_2 - R_3 \quad (3.4)$$

$$N^{e}_{CH4(a)} = N^{i}_{CH4(a)} \quad (3.5)$$

The material balance equations at the cathode are as follows:

$$N^{e}_{O2(c)} = N^{i}_{O2(c)} - \frac{R_3}{2} \quad (3.6)$$

$$N^{e}_{CO2(c)} = N^{i}_{CO2(c)} - R_3 \quad (3.7)$$

R_2 and R_3 are the rates of the water gas shift reaction and the electrochemical reaction respectively for the bulk volume in the anode. The superscript ‘i’ and ‘e’ denote the inlet and outlet of the anode and cathode and ‘a’ and ‘c’ denote anode and cathode respectively. The electrochemical reaction was assumed to be equal to the rate of fuel utilization.

Rate of fuel utilization was obtained from equation (3.8)

$$R_3 = \frac{JnA}{2F} \quad (3.8)$$

J is the current density in current per unit area, n is the number of cells in the stack and A is the geometric area of the cell.

The equilibrium constant for the WGS derived from equation (1.2) is expressed as equation (3.9)

$$K_{WGS} = \frac{N^e{}_{CO_2a} \times N^e{}_{H_2a}}{N^e{}_{COa} \times N^e{}_{H_2Oa}} \tag{3.9}$$

The equilibrium constant can be calculated using equation (3.10). This equation was originally developed by Chinchen *et al.,* 1988 [43] and used by Bove *et al.,* 2005 to develop a mathematical model for solid oxide fuel cell system simulation [37]

$$In\,[K_{WGS}] = \frac{5693.5}{T} + 1.077InT + 5.44 \times 10^{-4} T - 1.25 \times 10^{-7} T^2 - \frac{49170}{T^2} - 13.148 \tag{3.10}$$

The rate of water gas shift reaction at the direct internal reforming section was determined by solving the set of eight equations: (3.1), (3.2), (3.3), (3.4), (3.5), (3.8), (3.9) and (3.10). The result was a polynomial. Solution of the polynomial is explained in Appendix 3.

The material balance was used to solve for the anode and cathode outlet compositions of the cell. As will be discussed in a later section, the anode outlet was recycled to the cathode inlet through the anode gas oxidizer unit. Thus, it was very important to accurately solve for the anode outlet composition.

3.2.2 Energy Balance Model

It was necessary to develop energy balance model of the DIR-MCFC in order to quantify the heat generated by the fuel cell system.

The following are the assumptions made for the energy balance:

1. Heat transfer between cells is negligible
2. The operating voltage for each cell in the stack is uniform
3. Temperature in the fuel cell is uniform

The following were considered significant for developing the energy model: heat inflow and outflow, water gas shift (WGS) reaction, electrical work, cell reaction, resistance and heat loss.

The energy balance is given as:

$$Q_A^i + Q_C^i = Q_A^O + Q_C^O + Q_E - Q_{gen} + Q_{loss} \quad (3.11)$$

UniSim design calculates Q_A^i and Q_C^i based on the inlet condition of the fuel cell. The heat loss Q_{loss} from the DIR-MCFC was estimated to be 10% of the total heat flux of the cell. Miyake *et al.*, 1995 [38] estimated Q_{loss} to be 1% of the input heat. The heat loss accounts for losses through stack and insulation wall.

The total internal heat generation (Q_{gen}) accounts for the water gas shift reaction, electrochemical reaction and resistance to current. This was calculated using equation (3.12)

$$Q_{gen} = R_2 \cdot \Delta h_{WGS} + R_3 \cdot \Delta h_{el} + j^2 \cdot \sum R_i \quad (3.12)$$

Components which contribute to current resistance (R_i) are the anode reaction resistance (R_a), cathode reaction resistance (R_c) and the cell internal resistance (R_{ir}). These resistances, which are also referred to as cell losses, result in reduction in the cell voltage. While in some literatures, cell voltage losses were said to be caused mainly by activation irreversibility, mass transfer losses and ohmic losses, the current study did not use this approach. The method used in calculating the resistance to current in the cell adopted the approach of Morita *et al*., 2002 [39]. The anode and cathode resistances (R_a, R_c) were assumed to be due to polarization in the respective electrodes. They were calculated using the reactant gas composition and utilization as shown in equations (3.13) and (3.14) respectively. The internal resistance was assumed to be a function of temperature only (equation 3.15).

$$R_a\,(T,P_{H2}) = a(T)\,(P_{H_2})^{-0.5} = A_a\,exp(\frac{\Delta H_a}{RT})\,(P_{H_2})^{-0.5} \tag{3.13}$$

$$R_c\,(T, P_{O_2}, P_{CO_2}) = c_1(T)P(O_2)^{-0.75}\,P(CO_2)^{0.5} + c_2(T)\,M(CO_2)^{-1.0}$$

$$= A_{c1}\,exp(\frac{\Delta H_{c1}}{RT})\,P(O_2)^{-0.75}\,P(CO_2)^{0.5} + A_{c2}\,exp\,(\frac{\Delta H_{c2}}{RT})\,M(CO_2)^{-1.0} \tag{3.14}$$

$$R_{ir}\,(T) = A_{ir}\,exp(\frac{\Delta H_{ir}}{RT}) \tag{3.15}$$

Where T in equation 3.13 is temperature as a function of the partial pressure of hydrogen, T in equation 3.14 is temperature as a function of the partial pressure of oxygen and carbon dioxide, M is the gas concentration of carbon dioxide, A_a, A_{c1}, A_{c2}, A_{ir} are pre-exponential terms in the Arrhenius

type equations 3.13, 3.14, 3.15 while a, c_1, c_2 are constants. ΔH is used to represent an apparent activation energy to distinguish it from E which is used for potential.

Morita *et al.* observed that experimental data for each resistance at varying temperatures shows good linearity on Arrhenius plots; the temperature dependence of each resistance was determined by the equation. Morita *et al.* calculated the constants a, c_1 and c_2 in equation 3.13 and 3.14 using non-linear regression of experimental output voltages obtained at several gas conditions and the calculated output voltages. The values of the activation energy and frequency factor of the parameters calculated by Morita *et al.* for a Li_2CO_3/K_2CO_3 electrolyte cell at current density of $150mA/cm^2$ are presented in table (3.1). These values were used in the current study to determine the total cell resistance and the voltage losses of the DIR-MCFC.

Table 3.1 Frequency Factor and Apparent Activation Energy (ΔHx) of a Li_2CO_3/K_2CO_3 Electrolyte DIR-MCFC for Determination of Cell Resistance [Morita *et al.* ([39])

Internal Resistance:	A_{ir} (Ohms)	1.28×10^{-2}
	ΔH_{ir} (KJ/mol)	25.2
Anode Resistance:	A_a (Ohms)	1.39×10^{-6}
	ΔH_a (KJ/mol)	77.8
Cathode Resistance:	A_{c1} (Ohms)	1.97×10^{-6}
	ΔH_{c1} (KJ/mol)	83.4
	A_{c2} (Ohms)	2.2×10^{-3}
	ΔH_{c2} (KJ/mol)	22.8

3.2.3 Electrochemical model

The electrochemical model was developed based on the electrochemical reaction that occurs within the porous anode/electrolyte interface of the cell. The cell electrochemical reaction (Equation 1.5) was used to develop the electrochemical model of the fuel cell. The operating cell potential is described as

$$V = E^o - \eta_{ne} - jR_{tot} \tag{3.16}$$

E in equation (3.16) is the maximum reversible potential that is theoretically achievable (often approximated by the open circuit voltage), η_{ne} is the nernst loss, j is the current density and R_{tot} is the sum of the irreversibilities at the anode, the cathode and the electrolyte described in section 3.2.2 above.

The open circuit voltage (OCV) of the fuel cell was obtained from the Gibb's free energy change of hydrogen oxidation:

$$E = \frac{-\Delta G}{2F} \tag{3.17}$$

F is the Faraday's constant (96480 C mol^{-1})

The Nernst loss was calculated using the product gas composition as described by equation (3.18):

$$\eta_{ne} = \frac{RT}{2F} ln[\frac{P_{H2,an} \bullet (P_{O2,ca})^{\frac{1}{2}} \bullet P_{CO2,ca}}{P_{H2O,an} \bullet P_{CO2,an}}] \tag{3.18}$$

The cell electrical efficiency was obtained using the material balance, energy balance and electrochemical models that were developed. Equation (3.19) and equation (3.20) were used to determine these efficiencies. f in equation 3.20 accounts for the fraction of the heat generated that is not converted to useful heat, Q_u ($f = \frac{Q_U}{Q_{gen}}$),

$$\eta_{el} = \frac{W_{el}}{m_f h_f} \tag{3.19}$$

$$\eta_{en} = \frac{W_{el} + f * Q_{gen}}{m_f h_f} \tag{3.20}$$

η_{el} is the electrical efficiency, η_{en} is the overall heat plus electrical power efficiency, m_f and h_f are respectively the mass flowrate and enthalpy of the inlet fuel.

UniSim simulation process flowsheet software calculates the enthalpy at the inlet and outlet of both the anode and cathode based on the material balance model using the built-in thermodynamics parameter library.

3.4 Overall Efficiency

This section explains the calculation of the overall efficiency of the balance of plant. The overall system efficiency considers the individual efficiencies of the MCFC unit and the Turboexpander unit. See appendix C for an analysis of the efficiency of the Turboexpander. Since the MCFC generate useful heat, the efficiency of the combined heat and power of the MCFC was used to determine the global efficiency.

Thus, the global efficiency (η_g) of the balance of plant is given as equation 3.26

$$\eta_g = \left[\frac{h_{en} \times h_f}{h_f} + \frac{h_{te}(h_1 - h_{2s})}{(h_1 - h_{2s})} \right] \times \frac{1}{2} \tag{3.26}$$

3.5 Carbon Dioxide Emission Factors

This section explains the emission factors used to quantify the carbon dioxide produced by the combustion of natural gas in a furnace and the CO_2 emissions of coal-fired power plants. As explained in previous sections, burner in a NG letdown station combusts natural gas to preheat high pressure natural gas stream before pressure reduction. In the DFC-ERG, the heat generated by this burner is

replaced by the non- combustion thermal energy produced by the direct fuel cell. In order to analyse the emission reduction achieved by the DFC system, emission factors were determined based on the quantity of carbon dioxide produced per kWh of electrical energy generated.

An emission factor for coal power plant was also derived to be used to quantify the equivalent amount of carbon dioxide that would be produced by a coal fired plants currently operating in Ontario. The GHG mitigation potential of the DFC-ERG was carried out based on these emission factors.

The quality of fossil fuel (the primary source of green house gases), defined by the heating value and the quantity of carbon in the fuel, determine the energy in Kilowatt hour (kWh) and the amount of carbon dioxide emissions produced when the fuel is oxidized.

The heating value (LHV) of natural gas used in the current analysis was assumed to be 14.9kWh/kg (23,000BTU/Ib) or 34.6MJ/ m^3 (9.619 kWh/ m^3), while the heating value for coal was assumed to be 9.04 kWh/ kg (14,000BTU/Ib).

Assuming complete combustion of fossil fuel (natural gas or coal in this case) using air as the oxygen source, equation (3.27) summarizes the chemical reaction which produces heat, steam and carbon dioxide:

$$C_xH_y + (x + \frac{y}{4})O_2 \rightarrow Heat + xCO_2 + \left(\frac{y}{2}\right)H_2O \qquad (3.27)$$

Based on the stoichiometry, 12 kg of carbon combine with 32 kilograms of Oxygen to form 44 kilograms of Carbon dioxide assuming coal is 100% Carbon. This implies that, assuming complete combustion, 1 kg of Carbon will be oxidized by 2.667 kg of Oxygen to produce 3.667 kg of Carbon dioxide.

For this analysis, $1m^3$ of natural gas was assumed to contain 0.49 kg carbon. From the heating value of Natural gas, 1.79683 kg of Carbon dioxide will be emitted when 9.619 kWh of energy is generated.

Converting the unit of CO_2 emissions to metric tons and assuming that the furnace efficiency is 70%, *1MWh of heat generated from combustion of Natural gas produces 0.27 tonnes (0.30 tons) of CO_2.*

Although coal is an important source of energy for power generation, the combustion of coal adds a significant amount of carbon dioxide to the atmosphere per unit heat energy more than does the combustion of other fossil fuels. In coal fired power plants, energy stored in coal is converted to electrical power in the following sequence:

[Chemical Energy] → [Thermal Energy] → [Mechanical Energy] → [Electrical Energy]

The efficiency of the system determines the conversion of chemical energy to electrical energy and the amount of CO_2 emissions per kWh of electricity generated. Ontario currently has five coal-fired power plants at Thunder Bay, Nanticoke, Atikokan, Lennox and Lambton running with a combined capacity of about 4200 MW [6]. The amount of heat emitted during coal combustion in these plants depends on the nature of coal used; amount of carbon, hydrogen and oxygen present. In this study, it was assumed that bituminous coal with carbon content of 78% and heating value (dry basis) of 9.04kWh per kilogram (14,000 BTU/Ib) of coal was combusted to generate electrical power. From stoichiometric, 2.8603 kg carbon dioxide is produced when 9.04 kWh of energy is generated. It was assumed that the coal-fired power plants in Ontario operate at efficiency of 35%. Thus, *1 MWh of electricity generated in a coal-fired power plant will produce 0.905 tonnes (0.997 ton) of CO_2.*

The emissions conversion factors for natural gas furnace and coal fired power plant derived above are consistent with values used for emissions analysis by the United States Energy Information Administration (EIA).

Chapter 4

Simulation and System Analysis

This section explains the simulation of DFC-ERG system and analysis of Utilities Kingston pressure letdown station. As explained in chapter 3, the UniSim Design simulation software package was used to analyse the process flow diagrams of the systems. While the Enbridge's system in Toronto was simulated to verify the accuracy of the model and validate the performance claims of the DFC-ERG system as an energy recovery and greenhouse gas emissions reduction system, the Utilities Kingston NG usage was analysed as a possible situation where the traditional pressure regulating valve system could be replaced with the expander-fuel cell system.

4.1 Simulation of DFC-ERG system

The DFC-ERG system at the Enbridge Gas site in Toronto is a combined heat and power system which integrates a DIR-MCFC and a turboexpander in a combined cycle. The MCFC section consists of four 300kW stacks with 400 cells each. The DIR-MCFC was simulated to generate a total maximum electrical power output capacity of about 1.2 MW. Specifications used in designing and simulating the DFC are shown in Table 4.1. The balance-of-plant consists of the turboexpander, the anode gas oxidizer, pre-reformer unit, reforming unit, pumps and heat exchangers. The composition of natural gas used for this model is shown in Table 4.2.

Figure 4.1 shows the Enbridge system installed at the pressure letdown station in Toronto.

Table 4.1 Molten Carbonate Fuel Cell Stack Specification

Description	Specification
Operating Temperature:	618^{o}C
Ambient Temperature:	25^{o}C
Operating Pressure (absolute):	100 kPa
Fuel Utilization (fractional):	0.75
Oxidant Utilization (fractional):	0.30
Cell Geometric Area:	9000 cm^{2}
Number of Cells per stack:	400
Electrolyte Thickness:	0.2 mm
Ave. Stack Current Density:	100 mA/cm^{2}
Individual Stack output:	300 kW

As shown in the process flow diagram in Figure (4.2), natural gas enters the city gate through a high pressure line at flowrate of 2540kgmole/h, at an approximate pressure of 3450kPa and temperature of 27^{o}C (detailed results and specifications of the process flow diagram is shown in appendix A). These values will, however, vary with the time of day and the season. The stream is preheated in a heat exchanger by a heat source to about 61^{o}C before the pressure is reduced to about 400kPa either by the traditional regulating valve or by the turbo expander. The regulating valve acts as an optional by-pass

in this system simulation. With the regulating valve and the expander included in the process flow diagram, comparison between the traditional regulating valve and the DFC-ERG system was studied.

Table 4.2 Natural Gas Composition

Component	Mole Fraction
Methane (CH_4)	0.96
Ethane (C_2H_6)	0.006
Propane (C_3H_8)	0.002
Nitrogen (N_2)	0.031
Carbon Dioxide (CO_2)	0.001

The steam to methane ratio of the pre-reformer inlet streams was fixed at 3:1. This has been confirmed in literature as the ratio at which carbon deposition is avoided [40], thus preventing the danger of degrading the reforming catalysts.

Figure 4.1 Enbridge DFC-ERG Power Plant

The heat required to raise the temperature of the high pressure natural gas stream to 61^{o}C for the turboexpander operation was 3420MJ/h (950kW). The inlet temperature was raised to ensure that the temperature at the exhaust of the turboexpander met the requirement of the gas utility company, thus, avoiding frost heaving and water freezing in the pipeline. The quantity of heat required to raise the temperature of the turboexpander inlet gas, however, varies with the flowrate, pressure and temperature of the high pressure natural gas stream and the required condition of the expander outlet stream.

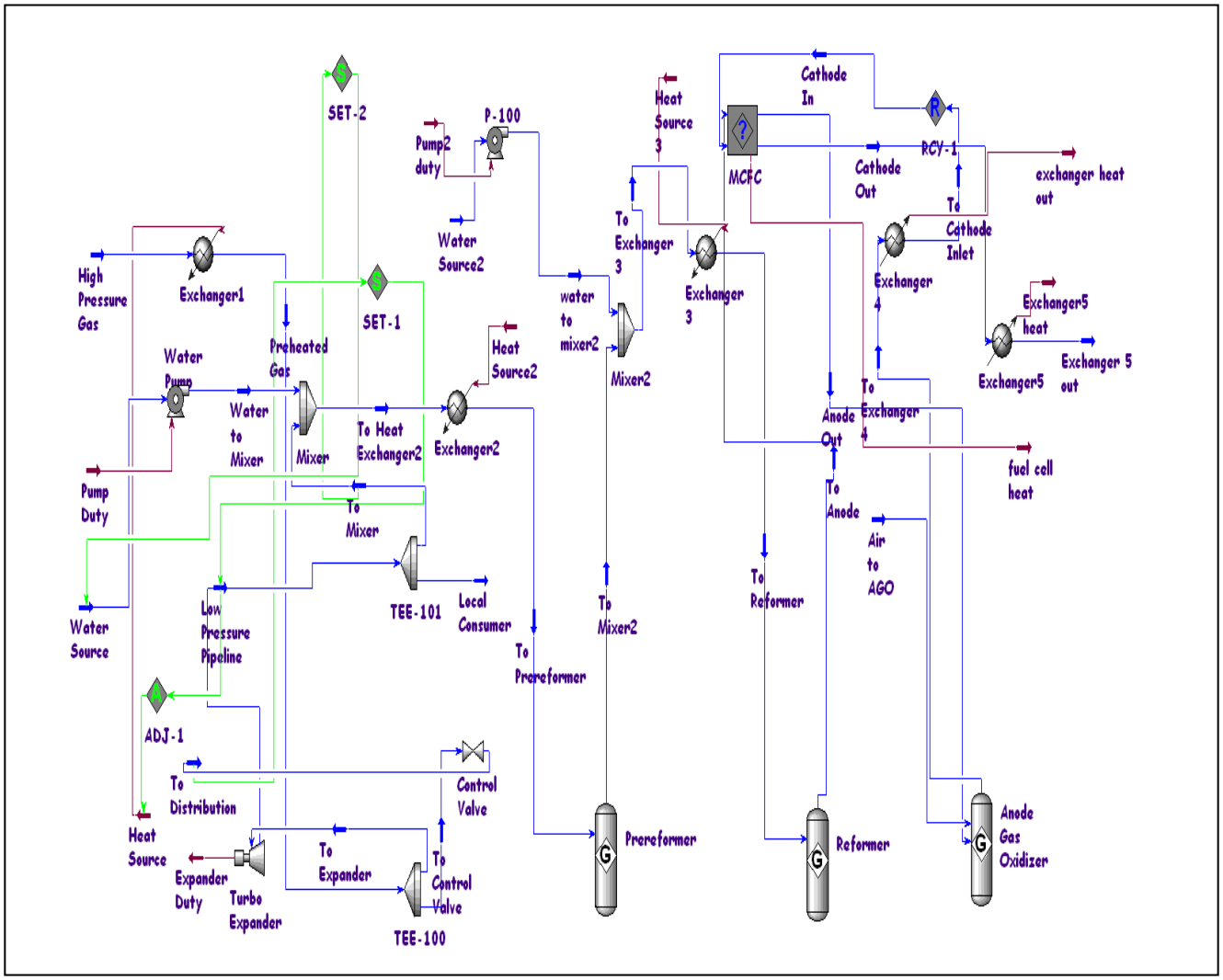

Figure 4.2 Process Flow Diagram for Direct Fuel Cell/ Turbine Energy Recovery System

About 0.5% (11kgmol/h) of the natural gas in the expander's outlet stream was sent to the pre-reforming section while the remaining 99.5% (2529kgmol/h) went to the distribution line. The reformer in this design represents the indirect internal reforming unit where hydrogen is produced from steam reforming and water gas shift reactions. The IIR and the DIR units were modelled as Gibbs reactors. The Gibbs reactor calculates the equilibrium composition of the outlet stream that minimizes the Gibbs free energy of the reacting system at the exit temperature.

As discussed in Chapter 3, the MCFC unit was modelled using a spreadsheet unit in UniSim and linked to a user defined unit operation. Energy and material balances for the fuel cell were used to

determine the outlet compositions of anode, cathode and the thermal and electrical output of the system. The anode outlet stream was recycled to the cathode inlet through the anode gas oxidizer (AGO). At the AGO unit, the anode outlet stream is oxidized by air pumped into the unit producing more carbon dioxide for the cathodic reaction (equation 1.4). Reactions 4.1, 4.2, 4.3 and 4.4 are the oxidation reactions that occur in the AGO unit.

$$CH_4 + 2O_2 + 7.52N_2 \rightarrow CO_2 + 2H_2O + 7.52\ N_2 \quad (4.1)$$

$$C_2H_6 + 3.5O_2 + 13.6N_2 \rightarrow 2CO_2 + 1.5H_2O + 13.6\ N_2 \quad (4.2)$$

$$C_3H_8 + 5O_2 + 18.8N_2 \rightarrow 3CO_2 + 4H_2O + 18.8\ N_2 \quad (4.3)$$

$$2CO + O_2 \rightarrow 2CO_2 \quad (4.4)$$

The oxidation reactions above were assumed to reach equilibrium, thus a Gibbs reactor was selected for AGO unit.

Heater and cooler unit operations were used as temperature regulators in the simulation. Pumps were used to supply water to the pre-reforming and reforming units for the steam reforming and water gas shift reactions.

The DIR-MCFC system generated electrical power of 1.13MW and excess thermal energy of 340kW for cell design specification reported in table 4.1 and reformate flowrate of 66kgmol/h. Results for this system are reported on table 4.3.

Table 4.3 Results for Enbridge 2.2 DFC-ERG System

Natural Gas Plant feed rate (kg/h)	42000
Turboexpander Inlet Pressure (KPa)	3450
Turboexpander Outlet Pressure (KPa)	400
Turboexpander Outlet Temperature (C)	3
Pre-heater thermal power required (kW)	950
Turboexpander Power (MW)	1.0
Fuel Cell Operating voltage (V)	0.78
CH_4 Conversion in MCFC (%)	95
Fuel Cell Electrical Power (MW)	1.2
Fuel Cell Excess Thermal Power (kW)	340
DFC Electrical Efficiency, η_{el} (%)	47
DFC Cogen Efficiency, η_{en} (%)	88
Turbine net efficiency, η_{tt} (%)	82
Global Plant Efficiency, η_g (%)	78

4.2 Utilities Kingston's City Gate DFC-ERG System

Utilities Kingston supplies electricity and natural gas in Kingston City Centre. Natural Gas is supplied to Utilities Kingston's gas pipeline network from the Trans-Canada high pressure pipeline and is received at the pressure letdown station in Glenburnie. The pressure is reduced at this city gate and delivered to the distribution network. Figure 4.3 shows Utilities Kingston's natural gas distribution pipeline network. There are other letdown stations on the distribution network but the current work focused on the city gate at Glenburnie which is the starting point of the distribution network.

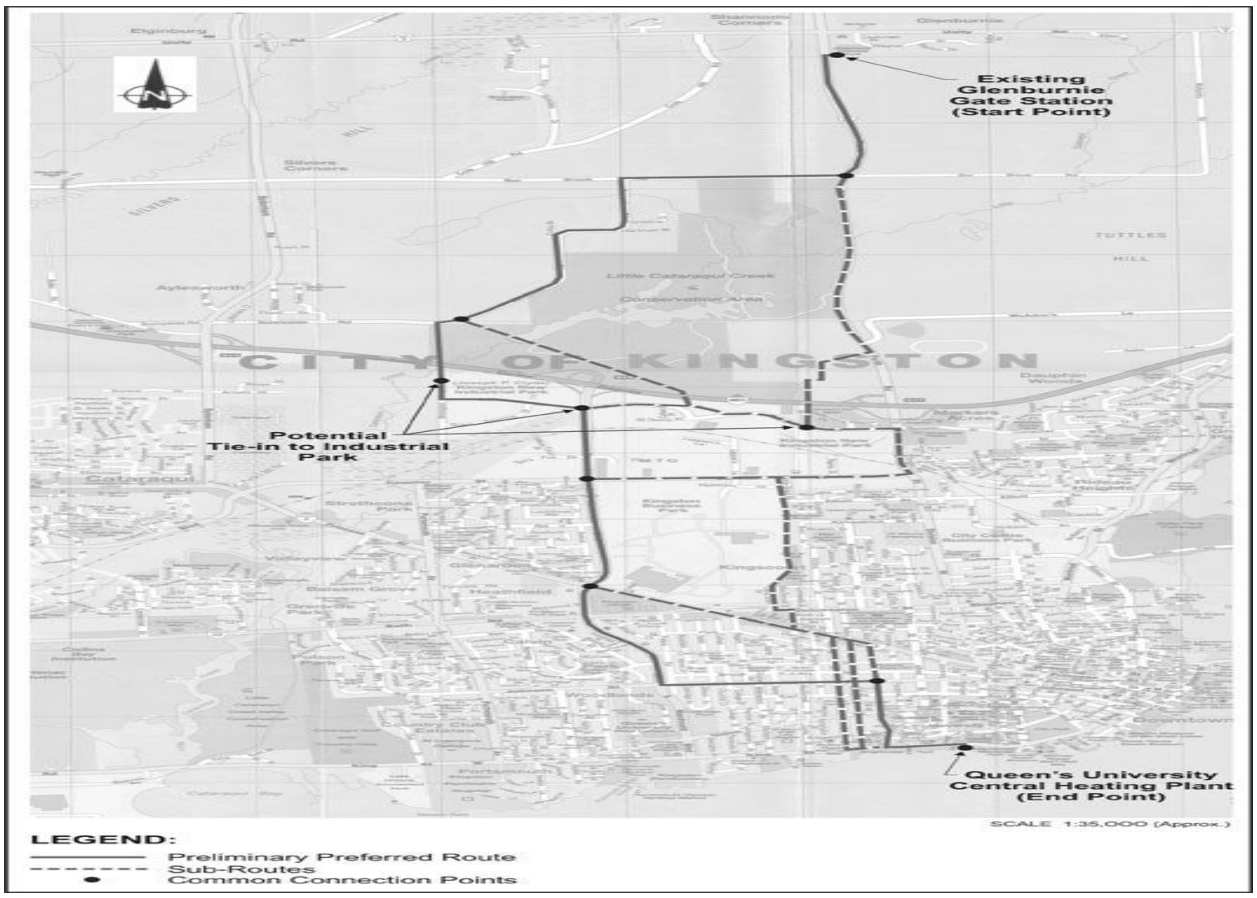

Figure 4.3 Utilities Kingston's Natural Gas Distribution Network (Utilities Kingston, 2005, [41])

Natural gas from the Trans-Canada pipeline enters the city gate via 6inch (15cm) line. The daily flowrate of the high pressure feed varies based on the time of day, ambient temperature and season. Pressure and temperature also vary seasonally from a low of near 4140 kPa (600psi) and 4^{o}C to a high of 6380 kPa (925psi) and 15^{o}C. After depressurising, natural gas leaves the station at a temperature of approximately 5^{o}C at a pressure of approximately 2240kPa (325psi) in an 8inch (20.3cm) city line and 3100 kPa (450psi) in a dedicated 12 inch (30.8cm) line for the Queen's gas turbine CHP plant.

The city gate currently uses the regulating valves shown in Fig 4.4 for pressure reduction and combustion furnaces (Fig 4.5) to pre-heat the high pressure gas before decompressing.

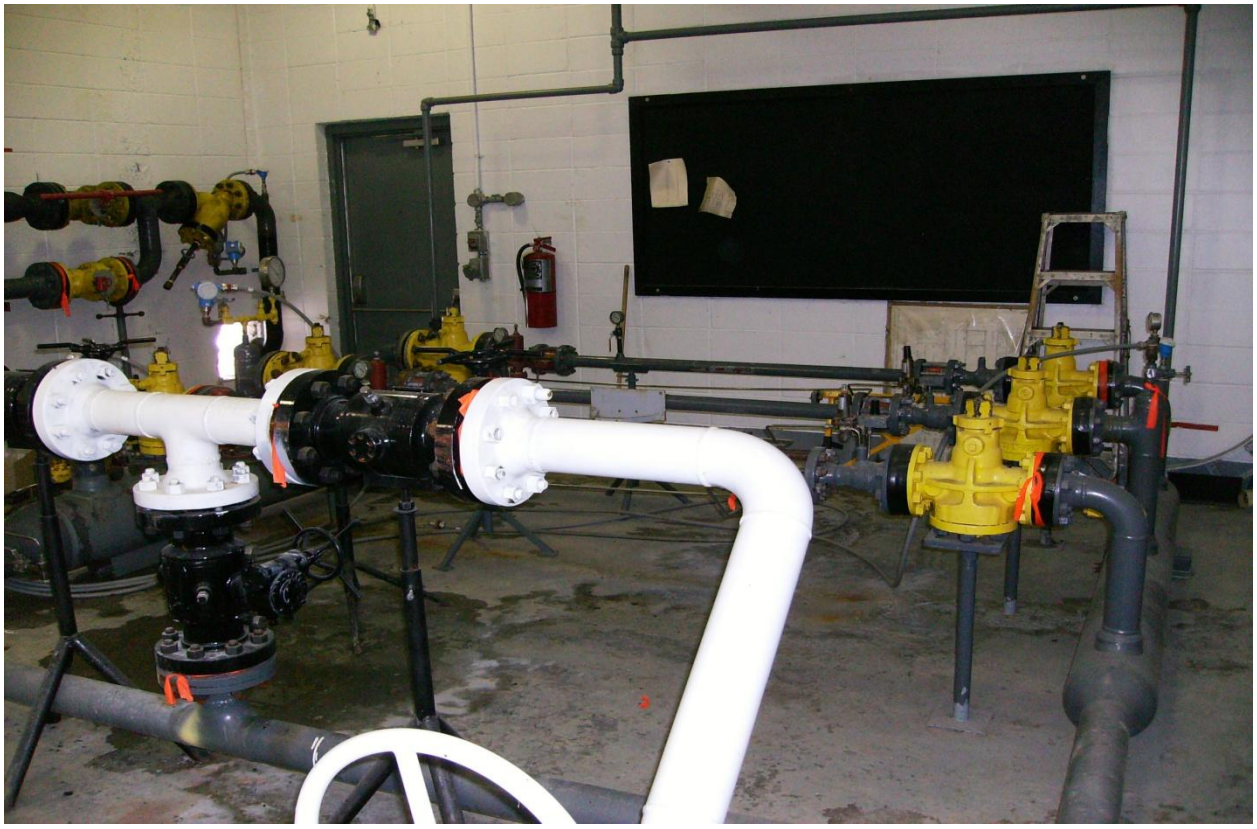

Figure 4.4 Glenburnie Pressure Regulation Valves

Most of the natural gas consumed by the furnace at the city gas is utilized for pre-heating but a small amount is also used by a space heater in the boiler room to keep the room temperature above freezing.

Figure 4.5 Glenburnie City gate Combustion Furnaces

The monthly natural gas consumption at the Glenburnie city gate for space and high pressure line preheating is highly seasonal as shown in Fig 4.6; More gas is consumed during the winter season when the ambient temperature is low (see Fig 4.7). In the summer less gas is burnt for heating the transmission pressure line and boiler room. Figure 4.6 shows the monthly trend for gas consumption at city gates using regulating valve. A deviation from the seasonal trend was however observed in the month of December of 2008. This was probably due to pipeline maintenance or upgrade.

The pre-heating loop consists of a shell and tube heat exchanger, a glycol pump and a glycol line. Glycol is used to transfer heat from the furnaces to the high pressure natural gas stream. Natural gas passes through the tube section of the heat exchanger while the glycol/water mixture flows through the shell.

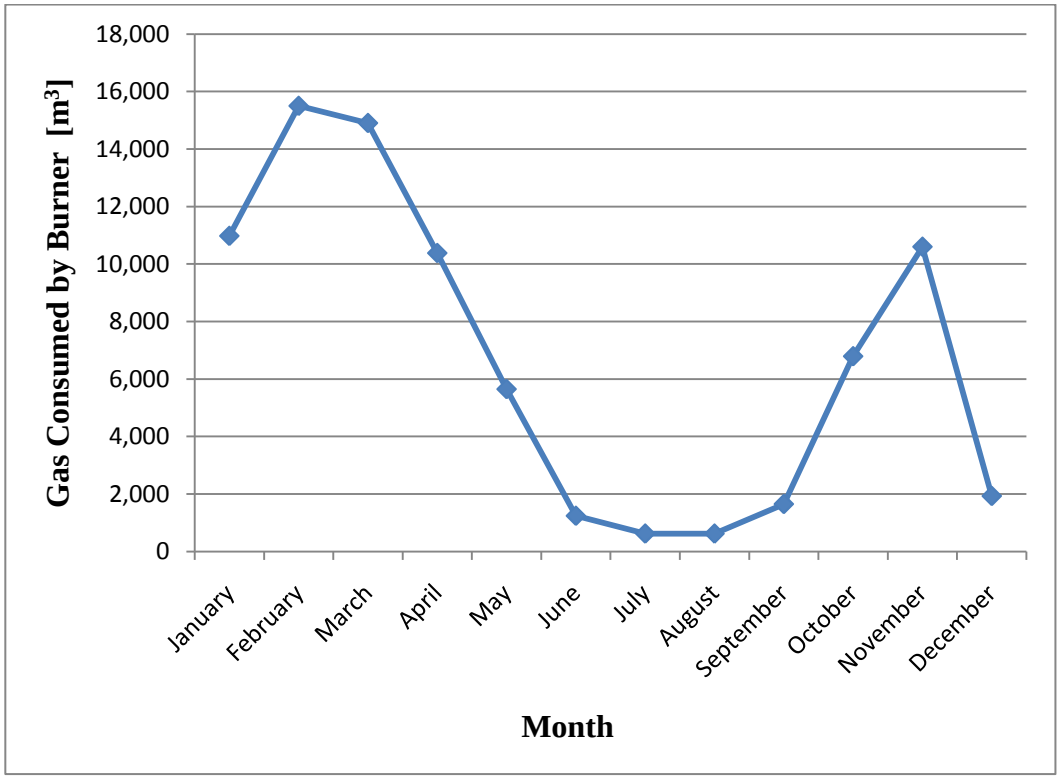

Figure 4.6 Glenburnie City Gate 2008 Monthly Natural Gas Consumption ([Phippen C, 2009 [42])

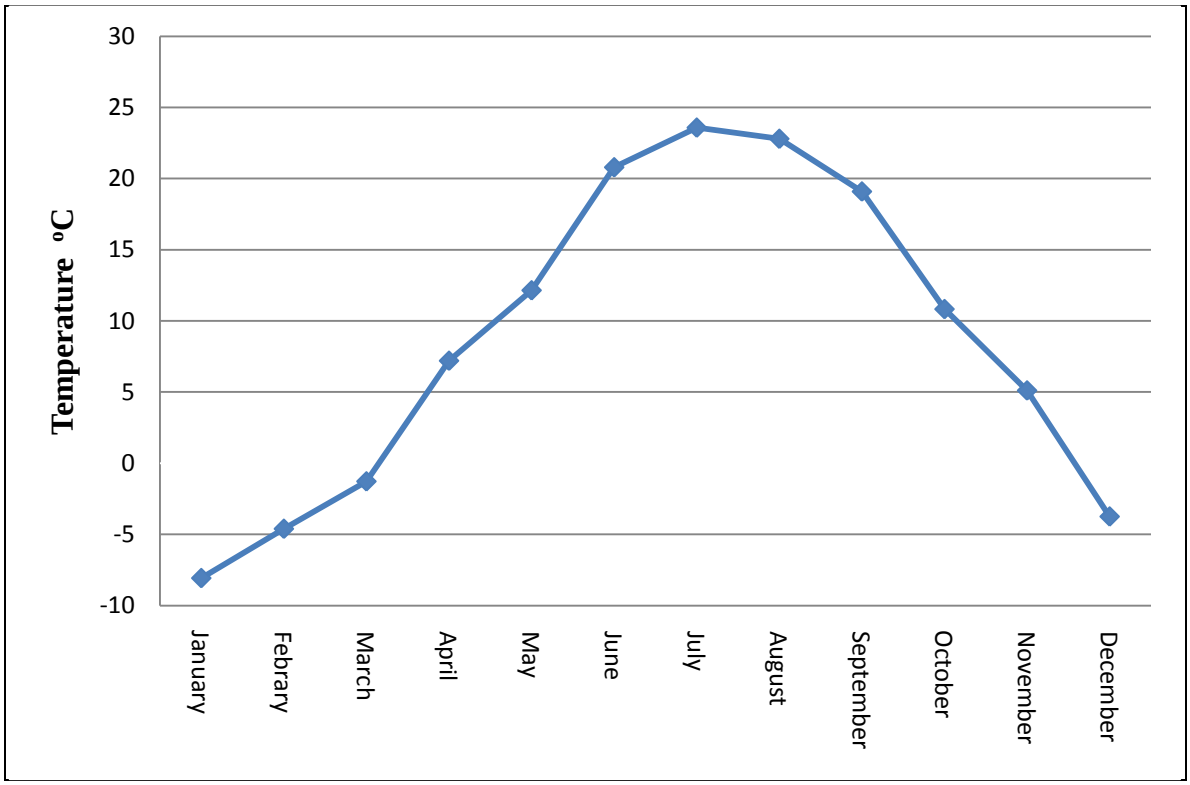

Figure 4.7 Kingston's Monthly Average Temperature (Phippen C, 2009 [42])

The flowrate of the high pressure feed stream is shown in Fig 4.8.

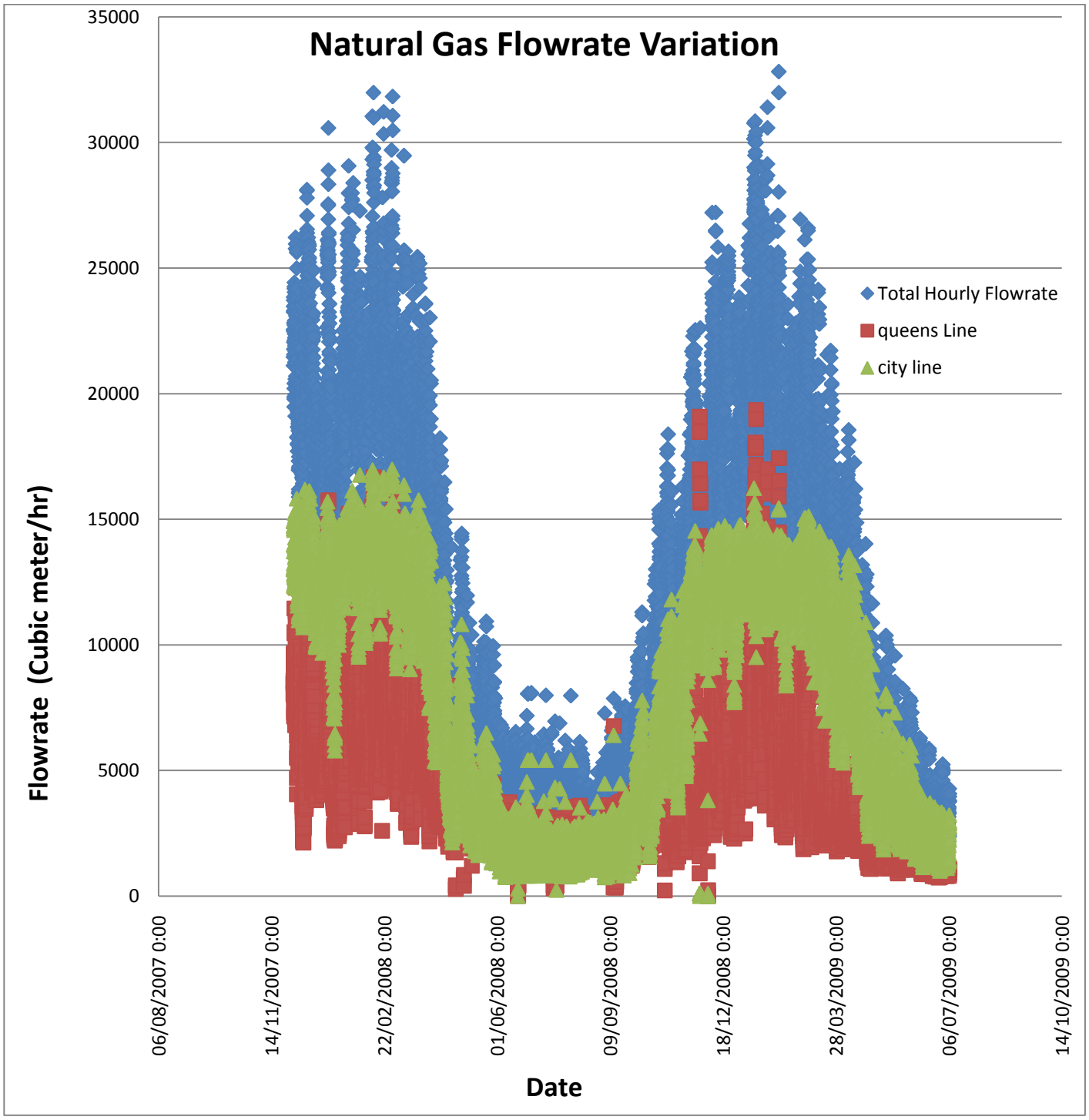

Figure 4.8 Pressured Natural Gas Feed Hourly Flowrate (Phippen C, 2009[42])

It is worth noting that the high pressure line is split into the city and the Queen's line before pressure reduction. This is because of the different output pressures required for the two lines. This study

focused mainly on pressure reduction for the low pressure line (city line). The data used for producing Fig 4.8 are those of 2007 to 2009. The data shows that significantly more natural gas is transmitted to the city gate in the winter months than is transmitted in the summer months. The summer/ winter variability in the flowrate is much less for the Queen's gas demand because demand for electrical power in the summer months is not significantly different than in the winter months as shown in Fig 4.9.

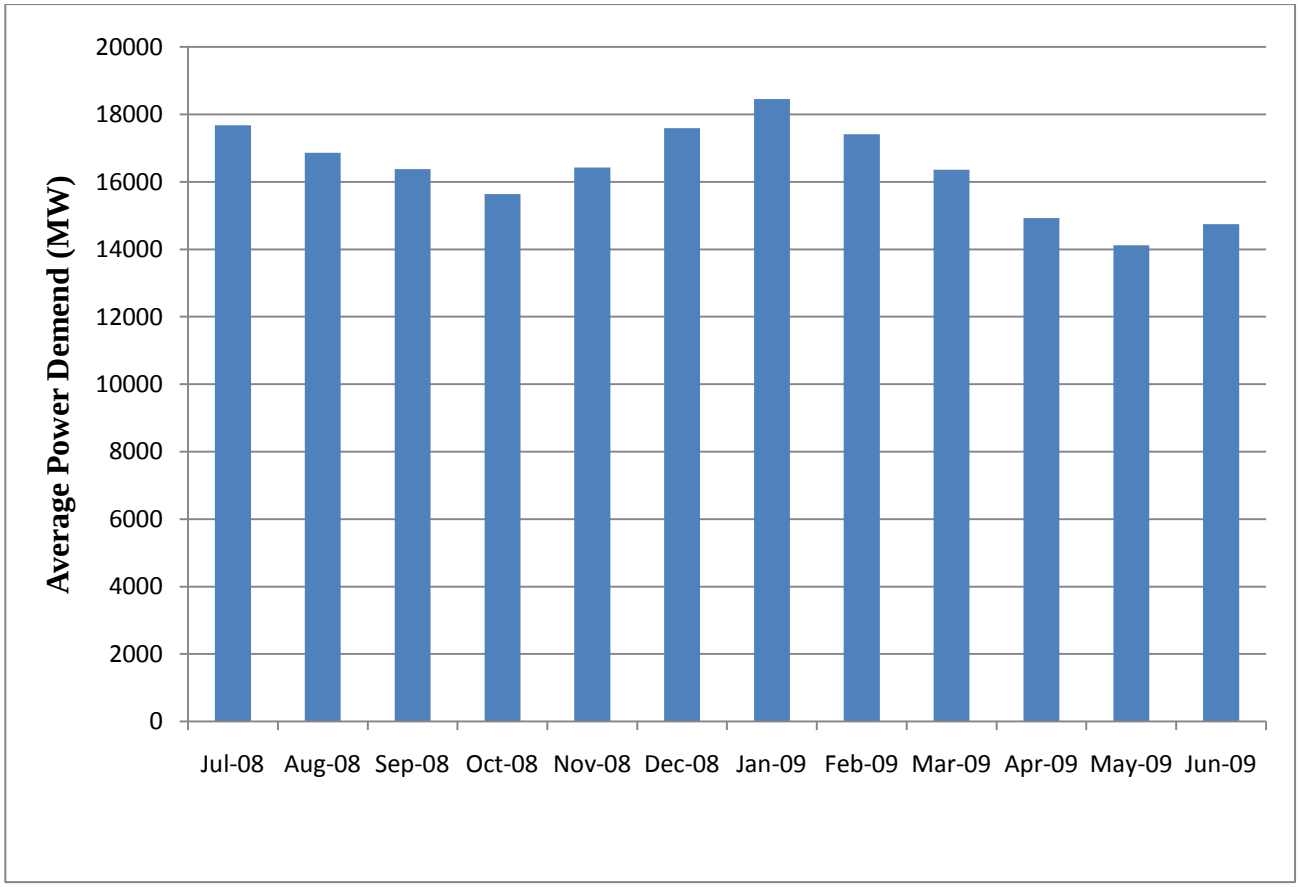

Figure 4.9 Ontario Average Hourly Power Demand (IESO [6])

The daily fluctuation of natural gas flowrate in the high pressure line is visible in Fig 4.10. One week hourly flowrate in the month of August 2008 was used in this graph. The flowrate of the natural gas in the city line peaks between 6am and 12noon. The flowrate however declined at night between 11pm and 1am.

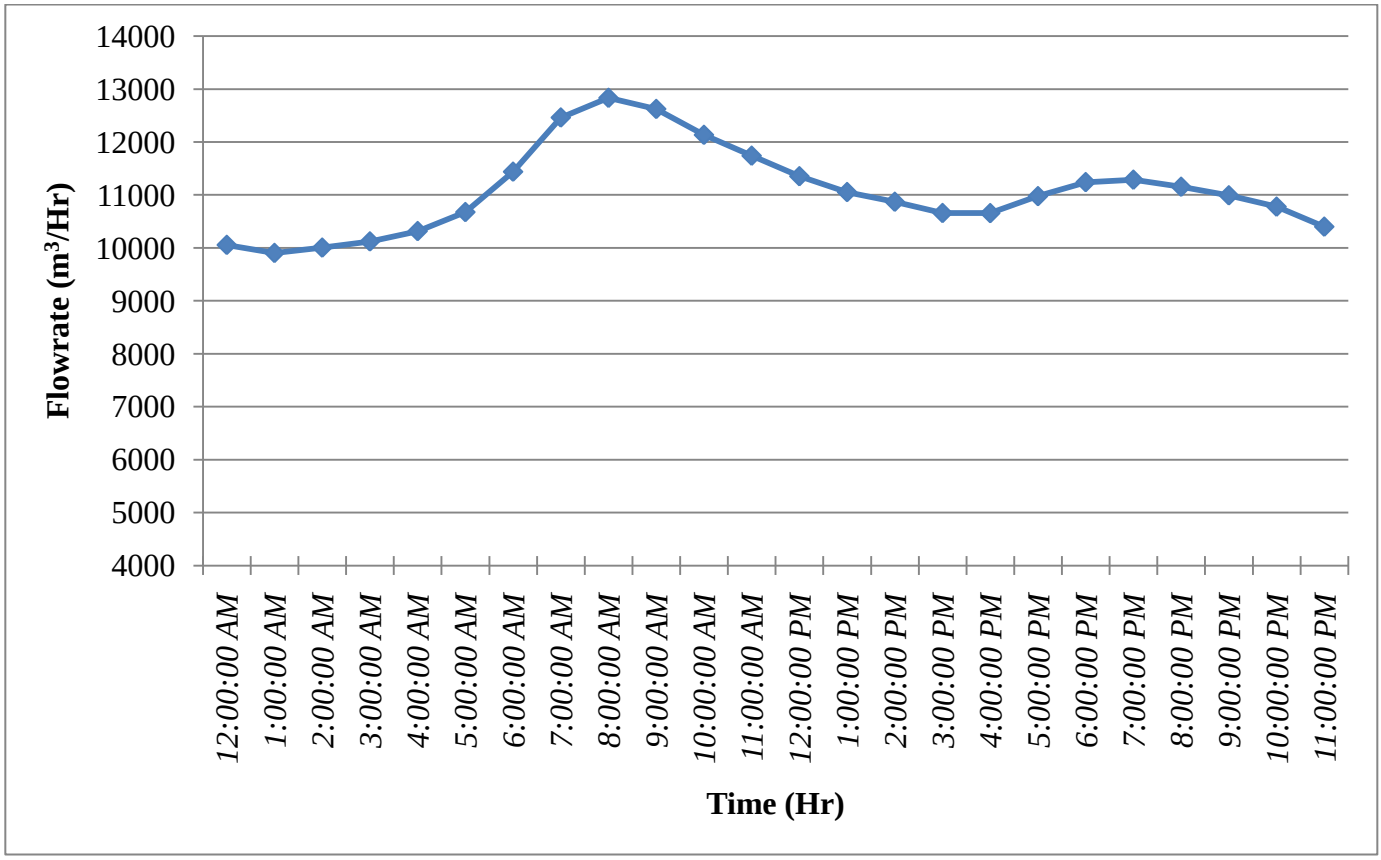

Figure 4.10 Glenburnie City Gate's Natural Gas Average Hourly Flowrate (Phippen C, 2009 [42])

The trend implies that the DFC-ERG system has a high power generation output potential during the period of high demand for power, between 7:00-8:30AM and 4:30–7:30PM which coincides with the period when coal-fired power is used to meet peak power demand.

The pressure of the turbine inlet stream is an important factor that determines the amount of power the expander can generate. Since the turbine outlet pressure is fixed, variation of the inlet pressure becomes very important. The higher the pressure ratio of the turboexpander the higher the efficiency

and the greater the power generated for a given flow. As shown on Figure 4.11, no particular pattern is observed in the 2008 city gate's natural gas pressure data. The highest pressure was in July while the lowest pressure was in December. High pressures were also observed in March and November.

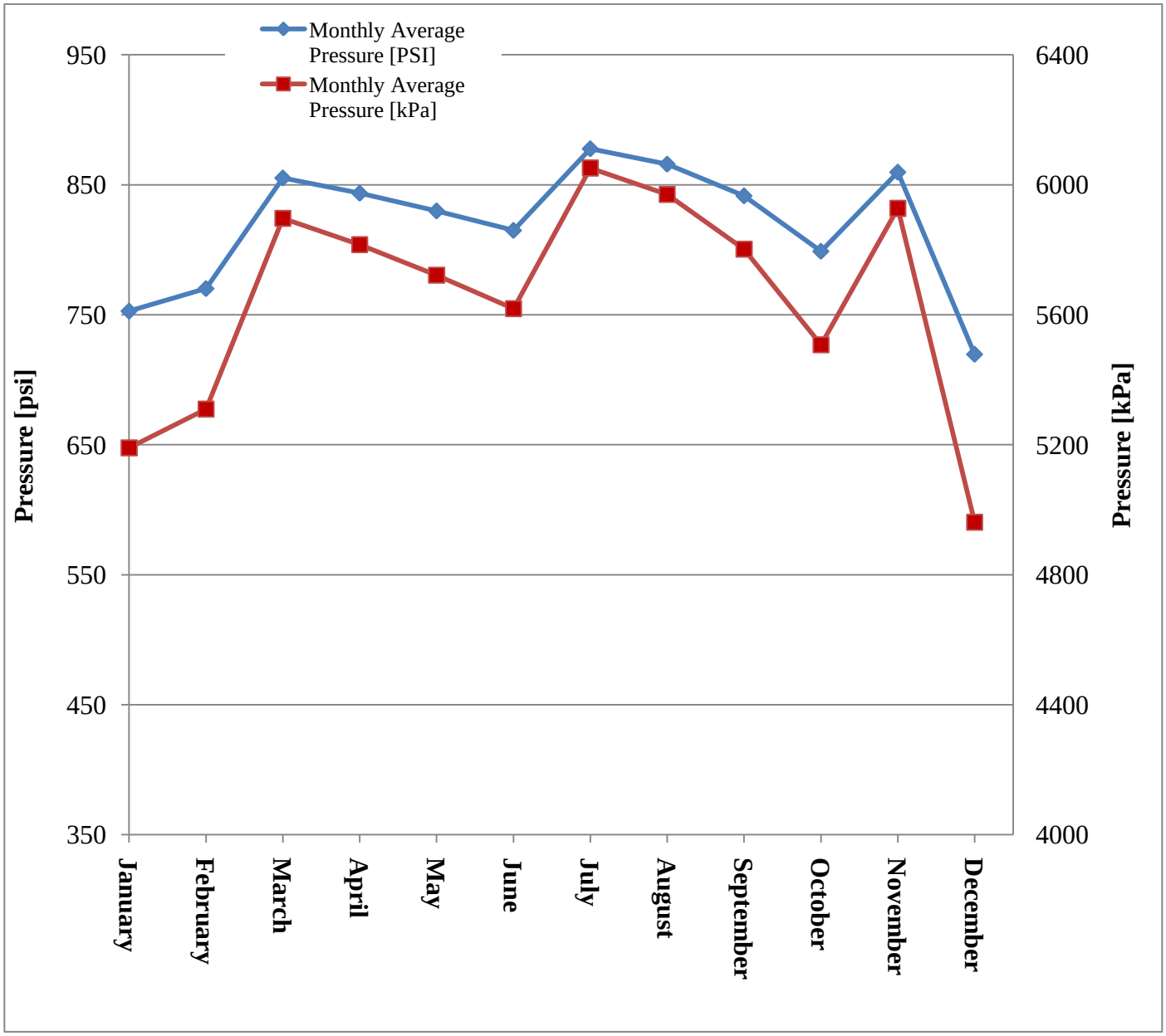

Figure 4.11 Glenburnie City gate's Natural Gas Inlet Pressure ([Phippen C, 2009, [42])

Glenburnie city gate data was used to analyse the DFC-ERG process simulation developed in UniSim to investigate the opportunities of the system at the city gate. The Direct fuel cell section was made to

operate at a constant power output while the expander output fluctuates with the varying conditions of the pressured feed stream. Results of the simulation are reported on Chapter 5.

Chapter 5

Results and Discussions

This chapter presents and discusses the results generated by the simulated Utilities Kingston energy recovery system. The MCFC stack was modeled to have the characteristics of the FuelCell Energy Inc. DFC300 system and the turboexpander simulation conformed to the characteristics of the Cryostar TG120. Comprehensive result of the simulated DFC-ERG system is presented in appendix A and the design specifications of the DFC300 and the TG120 are shown in appendix B.

The power generated and the preheating required by the turboexpander unit based on the Glenburnie letdown station's data were analysed. The CO_2 emissions of the hybrid energy recovery system was compared with emissions of the standard regulating valve system and also with the emissions of a coal-fired plant of equal power output as the DFC-ERG system. The variables used for analysing the performance of the MCFC unit were current density, cell operating voltage, cell power, steam to methane ratio and fuel utilization. The variables used for the analysis of the turboexpander are output power, required preheat, inlet flowrate and the inlet temperature.

Seasonal variation of power output from coal-fired plants in Ontario was compared with the seasonal flowrate of natural gas supplied to the Glenburnie city gate. The analysis provided insight to the use of city gates in Ontario as a possible source of utility grade clean energy and the possibility of replacing existing coal-fired power plants currently in operation in Ontario, thus supporting the province's goal of reducing emissions by 6% below 1990 emissions level by 2014.

5.1 Turboexpander Performance Analysis

The performance of the turboexpander strongly depends on the flowrate, temperature and pressure of the transnational natural gas line entering the city gate. Figure 5.1 shows the monthly variation of flowrate and temperature in Utilities Kingston's Glenburnie city gate in 2008. Average hourly flowrate per each month was plotted with Kingston's monthly average ambient temperature.

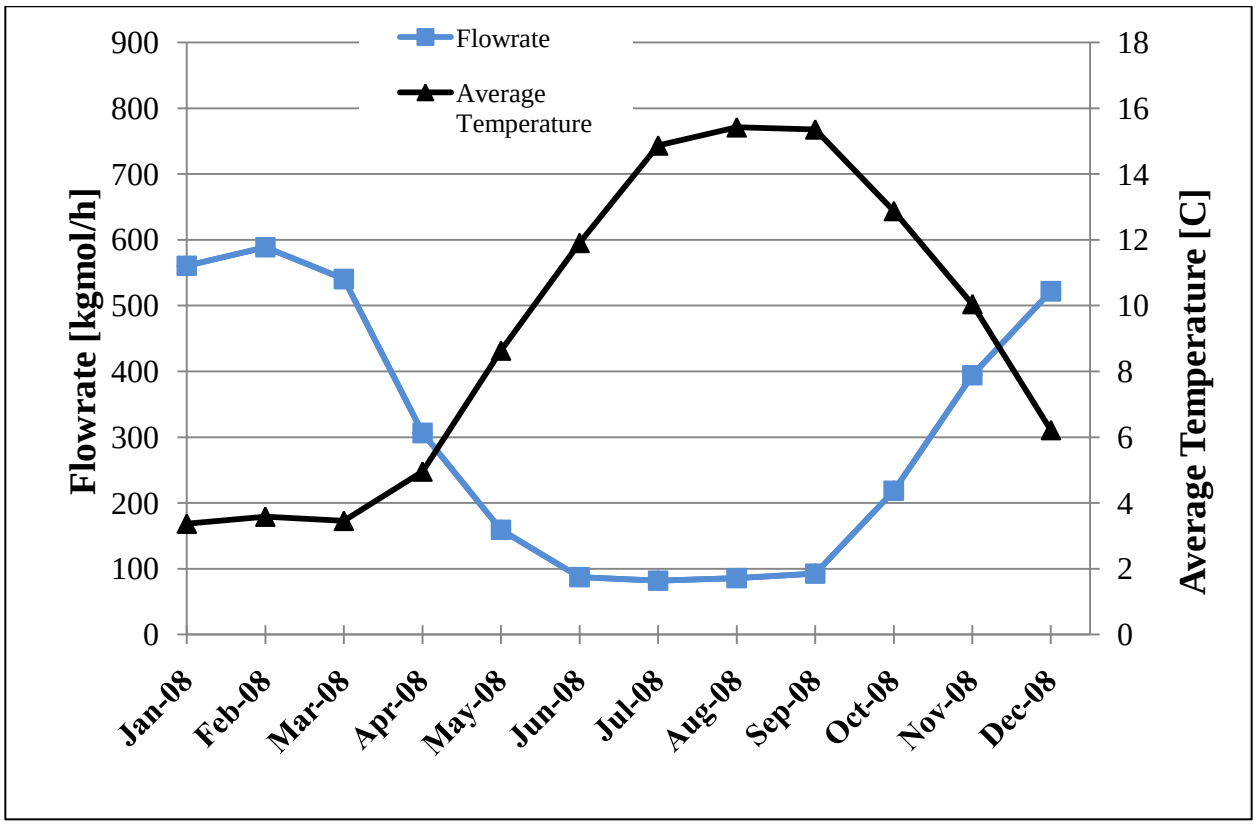

Figure 5.1 Glenburnie City Gate's Variation of Natural Gas flowrate with Ambient Temperature

The gas flow is highly seasonal with high flowrates during the winter season when the ambient temperature is low and low flowrate during the summer season when ambient temperature is high. Natural gas is used mainly for space and water heating in Kingston which explains why more natural gas is supplied to the city in winter than any other season. The trend observed in Fig 5.1 could be different in cities where natural gas is more widely used for power generation.

The estimated hourly average electrical power output of the simulated turboexpander is shown in Fig 5.2. The graph is based on the Glenburnie city gate natural gas inlet data for 2008. The effect of efficiency on the performance of the turboexpander was also investigated. In this graph, the expander isentropic efficiency was kept constant regardless of the fluctuating natural gas flowrate. This is, however, not true practically as the efficiency of a given turboexpander does depend on the flowrate. Depending on capital and operational cost considerations a combination of two turboexpander sized to achieve acceptable efficiencies in each season might be considered.

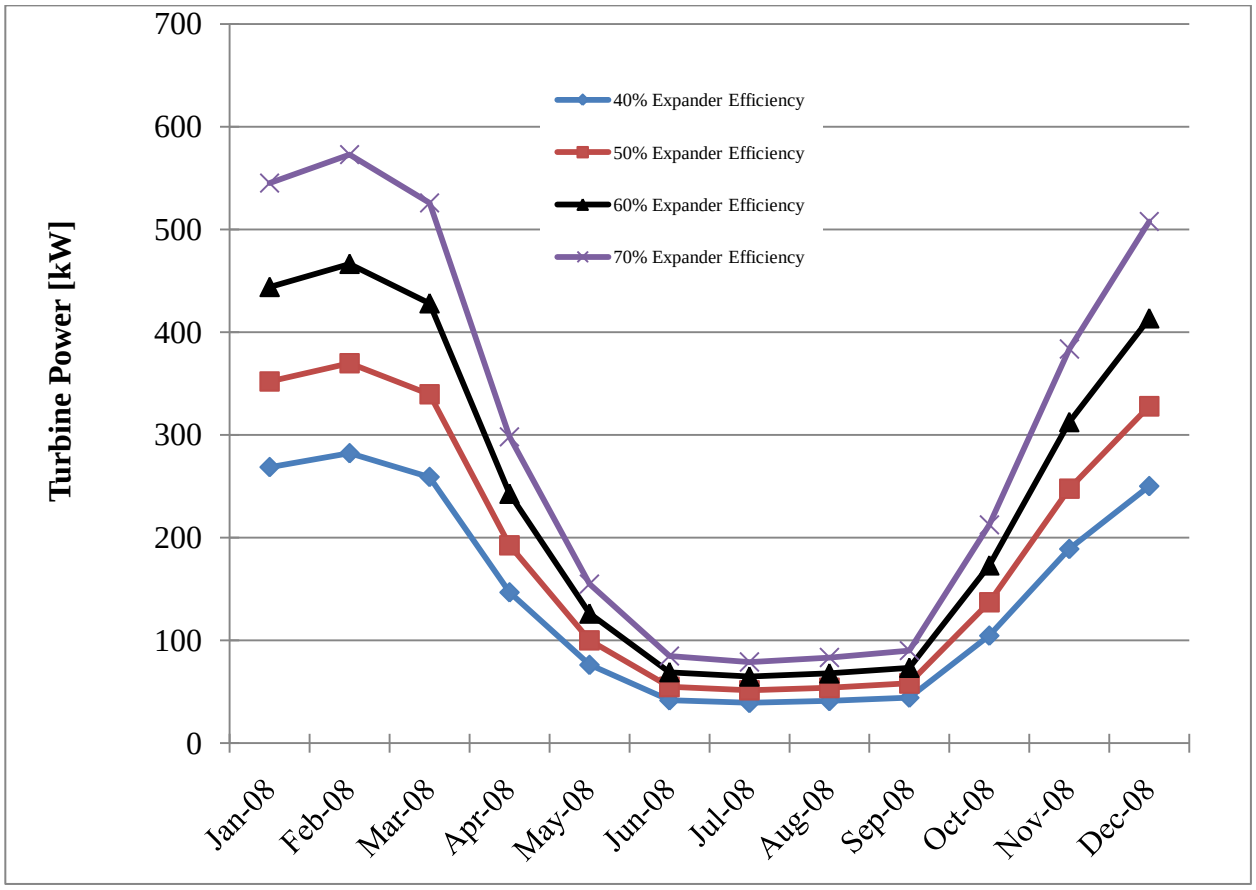

Figure 5.2 Average Hourly Electrical Power Output of Turboexpander

Less power was produced during the summer months with lowest output (39 kW) in the month of July for the turboexpander running at isentropic efficiency of 40%. The highest output was in February for a system running at isentropic efficiency of 70% (570 kW). As the isentropic efficiency increases, the electrical output of the turboexpander also increases.

The dependence of the turboexpander (Cryostar TG120) isentropic efficiency on the natural gas flowrate and pressure is shown in Fig. 5.3. The data for this plot was generated using the model developed by Madalloni and reviewed in Chapter 2 of this thesis. The upper and lower limits of the turboexpander efficiency were fixed at 90% and 40%, respectively. The model assumed that the expander efficiency varies only with flowrate and pressure. Hourly average flowrate and monthly average pressure of the natural gas entering the Glenburnie city gate were used as the input variables for the model and corresponding efficiency of the expander were generated.

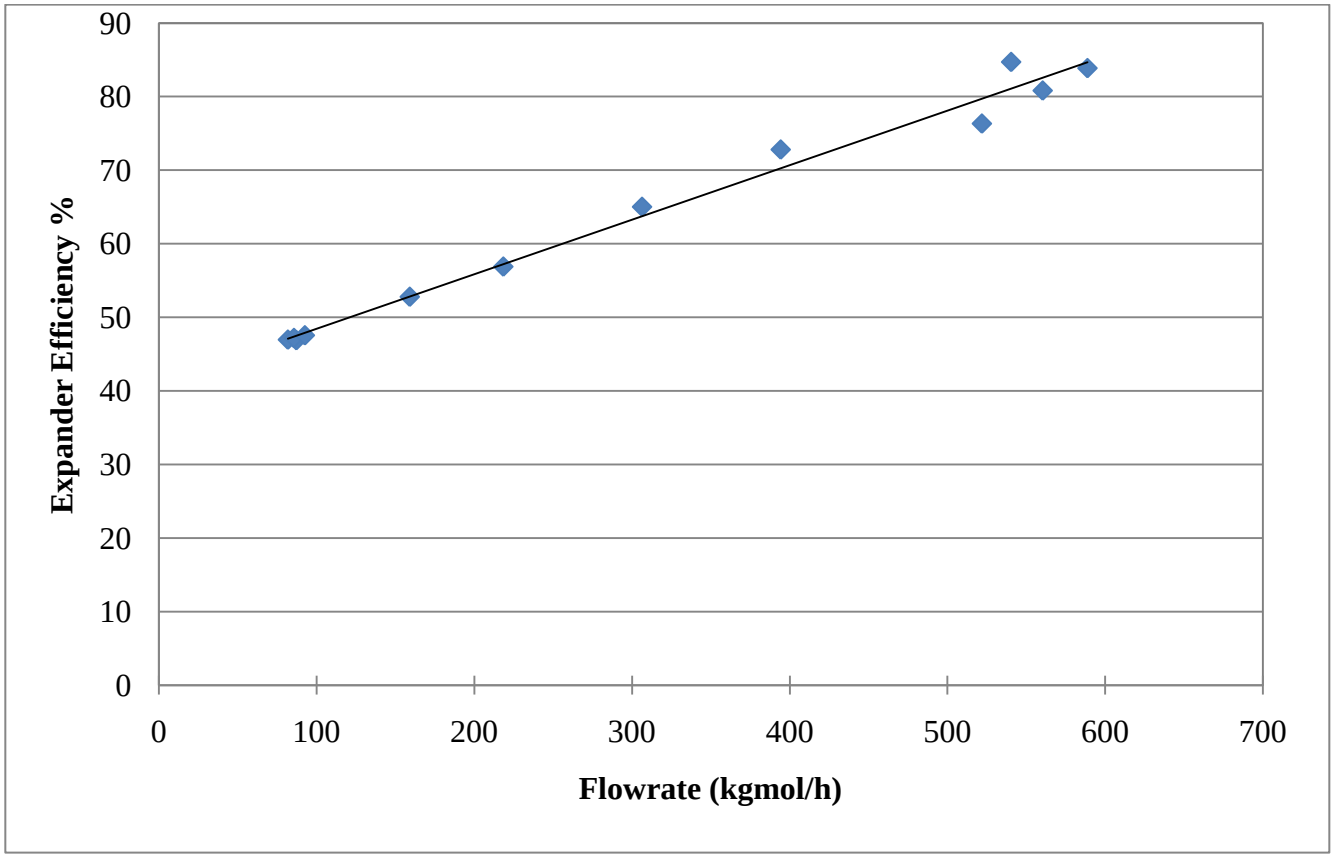

Figure 5.3 Dependence of Turboexpander Efficiency on Flowrate and Pressure (data points are based on typical monthly average flow and pressure for Glenburnie Letdown Station)

As the flowrate increases, the expander efficiency also increases. The turboexpander efficiency is less that 50% when the natural gas flowrate is less than 100kgmol/hr. This is the case in the summer months. The highest efficiency observed (84%) correspond to the flowrate of 540kgmol/h which is

due to the influence of pressure and flowrate on the efficiency. Figure 5.4 shows the effect of pressure and flowrate on the efficiency of the expander.

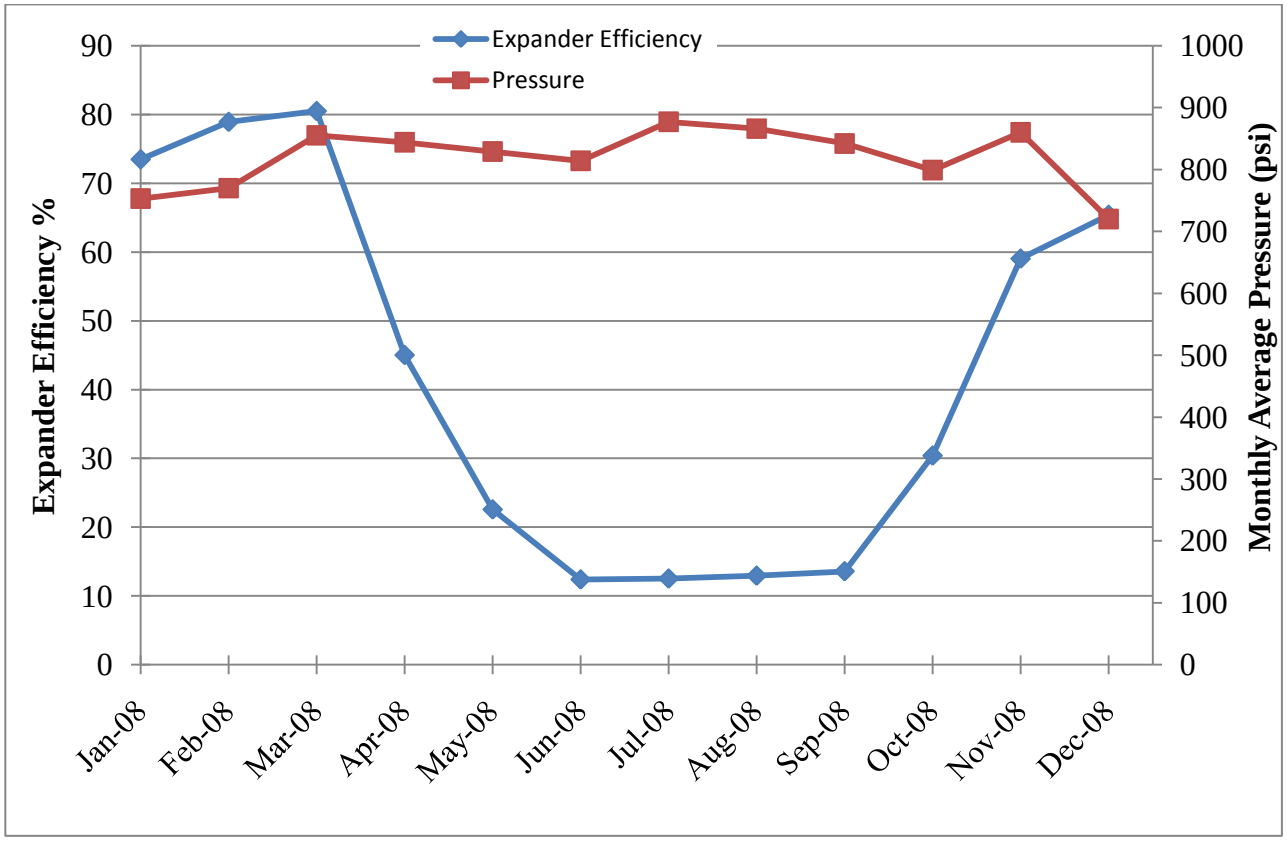

Figure 5.4 Seasonal Variation of Turboexpander Efficiency Natural Gas Pressure and Flow for Glenburnie Letdown Station

The preheating required at the turboexpander inlet steam depends on the flowrate of the natural gas entering the expander, the expander efficiency and the condition of the natural gas stream in the distribution line. In this simulation, the expander outlet condition was fixed at 3^{o}C and 22.4 bar (325 psi). Figure 5.5 shows the variation of the thermal load energy and the electrical power output of the expander with the flowrate of the natural gas pressured line.

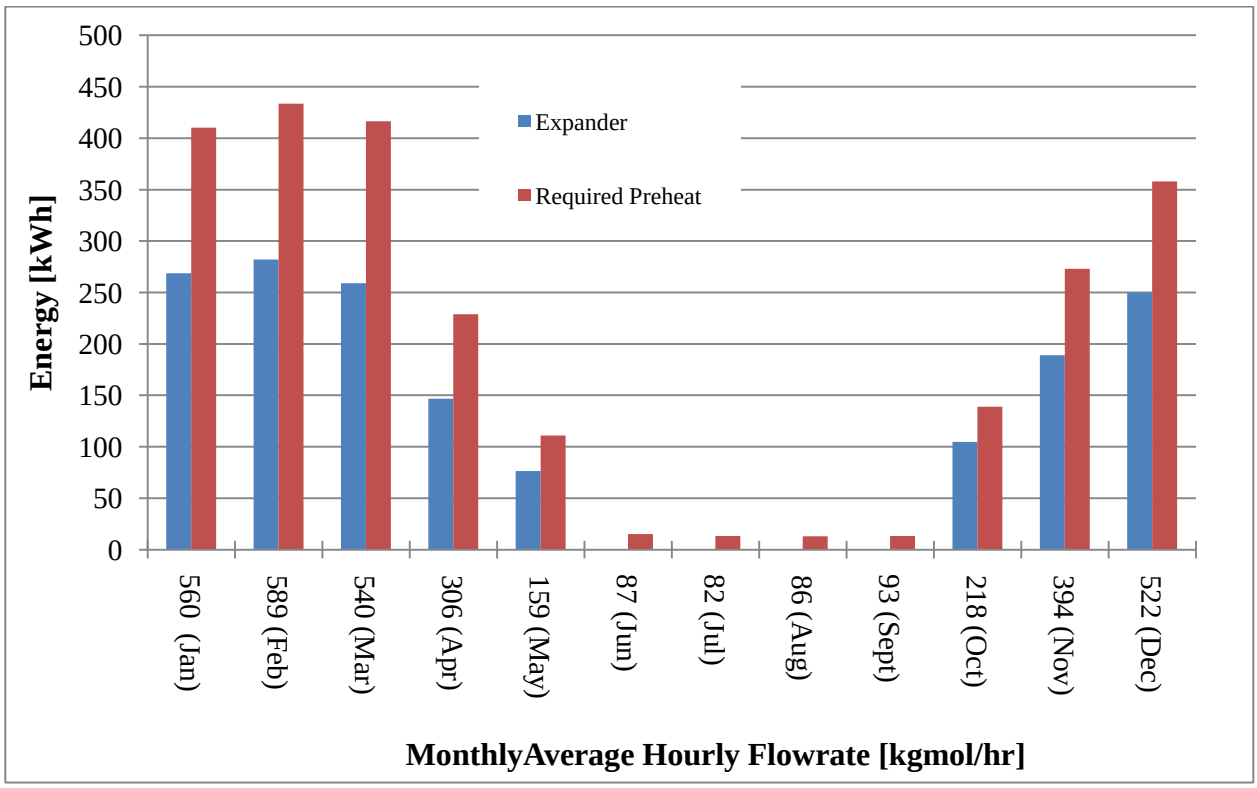

Figure 5.5 Dependence of preheat required on Turboexpander Electrical Power

More thermal energy is required for preheating during the winter season when the flowrate of the pressured gas entering the city is greatest whereas very little preheating is required during the summer season. In summer (June, July, August, September), because of the low efficiency and power generation, the turboexpander was shutdown and by-passed thus using the regulating valve as pressure reduction system. The turboexpander unit generated an average of 1140 MWh of electrical energy per year and the annual average preheat required by the simulated pressure reduction system was 1760 MWh which is approximately triple that of the regulating valve preheat alone. This shows the advantage of the turboexpander system over the regulating valve system, in that the addition of 1760 MWh of heating enables the turboexpander to convert pressure energy to electrical power which would be otherwise wasted in the regulating value system. However, if a boiler is used as the source of the additional thermal energy required to preheat the turboexpander natural gas inlet stream, then more CO_2 will be emitted to the environment at the letdown station compared to the emissions from using

the MCFC. Combining the MCFC unit with the turboexpander to provide thermal energy greatly offsets these additional CO_2 emissions by producing clean electricity. Figure 5.6 compares the hourly thermal output of the MCFC unit with the preheating requirements of the turboexpander and the regulating valve systems.

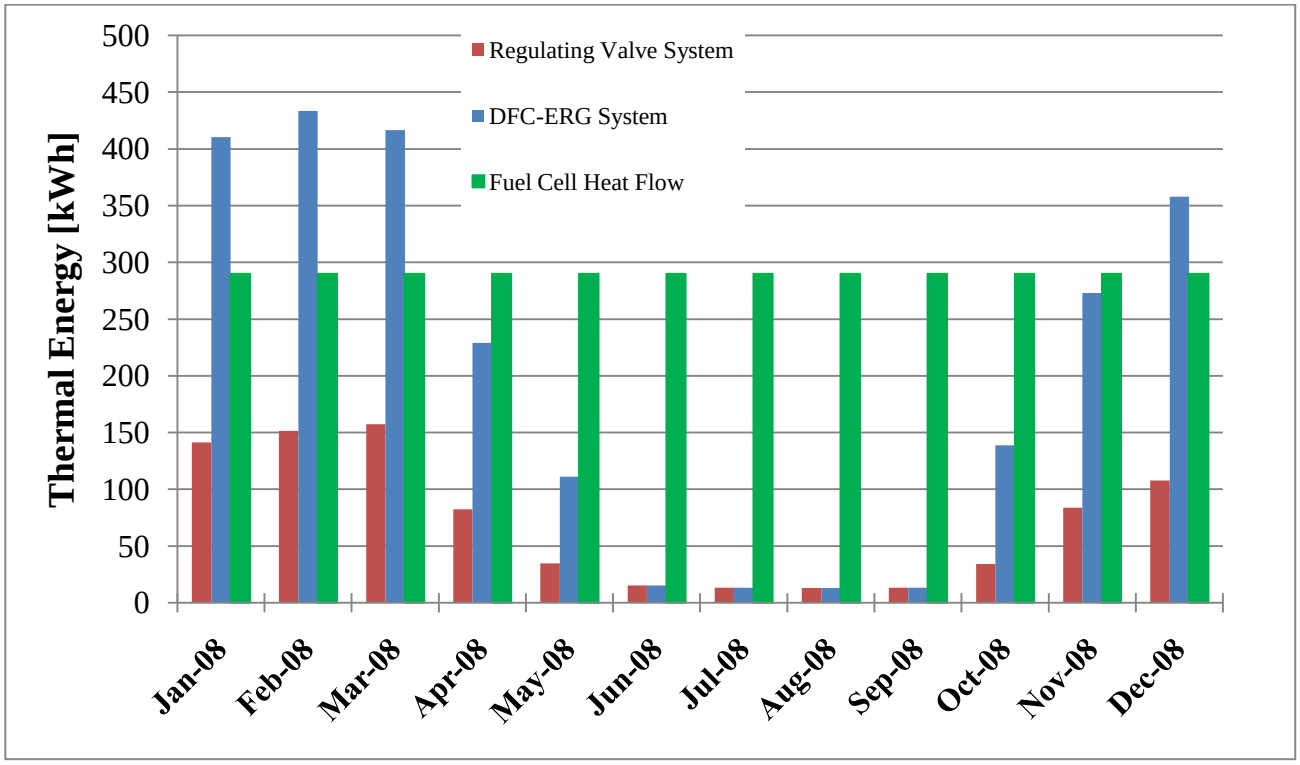

Figure 5.6 Comparison of Hourly Average Heating Duty of MCFC Unit with Average Hourly Preheating Requirements of the DFC-ERG and Regulating Valve Systems

The MCFC stack generated 290 kW non-combustion heat; a total of 2540 MWh non-combustion heat annually.

The thermal output of the fuel cell system was constant throughout the year because the electrical output was fixed at the nominal rated output of 300 kW for the standard system currently provided by FuelCell Energy Inc. who manufactures these systems. The rational for this scenario is that it maximizes the revenue generated by the fuel cell that would represent a major part of the investment of building this system. The fuel cell system can provide enough heat in April through November without any support from the boiler. The boiler was, however, required to provide additional heat in January, February, March and December. Figure 5.6 also shows that the annual thermal energy

required for preheating the expander natural gas inlet line (6340 GJ) is approximately three times more than the total annual thermal energy required for preheating the regulating valve inlet stream (2200 GJ). This implies that if the source of heat for the expander inlet stream is derived from a boiler system, the turboexpander system would emit about three times more CO_2 than the emissions of the regulating valve system.

However, the revenue from the sale of the electricity generated and the corresponding reduction in GHG emissions from coal-fired generation must be considered in evaluating the benefits of the turboexpander-fuel cell energy recovery system.

5.2 Molten Carbonate Fuel Cell Performance Analysis

The MCFC system specification was based on the required thermal output, electrical power output, as well as the size and cost of current available units. A single DFC 300 system provided the closest match to the requirements. It is a one stack unit with 400 cells and a net nominal electrical power output of 300 kW. The stack has electrical efficiency of about 47% (LHV) as claimed by the manufacturer, FuelCell Energy Inc.

Figure 5.7 shows the characteristic polarization curve of the cell used in the DFC 300 unit. The data for this graph were generated using Equation 3.20. The current density of the cell was varied and the corresponding cell voltage data generated. The steam to carbon ratio was also varied to investigate its effect on the cell operating voltage.

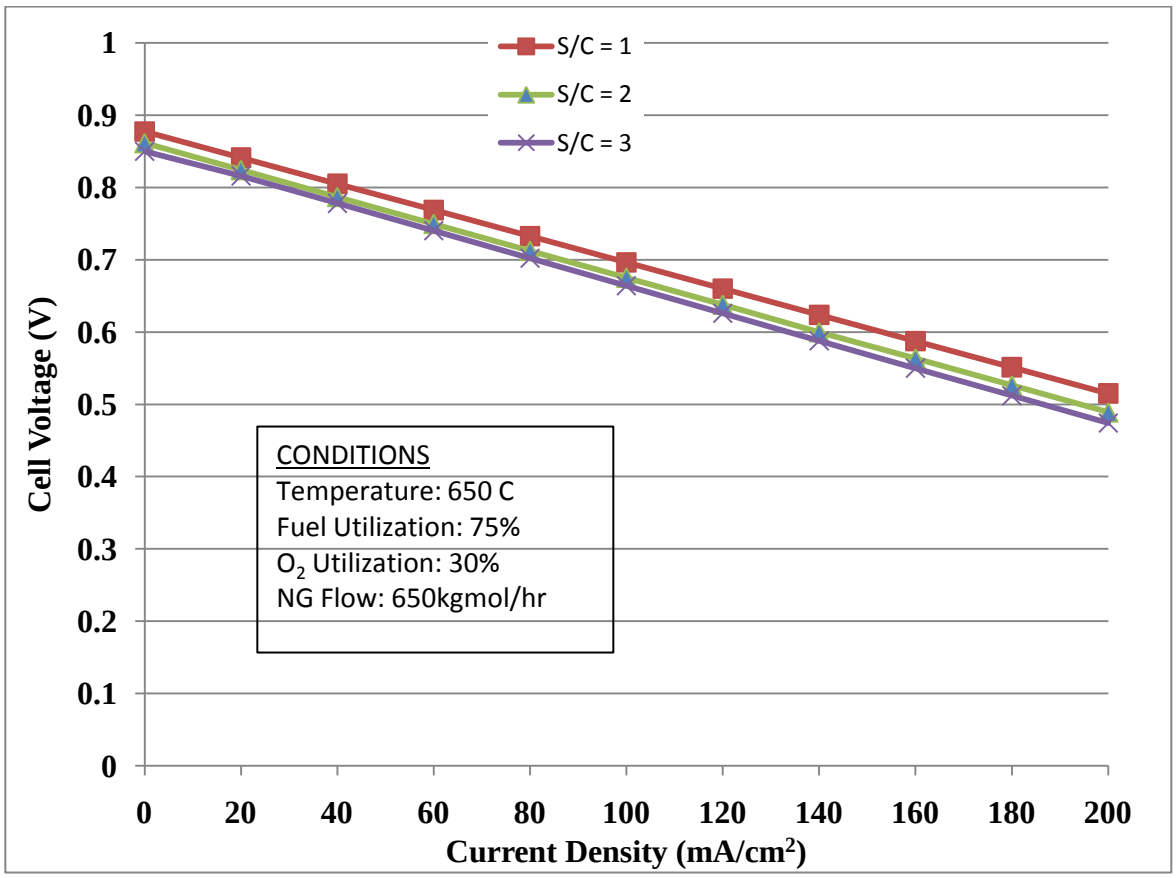

Figure 5.7 Fuel Cell Performance Curve

The MCFC performance curve agrees with typical characteristic curve of high temperature fuel cells [37]. The cell voltage was highest at steam to carbon ratio of 1 and lowest at steam to carbon ratio of 3. A steam to methane ratio greater than one is, however, required to prevent the formation of carbon that would deactivates the reforming catalyst in the cell. In this analysis, a steam to methane ratio of 3 was used.

The variation in the power output of DFC 300 system with fuel utilization is shown in Fig. 5.8

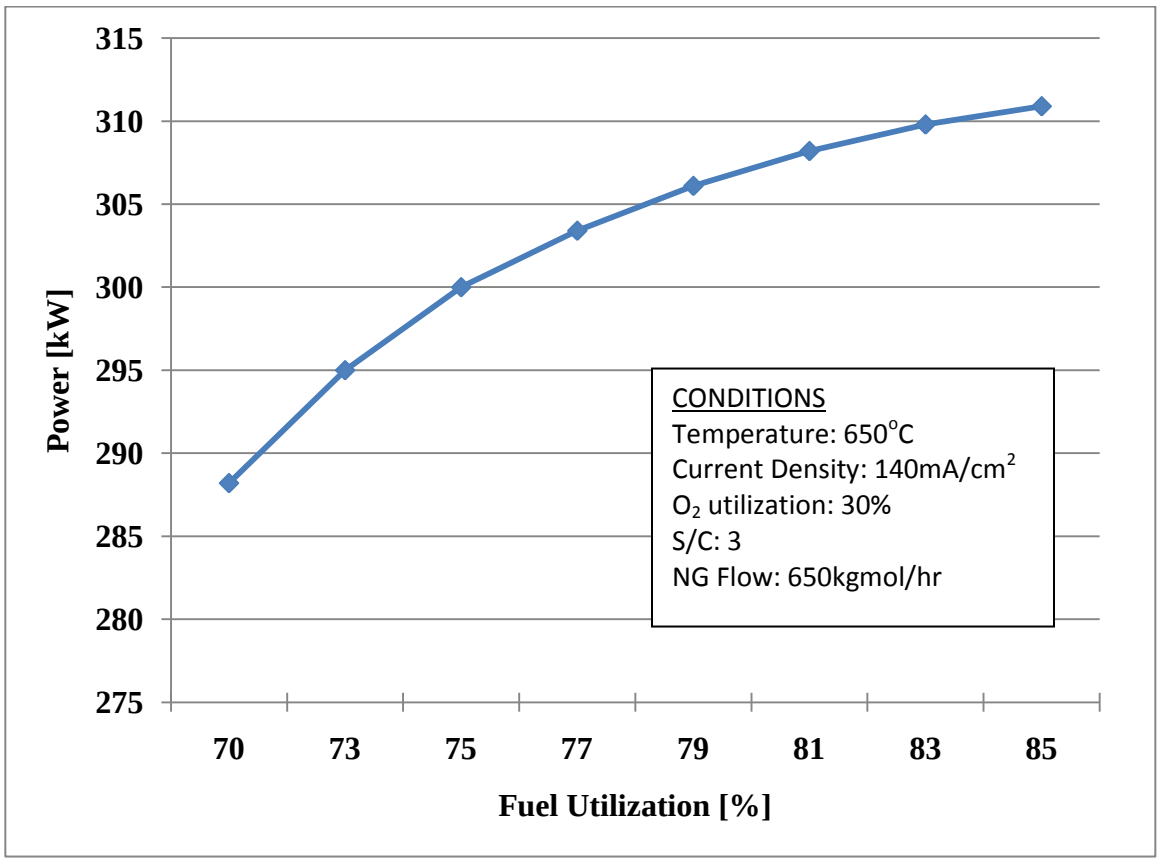

Figure 5.8 Effect of Fuel Utilization on the Output Power of Fuel Cell

As more methane is converted to hydrogen the electrical power output of the fuel cell system increases. The fuel utilization of the MCFC was fixed at 75%. This value corresponds to 300kW which is the electrical output of the DFC300. Fuel utilization also has an effect on the fuel efficiency. As a greater fraction of the fuel is utilized the stack fuel efficiency increases thus improving the performance of the system.

The effect of current density on stack efficiency and power density of the fuel cell is shown in Fig 5.9. As mentioned earlier, a MCFC model was developed and implemented in a process simulation developed in UniSim to predict the performance of the DFC300. At stack output power of 300kW the

predicted electrical efficiency is 47%.

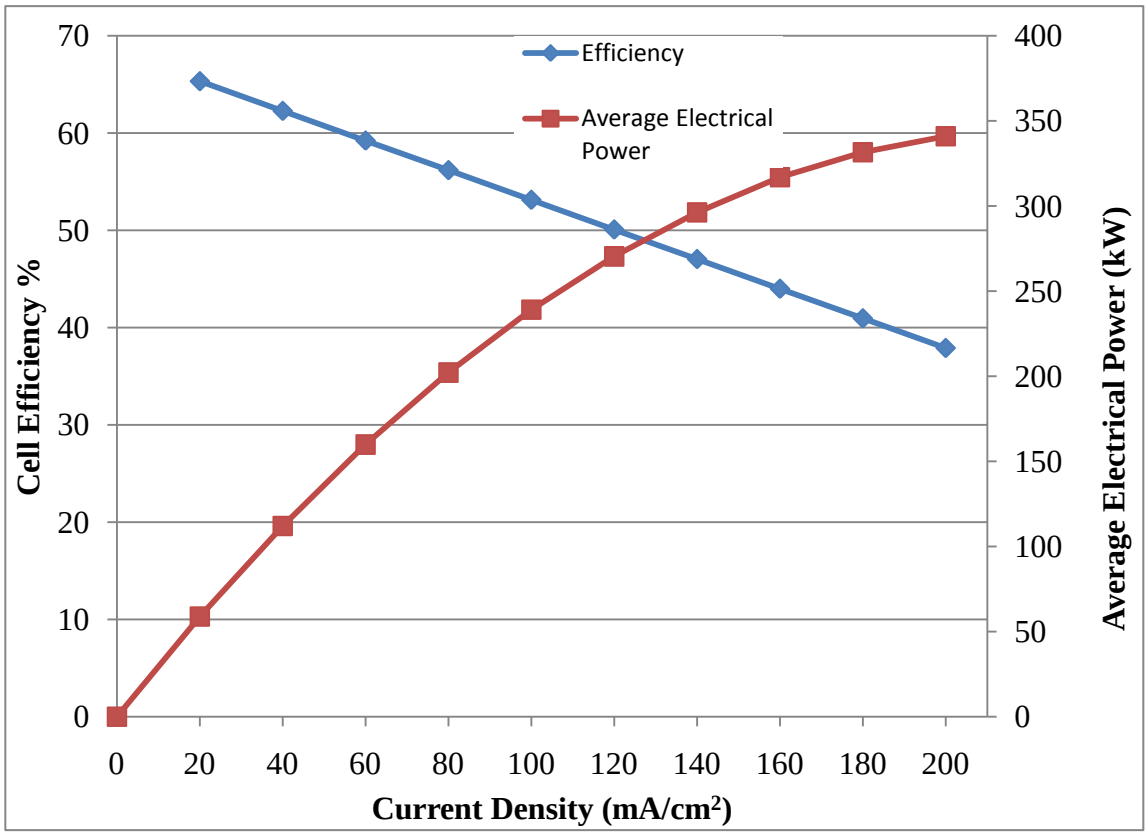

Figure 5.9 Dependence of Cell Efficiency and Electrical Power on Current Density

As the current density increases the cell efficiency decreases while the power density increases. At 47% efficiency, the current density was about 140mA/cm^2 and the power density was approximately 270kW. The current density used for the simulation was thus fixed at 140mA/cm^2.

Figure 5.10 shows the effect of current density on the thermal and electrical power output of the DFC 300. From 60 mA/cm^2 to 140 mA/cm^2, the predicted electrical power output of the DFC was greater then the thermal output. At 140 mA/ cm^2, the electrical power and thermal power were almost equal; 300 kW and 295 kW respectively. From 140 mA/cm^2 to 240 mA/cm^2, more thermal power is generated than electrical power.

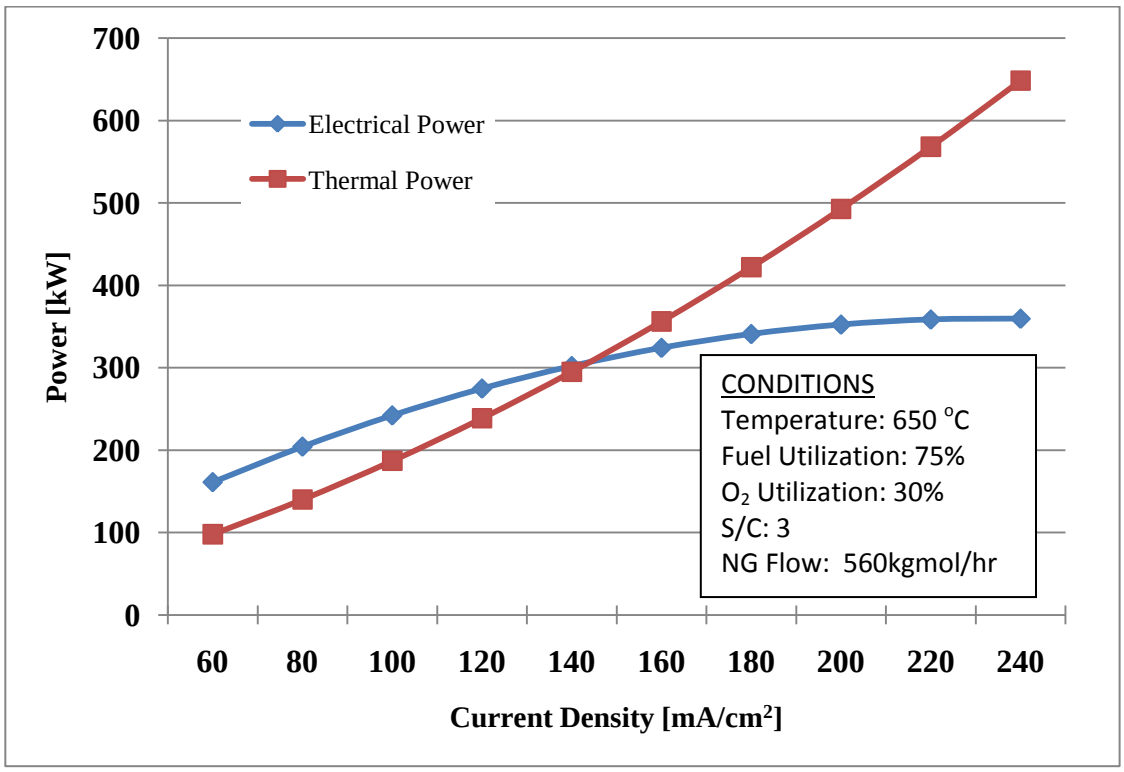

Figure 5.10 Dependence of DFC Output on Current Density

The reason for this trend is because as the current increases, I^2R losses increase generating heat.

5.3 CO_2 Emissions Analysis

In the systems CO_2 emissions analysis completed, the emissions of the regulating valve and the DFC-ERG systems were calculated based on the preheat requirements of the systems. The emission factor from combustion of natural gas (explained in section 3.4) was used for the conventional burner system CO_2 emissions while the emissions of the DFC-ERG system were calculated as the amount of CO_2 in the outlet stream plus the amount of CO_2 from the combustion of natural gas during the months when additional heat from the burner were required to supplement the heat produced by the DFC 300.

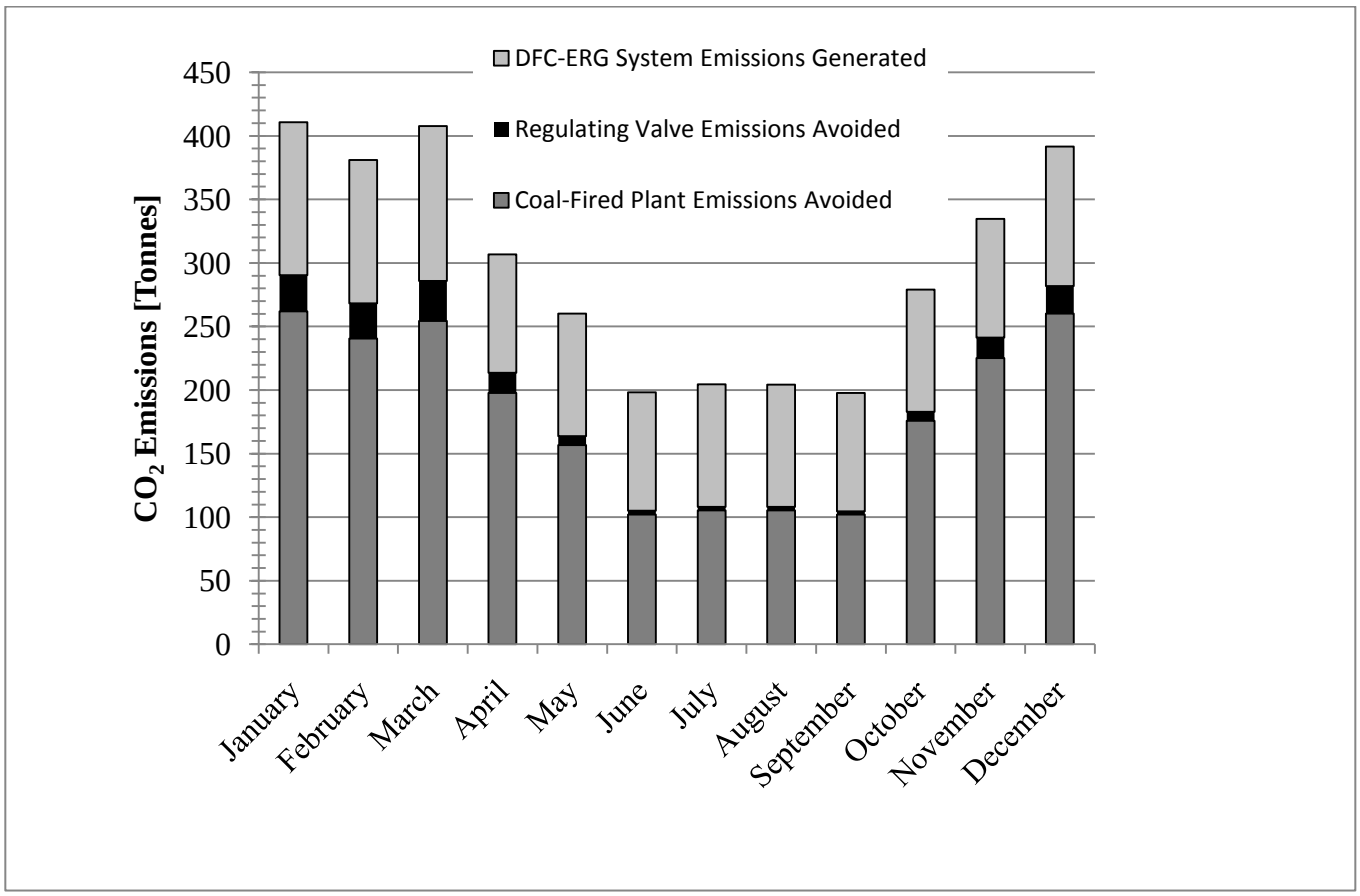

Figure 5.11: Reduction in CO_2 Emissions Assuming DFC-ERG Power Output Displaces Coal Power Generation and Regulating Valve Burner System.

Figure 5.11 shows monthly CO_2 mitigated by the DFC-ERG system if it's electrical power output displaces the electrical power generated by a coal-fired power plant and if it also replaces the regulating valve system at Glenburnie letdown station. The CO_2 emitted by the DFC-ERG system was highest during the winter months when the boiler was required to provide additional heat to supplement the heat provided by the MCFC unit.

The data for this figure assumed that the coal power plant generates the same power output as the electrical output of the Utilities Kingston's simulated DFC-ERG system. The simulated DFC-ERG system generated annual electrical output of 3773MWh and 1,220tonnes/yr of CO_2 using the 2008 city gate data. The regulating valve system emitted a total of 166 tonnes of CO_2/yr. A coal-fired plant with equivalent annual electrical output as the DFC-ERG emits 3,410 tonnes/yr of CO_2. Thus, the DFC-

ERC is capable of mitigating about 2190tonnes of CO_2 per annum if it displaces a coal-fired power plant with electrical power output.

Figure 5.12 shows typical coal-fired electrical power generation supplied to the Ontario electrical grid during the winter, spring, summer and fall of 2006 on a per hour of the day basis. Data for this figure was provided by the Independent Electricity System Operator (IESO). Data from 2006 was deliberately chosen because it was considered to be a year of normal economic activity in Ontario (i.e., not during recession).

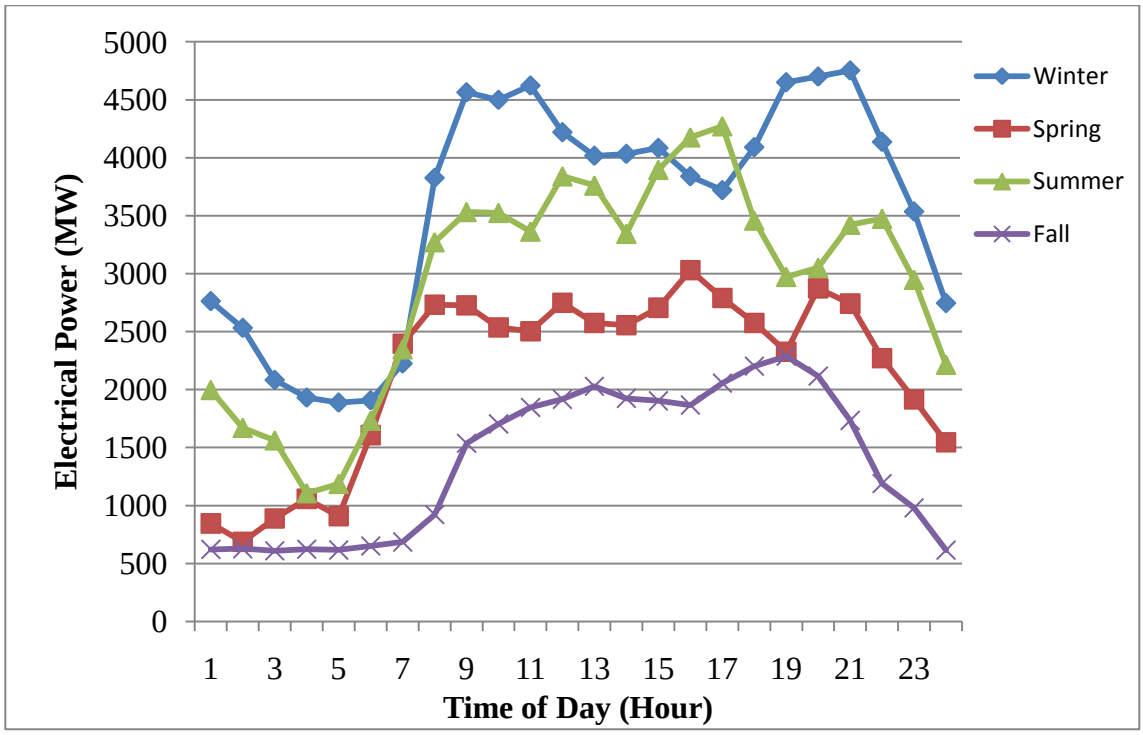

Figure 5.12 Seasonal Variation of Ontario Coal-Fired Plant Electrical Output in 2006

Figure 5.13 is Utilities Kingston's Glenburnie city gate hourly flowrates during winter, spring, summer, and fall of 2006. The winter and fall flowrate data used in this figure correspond to the same days as those used in Fig 5.12.

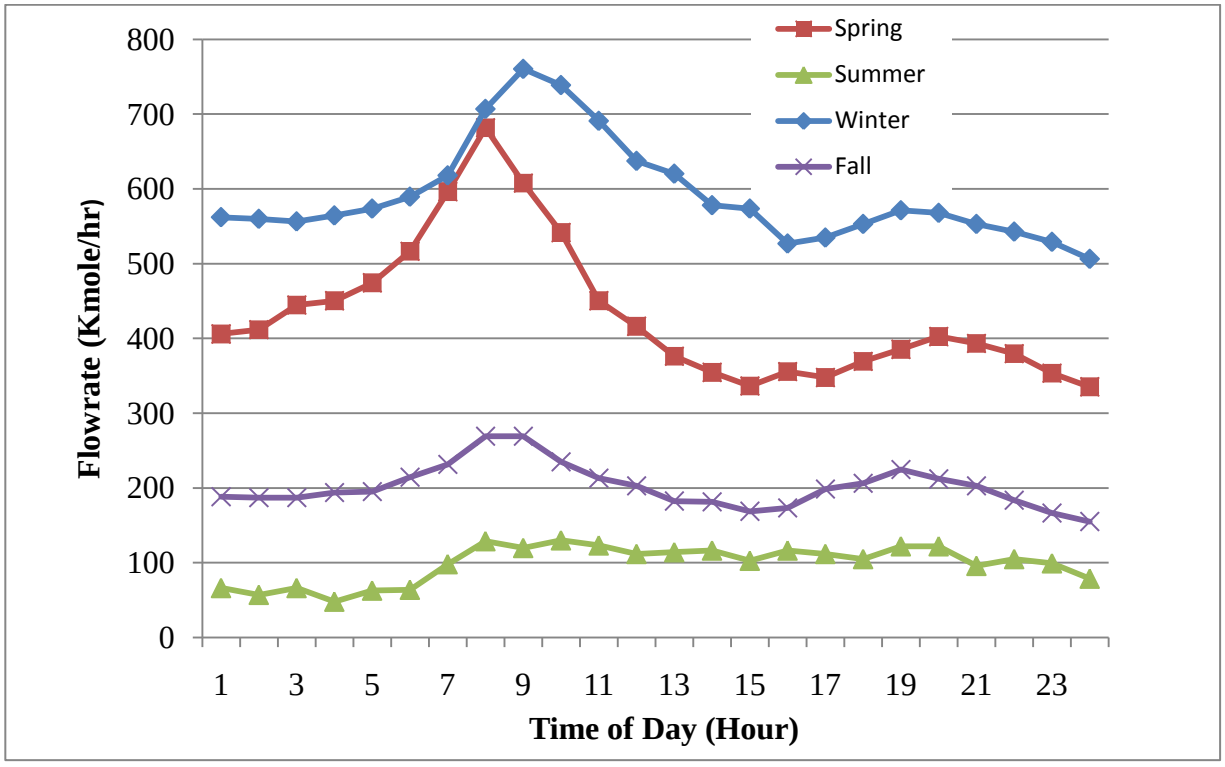

Figure 5.13 Kingston's Glenburnie City Gates Hourly and Seasonal Flowrate Variation

Due to the unavailability of the Glenburnie flowrate data of spring and summer for the exact days in 2006, the Glenburnie's 2005 flowrate data for exact days were used for spring and summer.

The trend in Fig 5.12 shows peaking of electrical output between 7:00am -11:00am and between 6pm-11pm. The morning peak region coincides with the time most people wake up, use electrical power and natural gas for appliances. The evening peak region coincides with the time people get home from their work day. For this data the electricity consumption is greater during the winter season and lowest during the fall season. Periodic extremely high consumption during high temperature periods in the summer when air conditioning is being used extensively were considered to be exceptions and were not considered in this analysis although this trend may change as global warming evolves.

The flowrate of the natural gas entering Glenburnie city gate during winter season is highest. If the DFC-ERG system was installed on all city gates in Ontario and all the city gates had trends similar to those shown in Fig 5.13, there is clearly an opportunity to reduce the need to use coal fired plants. During the summer season, however, when the electrical output of the coal fired plants is relatively high as shown in Fig 5.12, and the natural gas flowrates are low (as shown in Fig 5.13), the electrical output from the DFC-ERG would be less effective at displacing coal fired generation although the fuel cell system would still be able to provide a significant amount of distributed generation capacity.

Figure 5.14 shows the power output of the DFC-ERG system for the seasonal natural gas flowrates shown in Figure 5.13. The simulated DFC-ERG system has a maximum electrical power output of 840kW, this includes the 300kW electrical power output of the MCFC unit and the electrical power output of the turboexpander which depends on the flowrate and pressure of the natural gas inlet stream and cannot exceed the design limit specifications of Cryostar TG120: 600kW, 90% maximum efficiency.

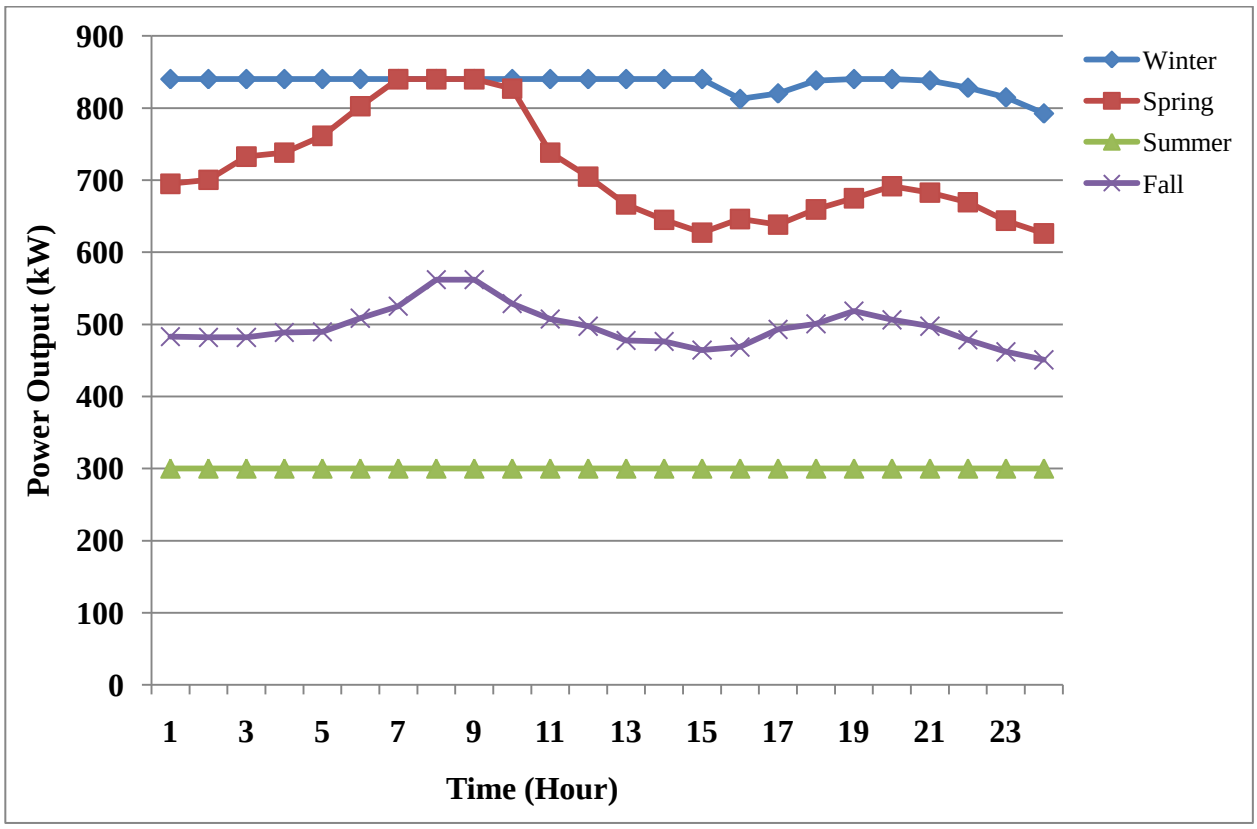

Figure 5.114 Seasonal Power Output of DFC-ERG System

During the summer season, the turboexpander efficiency is very low due to the low natural gas flowrate coming from the high pressure line. This makes it uneconomic to run the expander during the summer. Thus, the MCFC unit alone was kept in operation generating 300 kW of distributed electrical power to the grid. Excess heat generated by the fuel cell during this period would not be needed to heat the decompressed gas but could be used for providing hot water to the residential area at Glenburnie. With the flow parameters of the Glenburnie city gate, the DFC-ERG system generated peak electrical output during the winter season when the flowrate of the natural gas in the pressured line was highest. The system generated average daily electrical output of 20 MWh on a winter day, 17.1MWh on a spring day, 7.2 MWh on a summer day and 11.9 MWh on a fall day. If a coal powered plant was used to generate these quantities of electrical power, it would emit about 18 tonnes of CO_2 per day during the winter, 16 tonnes of CO_2 per day in the spring, 7 tonnes of CO_2 per day during the summer and 12 tonnes of CO_2 per day in the fall.

Figure 5.15 shows the seasonal CO_2 emissions of the DFC-ERG system based on electrical output shown in Figure 5.14.

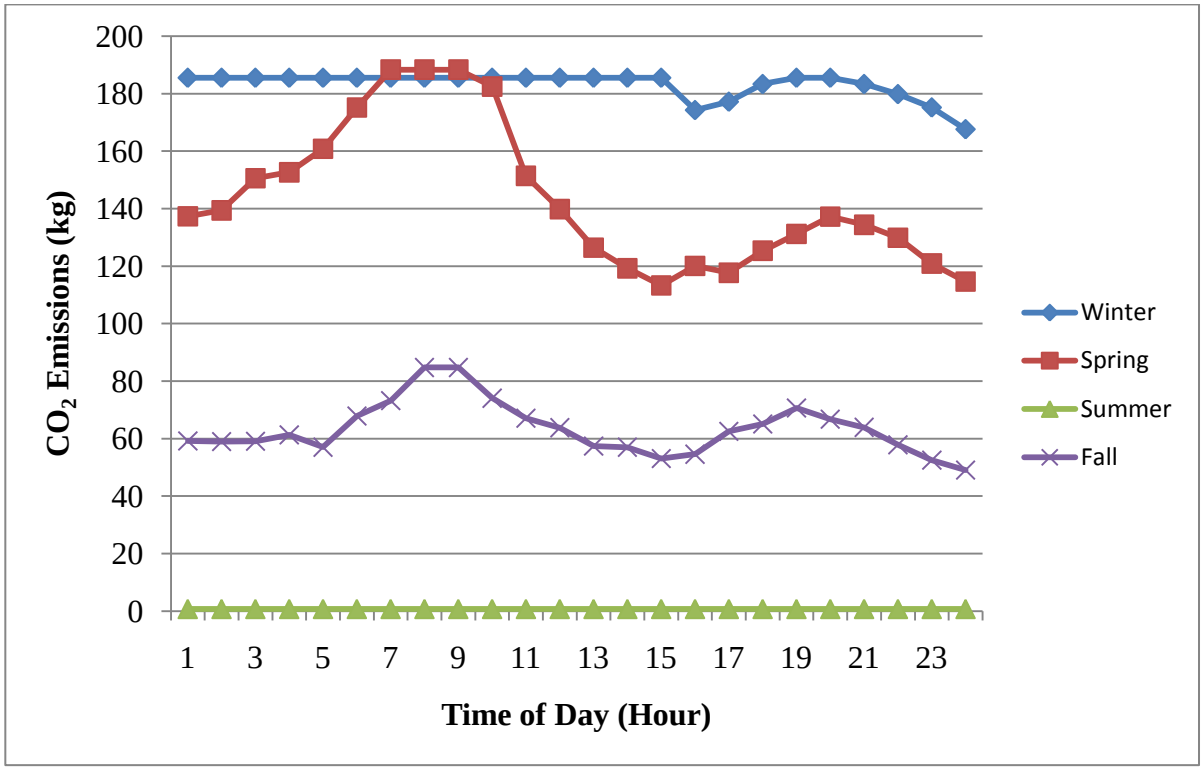

Figure 5.15 Seasonal CO_2 Emissions Analysis of DFC-ERG System

The winter season emissions were highest since more natural gas was burned to generate heat for preheating the turboexpander inlet steam. The emissions during the summer were lowest because the expander was shutdown due to low system efficiency and low output. The MCFC unit provided heat to the regulating valve during the summer season. The DFC-ERG system emitted a total of 4.4tonnes of CO_2 per day in winter, 3.5tonnes of CO_2 per day in spring, 0.018 tonnes of CO_2 per day in summer and 1.5tonnes of CO_2 per day in fall. Compared to the emissions of a coal-fired plant, the DFC-ERC can mitigate about 14 tonnes of CO_2 per day in winter, 12.5tonnes of CO_2 per day in spring, 7 tonnes of CO_2 per day in summer and 8.5 tonnes of CO_2 per day in fall.

5.4 Financial Analysis

The financial analysis assumed a cap and trade economy is in operation in Ontario and the CO_2 mitigated by the DFC-ERG system is sold under the clean development mechanism (CDM) program at a value of $15 per tonne of CO_2. The analysis also fix the price of electricity at $0.11 based on the current price offered for the purchase of electrical power generated by wind turbine through the Ontario Feed-In-Tariff program. The price of the thermal energy was assumed $0.05 per kWh equivalent to the price of natural gas in Ontario.

Figure 5.16 is the graph of the revenue that generated from the simulated DFC-ERG system for Glenburnie letdown station.

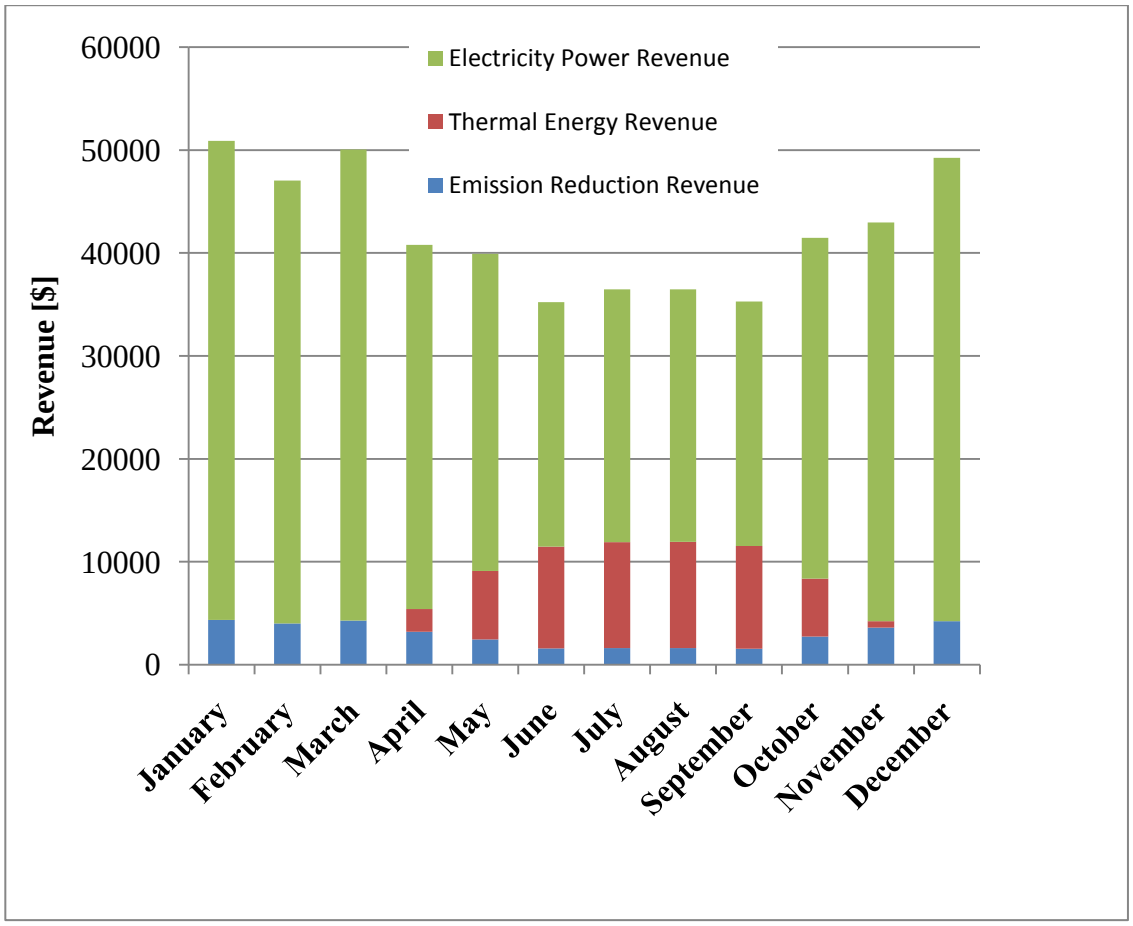

Figure 5.16 Annual Revenue Generated by the Simulated Glenburnie DFC-ERG System

The DFC-ERG system generates higher revenue during the winter months due to the high electrical power generated by the system during this season. Substantial revenue is also generated from sales of thermal energy during the summer season.

The simulated Glenburnie DFC-ERG system generates about $500,000.00 per annum from the sales of CO_2 ($35,000.00/yr), electrical energy ($410,000.00/yr) and thermal energy ($56,000.00/yr).

Chapter 6

Conclusions and Recommendations

6.1 Conclusions

An energy recovery and power generation system for natural gas pressure letdown stations application was successfully simulated. A case study using the Utilities Kingston city gate at Glenburnie was done. The DIR-MCFC unit in the simulation was modeled with the design specifications of the FuelCell Energy Inc's DFC300 system while the simulated turboexpander had design characteristics of Cryostar TG120. The power output of the turboexpander strongly depends on the natural gas inlet flowrate, temperature and pressure. High natural gas flowrate was observed during winter season; when the ambient temperature is low, and low natural gas flowrate was observed during the summer season; when ambient temperature is high. The highest average natural gas flowrate at the Glenburnie city gate in 2008 was 589kgmol/hr, in February, when the ambient temperature was 3.6^{o}C while the lowest average flowrate was 82kgmol/hr, in July, at 14.9^{o}C ambient temperature. At 70% isentropic efficiency, the average simulated power output of the turboexpander in February, when natural gas flowrate was highest, was 573 kW while in July when the natural gas flowrate was lowest, the average power output was 79 kW.

The efficiency of the simulated turboexpander varies linearly with the natural gas flowrate. When the natural gas flowrate was low, the efficiency of the expander was low. The maximum predicted efficiency of the expander (81%) was achieved in March while minimum efficiency observed (12.4%) was achieved in June. It is not economical to run the turboexpander unit during the summer season (i.e., June, July, August and September) because the efficiency and the generating capacity are too low to justify the maintenance and other operating costs.

The high pressure natural gas stream pre-heat requirement is dependent on the natural gas flowrate, temperature and the pressure of the natural gas exiting the turboexpander. The amount of heat required for preheating was greater in the winter season than in the summer season. Since the turboexpander was shutdown during the summer, the regulating valve system was used while the DIR-MCFC unit continued to generate both the required heat and electrical power. Preheating requirements for the turboexpander were estimated to be 6340GJ annually while the DFC-MCFC was estimated to generate a total annual average heat of 9150 GJ .The excess heat of 2810 GJ from the fuel cell could be used in the residential area of Glenburnie for hot water heating. The amount of heat generated by the fuel cell was adequate for preheating in spring, summer and fall; April, May, June, July, August, September, October and November. The heat generated by the fuel cell was however not adequate to preheat the turboexpander in the winter months; January, February March and December. The boiler system was used to provide additional heat during these months.

The DIR-MCFC stack was modelled to represent the operating characteristics of a DFC300 stack. This was achieved using the following parameters: current density at 140mA/cm^2, steam to methane ratio of 3, fuel utilization of 75% and oxygen utilization of 30%. The unit was optimized to produce the desired electrical power and thermal heating duty of 300 kW and 290 kW respectively. The performance curve of the MCFC is consistent with those of high temperature fuel cells.

A CO_2 emissions analysis and mitigation verification of the simulated DFC-ERG system was conducted. The emissions generated by DFC-ERG system (which also produced electricity from the recovered energy of depressurisation) was greater than the emissions generated by the regulating valve system by a factor of 7 using Glenburnie city gate's 2008 data. The simulated DFC-ERG system generated annual electrical energy of 3774MWh and 1220 tonnes of CO_2 per annum. It was verified

that this system would mitigate CO_2 emissions of 2190 tonnes if the power generated from the system replaced the same quantity of electrical power from a coal-fired plant.

Daily emission analysis of the DFC-ERG system was also completed. Compared with emissions of a coal-fired plant, the simulated DFC-ERG system mitigated 13.6 tonnes of CO_2 per day in winter, 12.5 tonnes of CO_2 per day in spring, 7 tonnes of CO_2 per day in summer and 8.5 tonnes of CO_2 per day in fall.

In a cap-and-trade economy, the CO_2 offset at about $15 per tonne would generate additional income of approximately $35,000.00 per annum as well as the $410,000.00 per annum from sales of electrical power and $56,000.00 per annum from sales of thermal energy. The simulated Glenburnie DFC-ERG system generated a total of $500,000.00 per annum.

6.2 Recommendations for Future Work

The simulation and analysis carried out in this thesis assumed a steady state system. A transient performance of the DFC-ERG should be undertaken to investigate the impact of start-up, shutdown and perturbation of the system. For example, preheating of the fuel cell stacks before restarts requires a considerable amount of natural gas combustion.

An improvement of the DIR-MCFC model based on actual operating specifications from FuelCell Energy Inc. would significantly improve the accuracy of the analysis. This would replace the model developed in the spreadsheet unit operation used UniSim. The spreadsheet uses visual basic programming language which cannot handle complex mathematical models such as intrinsic rate equation.

Validation of the simulation results should be done once operating data from Enbridge is available. This was the original intention for this study, however, delays in the supply of data from Enbridge required that the estimations based on information from open literature be used.

References

(1) Maddaloni JD, Rowe AM. Natural gas exergy recovery powering distributed hydrogen production. Int. J. Hydrogen Energy 2007 4;32(5):557-566.

(2) Jaroslav P. Use of Expansion Turbines in Natural Gas Pressure Reduction Station. 2004;9(3):258-260.

(3) Maddolani J, Rowe A, Bailey R, McDonald D. Impacts of Seasonality on Hydrogen Production Using Natural Gas Pressure Letdown Stations. 2005.

(4) David Teichroeb, Business Development Manager-Fuel Cell Market, Enbridge Gas. FCE, Enbridge in 'ultra-clean' hybrid power plant deal. Personal Communication

(5) Natural Resources Canada (NRCAN). Commercial And Institutional Consumption of Energy Survey (Summary Report). 2007;M141-17/2005E-PDF:1-47.

(6) The Independent Electricity Systems Organization. Ontario Existing Installed Generation [http://www.ieso.ca/imoweb/media/md_supply.asp].

(7) US Energy Information Administration. U.S. Natural Gas Imports by Country. [http://www.eia.gov/dnav/ng/ng_move_impc_s1_m.htm]

(8) Daneshi H, Khorashadi Zadeh H, Lotfjou Choobari A. Turboexpander as a distributed generator. Power and Energy Society General Meeting - Conversion and Delivery of Electrical Energy in the 21st Century, 2008 IEEE 2008:1-7.

(9) Ontario Energy Board. 2007 Yearbook of Natural Gas Distributors. 2008:1-2-6. [http://www.oeb.gov.on.ca/OEB/_Documents/Documents/2007_naturalgas_distributors.pdf]

(10) OEB. Natural Gas Pipeline System in Ontario. [http://www.oeb.gov.on.ca/documents/map_gas_pipelines.pdf]

(11) EG&G Services P. Inc. Fuel Cell Handbook. West Virginia: US Department of Energy, Office of Fossil Energy; 2000. [http://www.fuelcells.org/info/library/fchandbook.pdf]

(12) Lukas MD, Lee KY. Model-Based Analysis for the Control of Molten Carbonate Fuel Cell Systems. 2005;5(1):115-116-125.

(13) Williams MC, Strakey, JP, Singhal, SC. U.S Distributed generation fuel cell program. J. Power Sources 2004;131:79-85.

(14) Ghezel-Ayagh H, Sanderson R. High-Efficient Fuel Cell System, U.S. Patent 2002; No 6365290

(15) Ghezel-Ayagh H, Walzak J, Patel D, Daly J, Maru H, Sanderson R, *et al.* State of direct fuel cell/turbine systems development. J. Power Sources 2005;152:219-225.

(16) City of Toronto Council. A bi-Law to permit the production and distribution of energy from specific renewable devices and cogeneration devices. 2008 [http://www.toronto.ca/legdocs/mmis/2008/pg/bgrd/backgroundfile-10467.pdf]

(17) Teichroeb D. One Example of Industry's Fuel Cell Commercialization Efforts [http://www.fuelcellenergy.com/files/FCE%20DFC-ERG%20090507.pdf]

(18) Environment Canada. 1990-2006 Canada's Green House Gas Emissions- Understanding the trends. 2008:1-2-44. [http://www.ec.gc.ca/Publications/default.asp?lang=En&xml=75805F15-908C-4FB1-A285-6D437FF04C93]

(19) Hedman BA. Waste Energy Recovery Opportunity for Interstate Natural Gas Pipeline. 2008. [http://www.chpcenternw.org/NwChpDocs/NGas%20Compressor%20Stations%20Heat%20Recovery%20Analysis%20Hedman%20ICF%20for%20INGAA%2002%202008.pdf]

(20) Freni S, Maggio G. Energy Balance of Different Internal Reforming MCFC Configurations. Int. J. Energy Res. 2007 ;21(3):253-264.

(21) Baranak M, Atakül H. A basic model for analysis of molten carbonate fuel cell behavior. J. Power Sources 2007 10/25;172(2):831-839.

(22) Heidebrecht P, Sundmacher K. Molten carbonate fuel cell (MCFC) with internal reforming: model-based analysis of cell dynamics. Chem. Eng. Sci. 2003 0;58(3-6):1029-1036.

(23) Roberts RA, Brouwer J, Liese E, Gemmen RS. Dynamic Simulation of Carbonate Fuel Cell-Gas Turbine Hybrid Systems. 2006;128(2):294-301.

(24) Roberts RA, Jabbari F, Brouwer J, Gemmen R, Liese E. Dynamic Simulation of Carbonate Fuel Cell-Gas Turbine Hybrid Systems. J. Eng. Gas Turbines Power 2006; 128 (2):294-301

(25) Matelli JA, Bazzo E. A methodology for thermodynamic simulation of high temperature, internal reforming fuel cell systems. J. Power Sources 2005; 142(1-2):160-168.

(26) De Simon G, Parodi F, Fermeglia M, Taccani R. Simulation of process for electrical energy production based on molten carbonate fuel cells. J. Power Sources 2003 4/10; 115(2):210-218.

(27) Bosio B, Costamagna P, Parodi F. Modeling and experimentation of molten carbonate fuel cell reactors in a scale-up process. Chem. Eng. Sci. 1999 7;54(13-14):2907-2916.

(28) Marra D, Bosio B. Process analysis of 1 MW MCFC plant. Int. J. Hydrogen Energy 2007 5;32(7):809-818.

(29) Kang BS, Koh J, Lim HC. Effects of system configuration and operating condition on MCFC system efficiency. J. Power Sources 2002; 108(1-2):232-238.

(30) Sugiura K, Naruse I. Feasibility study of the co-generation system with direct internal reforming-molten carbonate fuel cell (DIR-MCFC) for residential use. J. Power Sources 2002 4/1; 106(1-2):51-59.

(31) Lunghi P, Bove R, Desideri U. Analysis and optimization of hybrid MCFC gas turbines plants. J. Power Sources 2003;118(1-2):108-117.

(32) Lunghi P, Bove R. Reliable Fuel Cell Simulation Using an Experimentally Driven Numerical Model. Fuel Cells 2002; 2(2):83-91.

(33) Amorelli A, Wilkinson MB, Bedont P, Capobianco P, Marcenaro B, Parodi F, *et al.* An experimental investigation into the use of molten carbonate fuel cells to capture CO_2 from gas turbine exhaust gases. Energy 2004; 29(9-10):1279-1284.

(34) Sims R, Rogner H, Gregory K. Carbon emission and mitigation cost comparisons between fossil fuel, nuclear and renewable energy resources for electricity generation. J. Energy Policy 2003 10; 31(13):1315-1326.

(35) Williams M, Wimer J, Sudhoff F, Archer D. Mathematical modelling of MCFC Cells/Stacks and networks.[http://www.anl.gov/PCS/acsfuel/preprint%20archive/Files/38_4_CHICAGO_08-93_1435.pdf]

(36) Weber A, Sauer B, Müller AC, Herbstritt D, Ivers-Tiffée E. Oxidation of H_2, CO and methane in SOFCs with Ni/YSZ-cermet anodes. Solid State Ionics 2002 12;152-153:543-550.

(37) Bove R, Lunghi P, M. Sammes N. SOFC mathematic model for systems simulations—Part 2: definition of an analytical model. Int. J. Hydrogen Energy 2005 2;30(2):189-200.

(38) Miyake Y, Nakanishi N, Nakajima T, Itoh Y, Saitoh T, Saiai A, *et al.* A study of heat and material balances in an internal-reforming molten carbonate fuel cell. J. Power Sources 1995 7;56(1):11-17.

(39) Morita H, Komoda M, Mugikura Y, Izaki Y, Watanabe T, Masuda Y, *et al*. Performance analysis of molten carbonate fuel cell using a Li/Na electrolyte. J.Power Sources 2002; 112(2):509-518.

(40) Jung-ho W, Kwan-Young L. Carbon deposition and alkali poisoning at each point of the reforming catalysts in DIR-MCFC. J. of Applied Electrochemistry 2004; 35(6):521-528.

(41) Utilities Kingston. Preliminary preferred route for Natural Gas. 2005 [http://www.utilitieskingston.com/Gas/ApplicationSteps.aspx]

(42) Phippen C. Utilities Kingston city gate data 2008. Personal Communication.

(43) G.C. Chinchen, P.J. Denny, J.R. Jennings, M.S. Spencer, K.C. Waugh, Synthesis of methanol. I: Catalysts and kinetics. Appl. Catal. (1988) 1–65

Appendix A

DFC-ERG System Simulation Results

Material Stream: High Pressure Gas

Fluid Package: Basis-1

Property Package: SRK

CONDITIONS

	Overall	Vapour Phase			
Vapour / Phase Fraction	1.0000	1.0000			
Temperature: (C)	14.01	14.01			
Pressure: (kPa)	6251	6251			
Molar Flow (kgmol/h)	155.1	155.1			
Mass Flow (kg/h)	2571	2571			
Std Ideal Liq Vol Flow (m3/h)	8.258	8.258			
Molar Enthalpy (kJ/kgmol)	-7.453e+004	-7.453e+004			
Molar Entropy (kJ/kgmol-C)	145.5	145.5			
Heat Flow (kJ/h)	-1.156e+007	-1.156e+007			
Liq Vol Flow @Std Cond (m3/h)					

PROPERTIES

	Overall	Vapour Phase			
Molecular Weight	16.58	16.58			
Molar Density (kgmol/m3)	2.941	2.941			
Mass Density (kg/m3)	48.77	48.77			
Act. Volume Flow (m3/h)	52.73	52.73			
Mass Enthalpy (kJ/kg)	-4495	-4495			
Mass Entropy (kJ/kg-C)	8.775	8.775			
Heat Capacity (kJ/kgmol-C)	44.02	44.02			
Mass Heat Capacity (kJ/kg-C)	2.655	2.655			
Lower Heating Value (kJ/kgmol)	7.833e+005	7.833e+005			
Mass Lower Heating Value (kJ/kg)	4.723e+004	4.723e+004			
Phase Fraction [Vol. Basis]		1.000			
Phase Fraction [Mass Basis]	4.941e-324	1.000			
Partial Pressure of CO2 (kPa)	6.251				
Cost Based on Flow (Cost/s)	0.0000	0.0000			
Act. Gas Flow (ACT_m3/h)	52.73	52.73			
Avg. Liq. Density (kgmol/m3)	18.78	18.78			
Specific Heat (kJ/kgmol-C)	44.02	44.02			
Std. Gas Flow (STD_m3/h)	3667	3667			
Std. Ideal Liq. Mass Density (kg/m3)	311.4	311.4			
Act. Liq. Flow (m3/s)					
Z Factor	0.8902	0.8902			
Watson K	18.77	18.77			
User Property					
Partial Pressure of H2S (kPa)	0.0000				
Cp/(Cp - R)	1.233	1.233			
Cp/Cv	1.558	1.558			
Heat of Vap. (kJ/kgmol)					
Kinematic Viscosity (cSt)	0.2571	0.2571			
Liq. Mass Density (Std. Cond) (kg/m3)					
Liq. Vol. Flow (Std. Cond) (m3/h)					
Liquid Fraction	0.0000	0.0000			
Molar Volume (m3/kgmol)	0.3400	0.3400			
Mass Heat of Vap. (kJ/kg)					
Phase Fraction [Molar Basis]	1.0000	1.0000			
Surface Tension (dyne/cm)					
Thermal Conductivity (W/m-K)	3.774e-002	3.774e-002			
Viscosity (cP)	1.254e-002	1.254e-002			

Material Stream: High Pressure Gas (continue

Fluid Package: Basis-1

Property Package: SRK

PROPERTIES

	Overall	Vapour Phase			
Reid VP at 37.8 C (kPa)					
True VP at 37.8 C (kPa)					
Liq. Vol. Flow - Sum(Std. Cond) (m3/h)	0.0000	0.0000			

COMPOSITION

Overall Phase — Vapour Fraction 1.0000

COMPONENTS	MOLAR FLOW (kgmol/h)	MOLE FRACTION	MASS FLOW (kg/h)	MASS FRACTION	LIQUID VOLUME FLOW (m3/h)	LIQUID VOLUME FRACTION
Methane	148.8666	0.9600	2388.2524	0.9288	7.9770	0.9660
Ethane	0.9304	0.0060	27.9775	0.0109	0.0787	0.0095
Propane	0.3101	0.0020	13.6762	0.0053	0.0270	0.0033
CO	0.0000	0.0000	0.0000	0.0000	0.0000	0.0000
CO2	0.1551	0.0010	6.8246	0.0027	0.0083	0.0010
Air	0.0000	0.0000	0.0000	0.0000	0.0000	0.0000
Nitrogen	4.8072	0.0310	134.6627	0.0524	0.1670	0.0202
Oxygen	0.0000	0.0000	0.0000	0.0000	0.0000	0.0000
H2O	0.0000	0.0000	0.0000	0.0000	0.0000	0.0000
Hydrogen	0.0000	0.0000	0.0000	0.0000	0.0000	0.0000
Total	155.0694	1.0000	2571.3934	1.0000	8.2579	1.0000

Vapour Phase — Phase Fraction 1.000

COMPONENTS	MOLAR FLOW (kgmol/h)	MOLE FRACTION	MASS FLOW (kg/h)	MASS FRACTION	LIQUID VOLUME FLOW (m3/h)	LIQUID VOLUME FRACTION
Methane	148.8666	0.9600	2388.2524	0.9288	7.9770	0.9660
Ethane	0.9304	0.0060	27.9775	0.0109	0.0787	0.0095
Propane	0.3101	0.0020	13.6762	0.0053	0.0270	0.0033
CO	0.0000	0.0000	0.0000	0.0000	0.0000	0.0000
CO2	0.1551	0.0010	6.8246	0.0027	0.0083	0.0010
Air	0.0000	0.0000	0.0000	0.0000	0.0000	0.0000
Nitrogen	4.8072	0.0310	134.6627	0.0524	0.1670	0.0202
Oxygen	0.0000	0.0000	0.0000	0.0000	0.0000	0.0000
H2O	0.0000	0.0000	0.0000	0.0000	0.0000	0.0000
Hydrogen	0.0000	0.0000	0.0000	0.0000	0.0000	0.0000
Total	155.0694	1.0000	2571.3934	1.0000	8.2579	1.0000

K VALUE

COMPONENTS	MIXED	LIGHT	HEAVY
Methane			
Ethane			
Propane			
CO			
CO2			
Air			
Nitrogen			
Oxygen			
H2O			
Hydrogen			

UNIT OPERATIONS

FEED TO	PRODUCT FROM	LOGICAL CONNECTION
Heater: Exchanger1		SpreadSheetCell: elecctrochemical Model@E25
		SpreadSheetCell: electrochemical Model@E29

UTILITIES

(No utilities reference this stream)

Material Stream: Low Pressure Pipeline

Fluid Package: Basis-1

Property Package: SRK

CONDITIONS

	Overall	Vapour Phase			
Vapour / Phase Fraction	1.0000	1.0000			
Temperature: (C)	3.000	3.000			
Pressure: (kPa)	450.0	450.0			
Molar Flow (kgmol/h)	155.1	155.1			
Mass Flow (kg/h)	2571	2571			
Std Ideal Liq Vol Flow (m3/h)	8.258	8.258			
Molar Enthalpy (kJ/kgmol)	-7.388e+004	-7.388e+004			
Molar Entropy (kJ/kgmol-C)	168.7	168.7			
Heat Flow (kJ/h)	-1.146e+007	-1.146e+007			
Liq Vol Flow @Std Cond (m3/h)					

PROPERTIES

	Overall	Vapour Phase			
Molecular Weight	16.58	16.58			
Molar Density (kgmol/m3)	0.1980	0.1980			
Mass Density (kg/m3)	3.283	3.283			
Act. Volume Flow (m3/h)	783.2	783.2			
Mass Enthalpy (kJ/kg)	-4455	-4455			
Mass Entropy (kJ/kg-C)	10.18	10.18			
Heat Capacity (kJ/kgmol-C)	35.69	35.69			
Mass Heat Capacity (kJ/kg-C)	2.152	2.152			
Lower Heating Value (kJ/kgmol)	7.833e+005	7.833e+005			
Mass Lower Heating Value (kJ/kg)	4.723e+004	4.723e+004			
Phase Fraction [Vol. Basis]		1.000			
Phase Fraction [Mass Basis]	4.941e-324	1.000			
Partial Pressure of CO2 (kPa)	0.4500				
Cost Based on Flow (Cost/s)	0.0000	0.0000			
Act. Gas Flow (ACT_m3/h)	783.2	783.2			
Avg. Liq. Density (kgmol/m3)	18.78	18.78			
Specific Heat (kJ/kgmol-C)	35.69	35.69			
Std. Gas Flow (STD_m3/h)	3667	3667			
Std. Ideal Liq. Mass Density (kg/m3)	311.4	311.4			
Act. Liq. Flow (m3/s)					
Z Factor	0.9900	0.9900			
Watson K	18.77	18.77			
User Property					
Partial Pressure of H2S (kPa)	0.0000				
Cp/(Cp - R)	1.304	1.304			
Cp/Cv	1.326	1.326			
Heat of Vap. (kJ/kgmol)	8909				
Kinematic Viscosity (cSt)	3.266	3.266			
Liq. Mass Density (Std. Cond) (kg/m3)					
Liq. Vol. Flow (Std. Cond) (m3/h)					
Liquid Fraction	0.0000	0.0000			
Molar Volume (m3/kgmol)	5.051	5.051			
Mass Heat of Vap. (kJ/kg)	537.3				
Phase Fraction [Molar Basis]	1.0000	1.0000			
Surface Tension (dyne/cm)					
Thermal Conductivity (W/m-K)	3.046e-002	3.046e-002			
Viscosity (cP)	1.072e-002	1.072e-002			
Cv (Semi-Ideal) (kJ/kgmol-C)	27.37	27.37			
Mass Cv (Semi-Ideal) (kJ/kg-C)	1.651	1.651			
Cv (kJ/kgmol-C)	26.92	26.92			
Mass Cv (kJ/kg-C)	1.623	1.623			
Cv (Ent. Method) (kJ/kgmol-C)	26.91	26.91			
Mass Cv (Ent. Method) (kJ/kg-C)	1.623	1.623			
Cp/Cv (Ent. Method)	1.326	1.326			

Material Stream: Low Pressure Pipeline (continued)

Fluid Package: Basis-1

Property Package: SRK

PROPERTIES

	Overall	Vapour Phase			
Reid VP at 37.8 C (kPa)					
True VP at 37.8 C (kPa)					
Liq. Vol. Flow - Sum(Std. Cond) (m3/h)	0.0000	0.0000			

COMPOSITION

Overall Phase

Vapour Fraction 1.0000

COMPONENTS	MOLAR FLOW (kgmol/h)	MOLE FRACTION	MASS FLOW (kg/h)	MASS FRACTION	LIQUID VOLUME FLOW (m3/h)	LIQUID VOLUME FRACTION
Methane	148.8666	0.9600	2388.2524	0.9288	7.9770	0.9660
Ethane	0.9304	0.0060	27.9775	0.0109	0.0787	0.0095
Propane	0.3101	0.0020	13.6762	0.0053	0.0270	0.0033
CO	0.0000	0.0000	0.0000	0.0000	0.0000	0.0000
CO2	0.1551	0.0010	6.8246	0.0027	0.0083	0.0010
Air	0.0000	0.0000	0.0000	0.0000	0.0000	0.0000
Nitrogen	4.8072	0.0310	134.6627	0.0524	0.1670	0.0202
Oxygen	0.0000	0.0000	0.0000	0.0000	0.0000	0.0000
H2O	0.0000	0.0000	0.0000	0.0000	0.0000	0.0000
Hydrogen	0.0000	0.0000	0.0000	0.0000	0.0000	0.0000
Total	155.0694	1.0000	2571.3934	1.0000	8.2579	1.0000

Vapour Phase

Phase Fraction 1.000

COMPONENTS	MOLAR FLOW (kgmol/h)	MOLE FRACTION	MASS FLOW (kg/h)	MASS FRACTION	LIQUID VOLUME FLOW (m3/h)	LIQUID VOLUME FRACTION
Methane	148.8666	0.9600	2388.2524	0.9288	7.9770	0.9660
Ethane	0.9304	0.0060	27.9775	0.0109	0.0787	0.0095
Propane	0.3101	0.0020	13.6762	0.0053	0.0270	0.0033
CO	0.0000	0.0000	0.0000	0.0000	0.0000	0.0000
CO2	0.1551	0.0010	6.8246	0.0027	0.0083	0.0010
Air	0.0000	0.0000	0.0000	0.0000	0.0000	0.0000
Nitrogen	4.8072	0.0310	134.6627	0.0524	0.1670	0.0202
Oxygen	0.0000	0.0000	0.0000	0.0000	0.0000	0.0000
H2O	0.0000	0.0000	0.0000	0.0000	0.0000	0.0000
Hydrogen	0.0000	0.0000	0.0000	0.0000	0.0000	0.0000
Total	155.0694	1.0000	2571.3934	1.0000	8.2579	1.0000

K VALUE

COMPONENTS	MIXED	LIGHT	HEAVY
Methane			
Ethane			
Propane			
CO			
CO2			
Air			
Nitrogen			
Oxygen			
H2O			
Hydrogen			

UNIT OPERATIONS

FEED TO	PRODUCT FROM	LOGICAL CONNECTION
Tee: TEE-101	Expander: Turbo Expander	Adjust: ADJ-1
		Set: SET-1

UTILITIES

(No utilities reference this stream)

Material Stream: Preheated Gas

Fluid Package: Basis-1

Property Package: SRK

CONDITIONS

	Overall	Vapour Phase			
Vapour / Phase Fraction	1.0000	1.0000			
Temperature: (C)	104.5	104.5			
Pressure: (kPa)	3447	3447			
Molar Flow (kgmol/h)	155.1	155.1			
Mass Flow (kg/h)	2571	2571			
Std Ideal Liq Vol Flow (m3/h)	8.258	8.258			
Molar Enthalpy (kJ/kgmol)	-7.038e+004	-7.038e+004			
Molar Entropy (kJ/kgmol-C)	162.8	162.8			
Heat Flow (kJ/h)	-1.091e+007	-1.091e+007			
Liq Vol Flow @Std Cond (m3/h)					

PROPERTIES

	Overall	Vapour Phase			
Molecular Weight	16.58	16.58			
Molar Density (kgmol/m3)	1.116	1.116			
Mass Density (kg/m3)	18.50	18.50			
Act. Volume Flow (m3/h)	139.0	139.0			
Mass Enthalpy (kJ/kg)	-4244	-4244			
Mass Entropy (kJ/kg-C)	9.820	9.820			
Heat Capacity (kJ/kgmol-C)	41.42	41.42			
Mass Heat Capacity (kJ/kg-C)	2.498	2.498			
Lower Heating Value (kJ/kgmol)	7.833e+005	7.833e+005			
Mass Lower Heating Value (kJ/kg)	4.723e+004	4.723e+004			
Phase Fraction [Vol. Basis]		1.000			
Phase Fraction [Mass Basis]	4.941e-324	1.000			
Partial Pressure of CO2 (kPa)	3.447				
Cost Based on Flow (Cost/s)	0.0000	0.0000			
Act. Gas Flow (ACT_m3/h)	139.0	139.0			
Avg. Liq. Density (kgmol/m3)	18.78	18.78			
Specific Heat (kJ/kgmol-C)	41.42	41.42			
Std. Gas Flow (STD_m3/h)	3667	3667			
Std. Ideal Liq. Mass Density (kg/m3)	311.4	311.4			
Act. Liq. Flow (m3/s)					
Z Factor	0.9838	0.9838			
Watson K	18.77	18.77			
User Property					
Partial Pressure of H2S (kPa)	0.0000				
Cp/(Cp - R)	1.251	1.251			
Cp/Cv	1.317	1.317			
Heat of Vap. (kJ/kgmol)	4192				
Kinematic Viscosity (cSt)	0.7774	0.7774			
Liq. Mass Density (Std. Cond) (kg/m3)					
Liq. Vol. Flow (Std. Cond) (m3/h)					
Liquid Fraction	0.0000	0.0000			
Molar Volume (m3/kgmol)	0.8961	0.8961			
Mass Heat of Vap. (kJ/kg)	252.8				
Phase Fraction [Molar Basis]	1.0000	1.0000			
Surface Tension (dyne/cm)					
Thermal Conductivity (W/m-K)	4.741e-002	4.741e-002			
Viscosity (cP)	1.438e-002	1.438e-002			
Cv (Semi-Ideal) (kJ/kgmol-C)	33.10	33.10			
Mass Cv (Semi-Ideal) (kJ/kg-C)	1.996	1.996			
Cv (kJ/kgmol-C)	31.45	31.45			
Mass Cv (kJ/kg-C)	1.897	1.897			
Cv (Ent. Method) (kJ/kgmol-C)	31.22	31.22			
Mass Cv (Ent. Method) (kJ/kg-C)	1.883	1.883			
Cp/Cv (Ent. Method)	1.327	1.327			

Material Stream: Preheated Gas (continued)

Fluid Package: Basis-1

Property Package: SRK

PROPERTIES

		Overall	Vapour Phase			
Reid VP at 37.8 C	(kPa)					
True VP at 37.8 C	(kPa)					
Liq. Vol. Flow - Sum(Std. Cond)	(m3/h)	0.0000	0.0000			

COMPOSITION

Overall Phase

Vapour Fraction 1.0000

COMPONENTS	MOLAR FLOW (kgmol/h)	MOLE FRACTION	MASS FLOW (kg/h)	MASS FRACTION	LIQUID VOLUME FLOW (m3/h)	LIQUID VOLUME FRACTION
Methane	148.8666	0.9600	2388.2524	0.9288	7.9770	0.9660
Ethane	0.9304	0.0060	27.9775	0.0109	0.0787	0.0095
Propane	0.3101	0.0020	13.6762	0.0053	0.0270	0.0033
CO	0.0000	0.0000	0.0000	0.0000	0.0000	0.0000
CO2	0.1551	0.0010	6.8246	0.0027	0.0083	0.0010
Air	0.0000	0.0000	0.0000	0.0000	0.0000	0.0000
Nitrogen	4.8072	0.0310	134.6627	0.0524	0.1670	0.0202
Oxygen	0.0000	0.0000	0.0000	0.0000	0.0000	0.0000
H2O	0.0000	0.0000	0.0000	0.0000	0.0000	0.0000
Hydrogen	0.0000	0.0000	0.0000	0.0000	0.0000	0.0000
Total	155.0694	1.0000	2571.3934	1.0000	8.2579	1.0000

Vapour Phase

Phase Fraction 1.000

COMPONENTS	MOLAR FLOW (kgmol/h)	MOLE FRACTION	MASS FLOW (kg/h)	MASS FRACTION	LIQUID VOLUME FLOW (m3/h)	LIQUID VOLUME FRACTION
Methane	148.8666	0.9600	2388.2524	0.9288	7.9770	0.9660
Ethane	0.9304	0.0060	27.9775	0.0109	0.0787	0.0095
Propane	0.3101	0.0020	13.6762	0.0053	0.0270	0.0033
CO	0.0000	0.0000	0.0000	0.0000	0.0000	0.0000
CO2	0.1551	0.0010	6.8246	0.0027	0.0083	0.0010
Air	0.0000	0.0000	0.0000	0.0000	0.0000	0.0000
Nitrogen	4.8072	0.0310	134.6627	0.0524	0.1670	0.0202
Oxygen	0.0000	0.0000	0.0000	0.0000	0.0000	0.0000
H2O	0.0000	0.0000	0.0000	0.0000	0.0000	0.0000
Hydrogen	0.0000	0.0000	0.0000	0.0000	0.0000	0.0000
Total	155.0694	1.0000	2571.3934	1.0000	8.2579	1.0000

K VALUE

COMPONENTS	MIXED	LIGHT	HEAVY
Methane			
Ethane			
Propane			
CO			
CO2			
Air			
Nitrogen			
Oxygen			
H2O			
Hydrogen			

UNIT OPERATIONS

FEED TO		PRODUCT FROM		LOGICAL CONNECTION
Tee:	TEE-100	Heater:	Exchanger1	

UTILITIES

(No utilities reference this stream)

Material Stream: Preheated Gas (continued)

Fluid Package: Basis-1

Property Package: SRK

DYNAMICS

Pressure Specification	(Inactive)	3447 kPa					
Flow Specification	(Inactive)	**Molar:**	155.1 kgmol/h	**Mass:**	2571 kg/h	**Std Ideal Liq Volume:**	8.258 m3/h

User Variables

NOTES

Description

Spreadsheet: Electrochemical Model

CONNECTIONS

Imported Variables

Cell	Object	Variable Description	Value
A1	SpreadSheetCell: Material and Energy Balan	C4: Cell operating Temperature	891.3
A4	SpreadSheetCell: Material and Energy Balan	C5: current density [mA/cm2]	138.0
A5	SpreadSheetCell: Material and Energy Balan	C2: User Variables (number of cells)	400
A6	SpreadSheetCell: Material and Energy Balan	C3: User Variables (Geometric Area)	9000
A11	Material Stream: Anode Out	Comp Mole Frac (Hydrogen)	0.1275
A12	Material Stream: Anode Out	Comp Mole Frac (CO2)	0.3771
A13	Material Stream: Anode Out	Comp Mole Frac (H2O)	0.4597
A15	Material Stream: Cathode Out	Comp Mole Frac (Oxygen)	0.3821
A16	Material Stream: Cathode Out	Comp Mole Frac (CO2)	0.0124
C14	SpreadSheetCell: Material and Energy Balan	F1: Hydrogen Fuel Utilization	0.7500
E18	SpreadSheetCell: Material and Energy Balan	D23: Useful heat (KW)	990.9 kJ/h
E19	Material Stream: To Anode	Heat Flow	-5.591e+005 kJ/h
F20	Expander: Turbo Expander	Adiabatic Efficiency	70
H18	Material Stream: Cathode Out	Heat Flow	5.400e+004 kJ/h
E25	Material Stream: High Pressure Gas	Pressure	6251 kPa
E29	Material Stream: High Pressure Gas	Mass Flow	2571 kg/h

Exported Variables' Formula Results

Cell	Object	Variable Description	Value
H1	MCFC	User Variables (Fuel Cell Work)	0.1043
C9	MCFC	User Variables (Open Circuit Voltage)	0.8162
C13	MCFC	User Variables (Cell Operating Voltage)	0.2099
H15	fuel cell heat	Power	403.0 kW

PARAMETERS

Exportable Variables

Cell	Visible Name	Variable Description	Variable Type	Value
A2	A2: Faraday's Constant [C]	Faraday's Constant [C]		9.650e+004
A3	A3: Universal Gas Constant [J/mol.K]	Universal Gas Constant [J/mol.K]		8.314
A7	A7: Ambient Temperature [K]	Ambient Temperature [K]		298.1
A8	A8:			8.314e-003
A17	A17: [RT/2F]	[RT/2F]		3.840e-002
A19	A19:			-1.763
A20	A20:			-3.411
B1	B1: Entropy [H2O] J/mol.K @ 298.15	Entropy [H2O] J/mol.K @ 298.15		188.8
B2	B2: Entropy [CO2] J/mol.K @ 298.15	Entropy [CO2] J/mol.K @ 298.15		213.8
B3	B3: Entropy [H2] J/mol.K @ 298.15	Entropy [H2] J/mol.K @ 298.15		130.7
B4	B4: Entropy [O2] J/mol.K @ 298.15	Entropy [O2] J/mol.K @ 298.15		205.1
B5	B5: Entropy [CO] J/mol.K @ 298.15	Entropy [CO] J/mol.K @ 298.15		197.8
B7	B7: change in enthalpy of formation [DH] [J/mol]	change in enthalpy of formation [DH] [J/mol]		-2.449e+005
B8	B8: Change in Gibbs free energy of formation DG	Change in Gibbs free energy of formation DG		-1.959e+005
B9	B9: Standard nernst potential	Standard nernst potential		1.015
B11	B11:			-0.1987
B13	B13: change in enthalpy of formation [DH] for WGS	change in enthalpy of formation [DH] for WGS [J/m		-3.298e+004
C1	C1: Enthalpy [H2O] J/mol @ 298.15	Enthalpy [H2O] J/mol @ 298.15		-2.418e+005
C2	C2: Enthalpy [CO2] J/mol @ 298.15	Enthalpy [CO2] J/mol @ 298.15		-3.935e+005
C3	C3: Enthalpy [H2] J/mol @ 298.15	Enthalpy [H2] J/mol @ 298.15		0.0000
C4	C4: Enthalpy [O2] J/mol @ 298.15	Enthalpy [O2] J/mol @ 298.15		0.0000
C5	C5: Enthalpy [CO] J/mol @ 298.15	Enthalpy [CO] J/mol @ 298.15		-1.106e+005
C7	C7: change in entropy of formation [DS][J/mol.K]	change in entropy of formation [DS][J/mol.K]		-55.01
C9	C9: User Variables (Open Circuit Voltage)	User Variables (Open Circuit Voltage)		0.8162
C11	C11: Losses; ohmic/activation/mass transfer [V]	Losses; ohmic/activation/mass transfer [V]		0.6062
C13	C13: User Variables (Cell Operating Voltage)	User Variables (Cell Operating Voltage)		0.2099
C15	C15: User Variables (Efficiency)	User Variables (Efficiency)		0.1680

Spreadsheet: Electrochemical Model (continued)

PARAMETERS

Exportable Variables

Cell	Visible Name	Variable Description	Variable Type	Value
C16	C16: STACK ELECTRICAL EFFICIENCY	STACK ELECTRICAL EFFICIENCY		0.1260
D1	D1: Specific heat capacity [H2O] J/mol.K @ 298.15	Specific heat capacity [H2O] J/mol.K @ 298.15		33.60
D2	D2: Specific heat capacity [CO2] J/mol.K @ 298.15	Specific heat capacity [CO2] J/mol.K @ 298.15		37.15
D3	D3: Specific heat capacity [H2] J/mol.K @ 298.15	Specific heat capacity [H2] J/mol.K @ 298.15		28.83
D4	D4: Specific heat capacity [O2] J/mol.K @ 298.15	Specific heat capacity [O2] J/mol.K @ 298.15		29.37
D5	D5: Specific heat capacity [CO] J/mol.K @ 298.15	Specific heat capacity [CO] J/mol.K @ 298.15		29.18
D7	D7: A(ir)-preexponential term for internal resistance	A(ir)-preexponential term for internal resistance		1.280e-002
D8	D8: Delta -H[ir] enthalpy for internal resistance [KJ/	Delta -H[ir] enthalpy for internal resistance [KJ/mol		25.20
D9	D9: Internal resistance [ohm/cm^2]	Internal resistance [ohm/cm^2]		0.3838
E1	E1: Specific heat capacity [H2O] J/mol.K @ A1	Specific heat capacity [H2O] J/mol.K @ A1		40.00
E2	E2: Specific heat capacity [CO2] J/mol.K @ A1	Specific heat capacity [CO2] J/mol.K @ A1		52.76
E3	E3: Specific heat capacity [H2] J/mol.K @ A1	Specific heat capacity [H2] J/mol.K @ A1		29.91
E4	E4: Specific heat capacity [O2] J/mol.K @ A1	Specific heat capacity [O2] J/mol.K @ A1		33.70
E5	E5: Specific heat capacity [CO] J/mol.K @ A1	Specific heat capacity [CO] J/mol.K @ A1		32.53
E7	E7: A(a)-preexponential term for anode reaction re	A(a)-preexponential term for anode reaction resista		1.390e-006
E8	E8: Delta -H[a] enthalpy for anode reaction resistan	Delta -H[a] enthalpy for anode reaction resistance		77.80
E9	E9: anode reaction resistance [ohms/cm^2]	anode reaction resistance [ohms/cm^2]		0.1412
E20	E20: anode heat flow [KW]	anode heat flow [KW]	Energy	155.3 kJ/h
E26	E26: Inlet Pressure (bar)	Inlet Pressure (bar)	Pressure	62.51 kPa
E27	E27: Design Inlet Pressure [bar]	Design Inlet Pressure [bar]		60.52
E28	E28: design mass flow (kg/s)	design mass flow (kg/s)		2.712
E30	E30: mass flow (kg/sec)	mass flow (kg/sec)	Mass Flow	0.7143 kg/h
F1	F1: Enthalpy [H2O] J/mol @ A1	Enthalpy [H2O] J/mol @ A1		-2.162e+005
F2	F2: Enthalpy [CO2] J/mol @ A1	Enthalpy [CO2] J/mol @ A1		-3.576e+005
F3	F3: Enthalpy [H2] J/mol @ A1	Enthalpy [H2] J/mol @ A1		1.806e+004
F4	F4: Enthalpy [O2] J/mol @ A1	Enthalpy [O2] J/mol @ A1		2.128e+004
F5	F5:			-9.032e+004
F7	F7: A(c1)-preexponential term for cathode reaction	A(c1)-preexponential term for cathode reaction res		1.970e-006
F8	F8: Delta -H[c1] enthalpy for anode reaction resista	Delta -H[c1] enthalpy for anode reaction resistance		83.40
F9	F9: C1(T]For anode ohmic resistance	C1(T]For anode ohmic resistance		3.493e-002
F10	F10:			<empty>
F18	F18: CELL ELECTRICAL EFFICIENCY	CELL ELECTRICAL EFFICIENCY		50.37
F19	F19: Cogen efficiency	Cogen efficiency		245.0
F21	F21: Global Efficiency	Global Efficiency		171.5
F25	F25: Expander efficiency:lower boundary [%]	Expander efficiency:lower boundary [%]		0.0000
F26	F26: expander efficiency:upper boundary [%]	expander efficiency:upper boundary [%]		90.00
G1	G1: Entropy [H2O] J/mol.K @ A1	Entropy [H2O] J/mol.K @ A1		108.5
G2	G2: Entropy [CO2] J/mol.K @ A1	Entropy [CO2] J/mol.K @ A1		67.13
G3	G3: Entropy [H2] J/mol.K @ A1	Entropy [H2] J/mol.K @ A1		91.76
G4	G4: Entropy [O2] J/mol.K @ A1	Entropy [O2] J/mol.K @ A1		143.6
G7	G7: A(c2)-preexponential term for cathode reaction	A(c2)-preexponential term for cathode reaction res		2.200e-003
G8	G8: Delta -H[c2] enthalpy for anode reaction resist	Delta -H[c2] enthalpy for anode reaction resistance		22.80
G9	G9: C2(T]For anode ohmic resistance	C2(T]For anode ohmic resistance		3.833
G25	G25: Operating Condition (OC)	Operating Condition (OC)		0.2720
G26	G26:			24.48
H1	H1: User Variables (Fuel Cell Work)	User Variables (Fuel Cell Work)		0.1043
H2	H2: fuel cell power KW	fuel cell power KW		104.3
H9	H9: Cathode reaction resistance [ohm/cm^2]	Cathode reaction resistance [ohm/cm^2]		3.868
H12	H12: Heat generated by fuel cell (kW)	Heat generated by fuel cell (kW)		516.7
H13	H13:			113.7
H15	H15: Power	Power	Power	403.0 kW
H16	H16:			403.0
H19	H19: Fuel Cell Heat	Fuel Cell Heat	Energy	-1.377e+004 kJ/h
H20	H20:		Energy	-3.825 kJ/h
I2	I2: Power Density (kW/cm2)	Power Density (kW/cm2)		1.159e-002

Spreadsheet: Electrochemical Model (continued)

User Variables

FORMULAS

Cell	Formula	Result
A8	=a3/1000	8.314e-003
A17	=(a3*a1)/(2*a2)	3.840e-002
A19	=@LN((a11*a15^0.5)/a13)	-1.763
A20	=@LN(A16/A12)	-3.411
B7	=(F1+F2)-(F2+F3+0.5*F4)	-2.449e+005
B8	=B7-(A1*C7)	-1.959e+005
B9	=-B8/(2*A2)	1.015
B11	=(A17*A19)+(A17*A20)	-0.1987
B13	=(F2+F3)-(F5+F1)	-3.298e+004
C7	=(G1+G2)-(G2+G3+0.5*G4)	-55.01
C9	=B9+B11	0.8162
C11	=(d9+e9+h9)*a4/1000	0.6062
C13	=c9-c11	0.2099
C15	=(c13/1.25)	0.1680
C16	=(c13/1.25)*C14	0.1260
D7	=1.28*10^-2	1.280e-002
D8	=25.2	25.20
D9	=d7*@EXP((d8)/(a8*a1))	0.3838
E1	=143.05-(58.040*A1^0.25)+(8.2751*A1^0.5)-(0.036989*A1)	40.00
E2	=-3.7357+(3.0529*A1^0.5)-(0.041034*A1)+(2.4198*(10^-6)*A1^2)	52.76
E3	=56.505-(22222.6*A1^-0.75)+(116500*A1^-1)-(560700*A1^-1.5)	29.91
E4	=37.432+(2.0102*(10^-5)*A1^-1.5)-(178570*A1^-1.5)+(2368800*A1^-2)	33.70
E5	=69.145-(0.022282*A1^0.75)-(2007.7*A1^-0.5)+(5589.64*A1^-0.75)	32.53
E7	=1.39*10^-6	1.390e-006
E8	=77.80	77.80
E9	=e7*@EXP((e8)/(a8*a1))*(a11^-0.5)	0.1412
E20	=-(e19/3.6/1000)	155.3 kJ/h
E26	=e25/100	62.51 kPa
E30	=e29/3600	0.7143 kg/h
F1	=C1+((E1*A1)-(D1*A7))	-2.162e+005
F2	=C2+((E2*A1)-(D2*A7))	-3.576e+005
F3	=C3+((E3*A1)-(D3*A7))	1.806e+004
F4	=C4+((E4*A1)-(D4*A7))	2.128e+004
F5	=C5+((E5*A1)-(D5*A7))	-9.032e+004
F7	=1.97*10^-6	1.970e-006
F8	=83.40	83.40
F9	=f7*(@EXP((f8)/(a8*a1)))*(a15^-0.75)*a16^0.5	3.493e-002
F18	=((H1*1000/E20)*c14)*100	50.37
F19	=((((H1*1000)+H15)/E20)*c14)*100	245.0
F21	=(f19*f20)/100	171.5
G1	=B1+((E1*@LN(A1^-1))-(D1*@LN(A7^-1)))	108.5
G2	=B2+((E2*@LN(A1^-1))-(D2*@LN(A7^-1)))	67.13
G3	=B3+((E3*@LN(A1^-1))-(D3*@LN(A7^-1)))	91.76
G4	=B4+((E4*@LN(A1^-1))-(D4*@LN(A7^-1)))	143.6
G7	=2.2*10^-3	2.200e-003
G8	=22.80	22.80
G9	=g7*(@EXP((g8)/(a8*a1)))*a16^-1	3.833
G25	=(1+((e26-e27)/e27))*(1+((e30-e28)/e28))	0.2720
G26	=((F26-F25)*G25)+F25	24.48
H1	=(c13*a4*a6*a5)/1000000000	0.1043
H2	=h1*1000	104.3
H9	=f9+g9	3.868
H12	=((a5*((a4*a6)/1000)*(1.25-c13))/1000)	516.7
H13	=H12*.22	113.7
H15	=H12-H13	403.0 kW

Spreadsheet: Electrochemical Model (continued)

Units Set: SI

FORMULAS

Cell	Formula	Result
H16	=H15	403.0
H19	=-H18*.255	-1.377e+004 kJ/h
H20	=h19/3.6/1000	-3.825 kJ/h
I2	=h2/a6	1.159e-002

Spreadsheet: Material and Energy Balance

CONNECTIONS

Imported Variables

Cell	Object	Variable Description	Value
A1	Material Stream: To Anode	Temperature	650.1 C
A2	Material Stream: To Anode	Pressure	101.3 kPa
A3	Material Stream: Cathode In	Temperature	650.0 C
A4	Material Stream: Cathode In	Pressure	101.3 kPa
A7	Material Stream: To Anode	Phase Comp Molar Flow (Vapour Phase-Methane)	0.0967 kgmol/h
A8	Material Stream: To Anode	Phase Comp Molar Flow (Vapour Phase-Ethane)	0.0000 kgmol/h
A9	Material Stream: To Anode	Phase Comp Molar Flow (Vapour Phase-Propane)	0.0000 kgmol/h
A10	Material Stream: To Anode	Phase Comp Molar Flow (Vapour Phase-CO)	0.4603 kgmol/h
A11	Material Stream: To Anode	Phase Comp Molar Flow (Vapour Phase-CO2)	0.5057 kgmol/h
A12	Material Stream: To Anode	Phase Comp Molar Flow (Vapour Phase-Air)	0.0000 kgmol/h
A13	Material Stream: To Anode	Phase Comp Molar Flow (Vapour Phase-Nitrogen)	0.0337 kgmol/h
A14	Material Stream: To Anode	Phase Comp Molar Flow (Vapour Phase-Oxygen)	0.0000 kgmol/h
A15	Material Stream: To Anode	Phase Comp Molar Flow (Vapour Phase-H2O)	1.7869 kgmol/h
A16	Material Stream: To Anode	Phase Comp Molar Flow (Vapour Phase-Hydrogen)	3.3886 kgmol/h
A19	Material Stream: Cathode In	Phase Comp Molar Flow (Vapour Phase-Methane)	0.0000 kgmol/h
A20	Material Stream: Cathode In	Phase Comp Molar Flow (Vapour Phase-Ethane)	0.0000 kgmol/h
A21	Material Stream: Cathode In	Phase Comp Molar Flow (Vapour Phase-Propane)	0.0000 kgmol/h
A22	Material Stream: Cathode In	Phase Comp Molar Flow (Vapour Phase-CO)	0.0000 kgmol/h
A23	Material Stream: Cathode In	Phase Comp Molar Flow (Vapour Phase-CO2)	3.6041 kgmol/h
A24	Material Stream: Cathode In	Phase Comp Molar Flow (Vapour Phase-Air)	49.5762 kgmol/h
A25	Material Stream: Cathode In	Phase Comp Molar Flow (Vapour Phase-Nitrogen)	0.0337 kgmol/h
A26	Material Stream: Cathode In	Phase Comp Molar Flow (Vapour Phase-Oxygen)	49.5767 kgmol/h
A27	Material Stream: Cathode In	Phase Comp Molar Flow (Vapour Phase-H2O)	5.3688 kgmol/h
A28	Material Stream: Cathode In	Phase Comp Molar Flow (Vapour Phase-Hydrogen)	0.0000 kgmol/h
C2	MCFC: MCFC	User Variables (number of cells)	400
C3	MCFC: MCFC	User Variables (Geometric Area)	9000
D14	Spreadsheet Cell: Electrochemical Model@B	B7: change in enthalpy of formation [DH] [J/mol]	-2.449e+005
D15	Spreadsheet Cell: Electrochemical Model@B	B13: change in enthalpy of formation [DH] for WGS [J/mol]	-3.298e+004
E14	SpreadSheetCell: Electrochemical Model@C	C13: User Variables (Cell Operating Voltage)	0.2099
E15	SpreadSheetCell: Electrochemical Model@D	D9: Internal resistance [ohm/cm^2]	0.3838
F14	SpreadSheetCell: Electrochemical Model@H	H1: MCFC power in [MW]	0.1043
E19	Material Stream: To Anode	Heat Flow	-5.591e+005 kJ/h
F19	Material Stream: Cathode In	Heat Flow	-5.507e+005 kJ/h
G19	Material Stream: Anode Out	Heat Flow	-2.099e+006 kJ/h
H19	Material Stream: Cathode Out	Heat Flow	5.400e+004 kJ/h
I2	Energy Stream: Heat Source2	Power	74.07 kW
I1	Energy Stream: Heat Source	Power	178.9 kW
I3	Energy Stream: Heat Source 3	Power	51.94 kW
I4	Energy Stream: exchanger heat out	Power	-430.3 kW
I5	SpreadSheetCell: Electrochemical Model@H	H15: Net fuelcell thermal power (kW)	403.0 kW
I6	Energy Stream: Exchanger5 heat	Power2	575.8 kW
H1	Energy Stream: Pump Duty	Power	8.482e-004 kW
H2	Energy Stream: Pump2 duty	Power	0.0000 kW
H3	Energy Stream: Expander Duty	Power	150.8 kW
H4	SpreadSheetCell: Electrochemical Model@H	H2: fuel cell power KW	104.3
F25	Material Stream: To Mixer	Comp Molar Flow (Methane)	1.0421 kgmol/h
G1	Material Stream: To Mixer	Comp Molar Flow (Methane)	1.0421 kgmol/h

Exported Variables' Formula Results

Cell	Object	Variable Description	Value
B1	Anode Out	Temperature	650.1 C
B2	Anode Out	Pressure	101.3 kPa
B3	Cathode Out	Temperature	650.0 C
B4	Cathode Out	Pressure	101.3 kPa
B7	Anode Out	Phase Comp Molar Flow (Vapour Phase-Methane)	0.0967 kgmol/h

Spreadsheet: Material and Energy Balance (continued)

CONNECTIONS

Exported Variables' Formula Results

Cell	Object	Variable Description	Value
B8	Anode Out	Phase Comp Molar Flow (Vapour Phase-Ethane)	0.0000 kgmol/h
B9	Anode Out	Phase Comp Molar Flow (Vapour Phase-Propane)	0.0000 kgmol/h
B12	Anode Out	Phase Comp Molar Flow (Vapour Phase-Air)	0.0000 kgmol/h
B13	Anode Out	Phase Comp Molar Flow (Vapour Phase-Nitrogen)	0.0337 kgmol/h
B14	Anode Out	Phase Comp Molar Flow (Vapour Phase-Oxygen)	0.0000 kgmol/h
B15	Anode Out	Phase Comp Molar Flow (Vapour Phase-H2O)	4.0517 kgmol/h
B16	Anode Out	Phase Comp Molar Flow (Vapour Phase-Hydrogen)	1.1238 kgmol/h
B19	Cathode Out	Phase Comp Molar Flow (Vapour Phase-Methane)	0.0000 kgmol/h
B20	Cathode Out	Phase Comp Molar Flow (Vapour Phase-Ethane)	0.0000 kgmol/h
B21	Cathode Out	Phase Comp Molar Flow (Vapour Phase-Propane)	0.0000 kgmol/h
B22	Cathode Out	Phase Comp Molar Flow (Vapour Phase-CO)	0.0000 kgmol/h
B24	Cathode Out	Phase Comp Molar Flow (Vapour Phase-Air)	49.5762 kgmol/h
B25	Cathode Out	Phase Comp Molar Flow (Vapour Phase-Nitrogen)	0.0337 kgmol/h
B26	Cathode Out	Phase Comp Molar Flow (Vapour Phase-Oxygen)	34.7037 kgmol/h
B23	Cathode Out	Phase Comp Molar Flow (Vapour Phase-CO2)	1.1305 kgmol/h
B27	Cathode Out	Phase Comp Molar Flow (Vapour Phase-H2O)	5.3688 kgmol/h
B28	Cathode Out	Phase Comp Molar Flow (Vapour Phase-Hydrogen)	0.0000 kgmol/h
B10	Anode Out	Phase Comp Molar Flow (Vapour Phase-CO)	0.1836 kgmol/h
B11	Anode Out	Phase Comp Molar Flow (Vapour Phase-CO2)	3.3238 kgmol/h
D21	MCFC	User Variables (Fuel Cell Useful heat)	-3.964e+006

PARAMETERS

Exportable Variables

Cell	Visible Name	Variable Description	Variable Type	Value
B1	B1: Temperature	Temperature	Temperature	650.1 C
B2	B2: Pressure	Pressure	Pressure	101.3 kPa
B3	B3: Temperature	Temperature	Temperature	650.0 C
B4	B4: Pressure	Pressure	Pressure	101.3 kPa
B7	B7: Phase Comp Molar Flow (Vapour Phase-Meth	Phase Comp Molar Flow (Vapour Phase-Methane)	Comp. Mole Flow	0.0967 kgmol/h
B8	B8: Phase Comp Molar Flow (Vapour Phase-Ethan	Phase Comp Molar Flow (Vapour Phase-Ethane)	Comp. Mole Flow	0.0000 kgmol/h
B9	B9: Phase Comp Molar Flow (Vapour Phase-Propa	Phase Comp Molar Flow (Vapour Phase-Propane)	Comp. Mole Flow	0.0000 kgmol/h
B10	B10: Phase Comp Molar Flow (Vapour Phase-CO)	Phase Comp Molar Flow (Vapour Phase-CO)	Comp. Mole Flow	0.1836 kgmol/h
B11	B11: Phase Comp Molar Flow (Vapour Phase-CO2	Phase Comp Molar Flow (Vapour Phase-CO2)	Comp. Mole Flow	3.3238 kgmol/h
B12	B12: Phase Comp Molar Flow (Vapour Phase-Air)	Phase Comp Molar Flow (Vapour Phase-Air)	Comp. Mole Flow	0.0000 kgmol/h
B13	B13: Phase Comp Molar Flow (Vapour Phase-Nitro	Phase Comp Molar Flow (Vapour Phase-Nitrogen)	Comp. Mole Flow	0.0337 kgmol/h
B14	B14: Phase Comp Molar Flow (Vapour Phase-Oxy	Phase Comp Molar Flow (Vapour Phase-Oxygen)	Comp. Mole Flow	0.0000 kgmol/h
B15	B15: Phase Comp Molar Flow (Vapour Phase-H2O	Phase Comp Molar Flow (Vapour Phase-H2O)	Comp. Mole Flow	4.0517 kgmol/h
B16	B16: Phase Comp Molar Flow (Vapour Phase-Hyd	Phase Comp Molar Flow (Vapour Phase-Hydrogen	Comp. Mole Flow	1.1238 kgmol/h
B17	B17:		Comp. Mole Flow	8.8133 kgmol/h
B19	B19: Phase Comp Molar Flow (Vapour Phase-Met	Phase Comp Molar Flow (Vapour Phase-Methane)	Comp. Mole Flow	0.0000 kgmol/h
B20	B20: Phase Comp Molar Flow (Vapour Phase-Etha	Phase Comp Molar Flow (Vapour Phase-Ethane)	Comp. Mole Flow	0.0000 kgmol/h
B21	B21: Phase Comp Molar Flow (Vapour Phase-Prop	Phase Comp Molar Flow (Vapour Phase-Propane)	Comp. Mole Flow	0.0000 kgmol/h
B22	B22: Phase Comp Molar Flow (Vapour Phase-CO)	Phase Comp Molar Flow (Vapour Phase-CO)	Comp. Mole Flow	0.0000 kgmol/h
B23	B23: Phase Comp Molar Flow (Vapour Phase-CO2	Phase Comp Molar Flow (Vapour Phase-CO2)	Comp. Mole Flow	1.1305 kgmol/h
B24	B24: Phase Comp Molar Flow (Vapour Phase-Air)	Phase Comp Molar Flow (Vapour Phase-Air)	Comp. Mole Flow	49.5762 kgmol/h
B25	B25: Phase Comp Molar Flow (Vapour Phase-Nitro	Phase Comp Molar Flow (Vapour Phase-Nitrogen)	Comp. Mole Flow	0.0337 kgmol/h
B26	B26: Phase Comp Molar Flow (Vapour Phase-Oxy	Phase Comp Molar Flow (Vapour Phase-Oxygen)	Comp. Mole Flow	34.7037 kgmol/h
B27	B27: Phase Comp Molar Flow (Vapour Phase-H2O	Phase Comp Molar Flow (Vapour Phase-H2O)	Comp. Mole Flow	5.3688 kgmol/h
B28	B28: Phase Comp Molar Flow (Vapour Phase-Hyd	Phase Comp Molar Flow (Vapour Phase-Hydrogen	Comp. Mole Flow	0.0000 kgmol/h
B29	B29:		Comp. Mole Flow	90.8129 kgmol/h
C1	C1:			9.650e+004
C4	C4: Cell operating Temperature	Cell operating Temperature		891.3
C5	C5: current density [mA/cm2]	current density [mA/cm2]		138.0
C6	C6: Cell curent [A]	Cell curent [A]		1242

Spreadsheet: Material and Energy Balance (continued)

PARAMETERS

Exportable Variables

Cell	Visible Name	Variable Description	Variable Type	Value
C7	C7: Hydrogen Utilization [kgmol/h]	Hydrogen Utilization [kgmol/h]	Comp. Mole Flow	2.4737 kgmol/h
C8	C8: Oxygen fuel utilization [kgmol/h]	Oxygen fuel utilization [kgmol/h]	Comp. Mole Flow	14.8730 kgmol/h
C9	C9: LN[Keq] for WSG	LN[Keq] for WSG		0.8892
C10	C10: kwg	kwg		2.433
C16	C16:		Comp. Mole Flow	0.9149 kgmol/h
D1	D1: Rate of Steam reforming reaction (r1)[kgmol/h]	Rate of Steam reforming reaction (r1)[kgmol/h]		0.0000
D2	D2: rate of water gas shift reaction (r2) [kgmol/h]	rate of water gas shift reaction (r2) [kgmol/h]	Comp. Mole Flow	0.2766 kgmol/h
D3	D3: rate of electrochemical reaction [r3][kgmol/h]	rate of electrochemical reaction [r3][kgmol/h]	Comp. Mole Flow	2.5414 kgmol/h
D17	D17: Current in Ampere [A]	Current in Ampere [A]		1242
D19	D19: Qgen in [KJ/hr]	Qgen in [KJ/hr]	Comp. Mole Flow	-5.328378384e+06 kgm
D21	D21: User Variables (Fuel Cell Useful heat)	User Variables (Fuel Cell Useful heat)		-3.964e+006
D22	D22: Useful heat in Joules/sec	Useful heat in Joules/sec	Energy	-1.101e+006 kJ/h
D23	D23: Power	Power	Energy	990.9 kJ/h
E1	E1: a	a		1.433
E2	E2: b	b	Comp. Mole Flow	-15.3808 kgmol/h
E3	E3: c	c	Comp. Mole Flow	2.0457 kgmol/h
E4	E4:		Comp. Mole Flow	-0.2766 kgmol/h
E5	E5:		Comp. Mole Flow	0.2766 kgmol/h
E21	E21:		Energy	-3.964e+006 kJ/h
F1	F1: Hydrogen Fuel Utilization	Hydrogen Fuel Utilization		0.7500
F2	F2: Oxygen utilization	Oxygen utilization		0.3000
F15	F15: mcfc work in [KJ/h]	mcfc work in [KJ/h]		3.755e+005
F26	F26:		Comp. Mole Flow	3.1262 kgmol/h
G2	G2:		Comp. Mole Flow	3.1262 kgmol/h
G20	G20:		Energy	2.474e+006 kJ/h
H5	H5:		Power	255.1 kW
I7	I7:		Power	243.6 kW

User Variables

FORMULAS

Cell	Formula	Result
B1	=A1	650.1 C
B2	=A2	101.3 kPa
B3	=A3	650.0 C
B4	=A4	101.3 kPa
B7	=A7-d1	0.0967 kgmol/h
B8	=A8	0.0000 kgmol/h
B9	=A9	0.0000 kgmol/h
B10	=a10+d1-d2	0.1836 kgmol/h
B11	=a11+d2+d3	3.3238 kgmol/h
B12	=A12	0.0000 kgmol/h
B13	=A13	0.0337 kgmol/h
B14	=A14	0.0000 kgmol/h
B15	=a15-d1-d2+d3	4.0517 kgmol/h
B16	=a16+3*d1+d2-d3	1.1238 kgmol/h
B17	=b7+b8+b9+b10+b11+b12+b13+b14+b15+b16	8.8133 kgmol/h
B19	=A19	0.0000 kgmol/h
B20	=A20	0.0000 kgmol/h
B21	=A21	0.0000 kgmol/h
B22	=A22	0.0000 kgmol/h
B23	=A23-C7	1.1305 kgmol/h
B24	=A24	49.5762 kgmol/h
B25	=A25	0.0337 kgmol/h
B26	=A26-C8	34.7037 kgmol/h

Spreadsheet: Material and Energy Balance (continued)

FORMULAS

Cell	Formula	Result
B27	=A27	5.3688 kgmol/h
B28	=A28	0.0000 kgmol/h
B29	=B19+B20+B21+B22+B23+B24+B25+B26+B27+B28	90.8129 kgmol/h
C4	=618.15+273.15	891.3
C6	=C5*9000/1000	1242
C7	=A16-C16	2.4737 kgmol/h
C8	=0.30*A26	14.8730 kgmol/h
C9	=(5693.5/C4)+(1.077*(@LN(C4)))+(0.000544*C4)-(0.0000001125*C4^2)-(49170/(C4^2))-(13.148)	0.8892
C10	=@EXP(C9)	2.433
C16	=A16-(0.73*A16)	0.9149 kgmol/h
D1	=0	0.0000
D2	=e5	0.2766 kgmol/h
D3	=0.75*A16	2.5414 kgmol/h
D17	=(C5/1000)*C3	1242
D19	=-(((D2*D15/1000)+(D3*D14/1000))+(E15*C3*D17^2))/1000	-5.328378384e+06 kgm
D21	=(d19+e19+f19)+(g20)	-3.964e+006
D22	=d21/3.6	-1.101e+006 kJ/h
D23	=-(d22/1000)*.90	990.9 kJ/h
E1	=c10-1	1.433
E2	=-((a15*c10)+(2*c10*d1)+(a10*c10)+(c10*c7)+(a16)+(3*d1)+a11)	-15.3808 kgmol/h
E3	=(a10*a15*c10)+(a15*c10*d1)-(a10*c10*d1)-(c10*d1^2)+(a10*c10*c7)+(c10*d1*c7)-(a16*a11)-(a16*c7)-(3*a11*d1)-(3*d1*c7)+(a1	2.0457 kgmol/h
E4	=-(-e2-@SQRT(e2^2-(4*e1*e3)))/2*e1	-0.2766 kgmol/h
E5	=-e4	0.2766 kgmol/h
E21	=(d19+e19+f19)+g20	-3.964e+006 kJ/h
F1	=d3/a16	0.7500
F2	=C8/A26	0.3000
F15	=F14*1000000*3.6	3.755e+005
F26	=f25*3	3.1262 kgmol/h
G2	=3*g1	3.1262 kgmol/h
G20	=(-g19+f15)	2.474e+006 kJ/h
H5	=H4+H3-H2-H1	255.1 kW
I7	=I6+i5+i4-i3-i2-i1	243.6 kW

Gibbs Reactor: Anode Gas Oxidizer

CONNECTIONS

Inlet Stream Connections

Stream Name	From Unit Operation
Anode Out	MCFC
Air to AGO	MCFC

Outlet Stream Connections

Stream Name	To Unit Operation
To Exchanger 4	Cooler: Exchanger 4
Dummy 2	

Energy Stream Connections

Stream Name	From Unit Operation

PARAMETERS

Physical Parameters		Optional Heat Transfer: Heating	
Delta P	Vessel Volume	Duty	Energy Stream
0.0000 kPa		0.0000 kJ/h	

User Variables

REACTION DETAILS

MOLE FLOW SPECIFICATIONS

Components	Total Feed (kgmol/h)	Total Prod (kgmol/h)	Inerts	Frac Spec	Fixed Spec (kgmol/h)
Methane	9.667e-002	3.676e-037	No		
Ethane	2.839e-007	6.831e-037	No		
Propane	2.279e-012	9.197e-037	No		
CO	0.1836	9.308e-026	No		
CO2	3.324	3.604	No		
Air	100.0	49.58	No		
Nitrogen	3.365e-002	3.365e-002	No		
Oxygen	9.110e-023	49.58	No		
H2O	4.052	5.369	No		
Hydrogen	1.124	2.620e-023	No		

ATOM MATRIX DATA

	C	H	O	N		
Methane	1.000	4.000	0.0000	0.0000		
Ethane	2.000	6.000	0.0000	0.0000		
Propane	3.000	8.000	0.0000	0.0000		
CO	1.000	0.0000	1.000	0.0000		
CO2	1.000	0.0000	2.000	0.0000		
Air	0.0000	0.0000	2.000	0.0000		
Nitrogen	0.0000	0.0000	0.0000	2.000		
Oxygen	0.0000	0.0000	2.000	0.0000		
H2O	0.0000	2.000	1.000	0.0000		
Hydrogen	0.0000	2.000	0.0000	0.0000		

RATING

Sizing

Cylinder	Vertical	Reactor has a Boot: No
Volume	Diameter	Height

Nozzles

Gibbs Reactor: Anode Gas Oxidizer (continued)

Base Elevation Relative to Ground Level	0.0000 m	Diameter	Height

		Anode Out	Air to AGO	To Exchanger 4
Diameter	(m)	5.000e-002	5.000e-002	5.000e-002
Elevation (Base)	(m)	0.0000	0.0000	0.0000
Elevation (Ground)	(m)	0.0000	0.0000	0.0000
Elevation (% of Height)	(%)			

		Dummy 2
Diameter	(m)	5.000e-002
Elevation (Base)	(m)	0.0000
Elevation (Ground)	(m)	0.0000
Elevation (% of Height)	(%)	

CONDITIONS

Name		Anode Out	Air to AGO	Dummy 2	To Exchanger 4
Vapour		1.0000	1.0000	0.0000	1.0000
Temperature	(C)	650.1032	25.0000	213.8103	213.8103
Pressure	(kPa)	101.3250	101.3250	101.3250	101.3250
Molar Flow	(kgmol/h)	8.8133	100.0000	0.0000	108.1595
Mass Flow	(kg/h)	229.1748	2895.0001	0.0000	3277.9658
Std Ideal Liq Vol Flow	(m3/h)	0.2956	3.2914	0.0000	3.3165
Molar Enthalpy	(kJ/kgmol)	-2.382e+005	-6.986	-1.941e+004	-1.941e+004
Molar Entropy	(kJ/kgmol-C)	219.5	118.2	158.0	158.0
Heat Flow	(kJ/h)	-2.0990e+06	-6.9865e+02	0.0000e-01	-2.0997e+06

PROPERTIES

Name		Anode Out	Air to AGO	Dummy 2	To Exchanger 4	
Molecular Weight		26.00	28.95	30.31	30.31	
Molar Density	(kgmol/m3)	1.320e-002	4.089e-002	2.502e-002	2.502e-002	
Mass Density	(kg/m3)	0.3432	1.184	0.7583	0.7583	
Act. Volume Flow	(m3/h)	667.7	2446	0.0000	4323	
Mass Enthalpy	(kJ/kg)	-9159	-0.2413	-640.5	-640.5	
Mass Entropy	(kJ/kg-C)	8.442	4.082	5.214	5.214	
Heat Capacity	(kJ/kgmol-C)	43.90	28.73	31.10	31.10	
Mass Heat Capacity	(kJ/kg-C)	1.688	0.9924	1.026	1.026	
Lower Heating Value	(kJ/kgmol)	4.555e+004	0.0000	5.886e-020	5.886e-020	
Mass Lower Heating Value	(kJ/kg)	1752		1.942e-021	1.942e-021	
Phase Fraction [Vol. Basis]						
Phase Fraction [Mass Basis]		4.941e-324	4.941e-324	2.122e-314	2.122e-314	
Partial Pressure of CO2	(kPa)	38.21	0.0000	0.0000	3.376	
Cost Based on Flow	(Cost/s)	0.0000	0.0000	0.0000	0.0000	
Act. Gas Flow	(ACT_m3/h)	667.7	2446		4323	
Avg. Liq. Density	(kgmol/m3)	29.82	30.38		32.61	
Specific Heat	(kJ/kgmol-C)	43.90	28.73	31.10	31.10	
Std. Gas Flow	(STD_m3/h)	208.4	2364	0.0000	2557	
Std. Ideal Liq. Mass Density	(kg/m3)	775.3	879.6	988.4	988.4	
Act. Liq. Flow	(m3/s)			0.0000	0.0000	
Z Factor		1.000	0.9997			
Watson K		9.121	5.914	5.476	5.476	
User Property						
Partial Pressure of H2S	(kPa)	0.0000	0.0000	0.0000	0.0000	
Cp/(Cp - R)		1.234	1.407	1.365	1.365	
Cp/Cv		1.234	1.410	1.366	1.366	
Heat of Vap.	(kJ/kgmol)	5.887e+004	5710	1.605e+004	1.605e+004	
Kinematic Viscosity	(cSt)	97.98	15.91	5.098	36.15	
Liq. Mass Density (Std. Cond)	(kg/m3)	809.6				
Liq. Vol. Flow (Std. Cond)	(m3/h)	0.2831		0.0000		
Liquid Fraction		0.0000	0.0000	1.000	0.0000	
Molar Volume	(m3/kgmol)	75.76	24.46	39.97	39.97	
Mass Heat of Vap.	(kJ/kg)	2264	197.2	529.4	529.4	
Phase Fraction [Molar Basis]		1.0000	1.0000	0.0000	1.0000	

Gibbs Reactor: Anode Gas Oxidizer (continued)

PROPERTIES

Name		Anode Out	Air to AGO	Dummy 2	To Exchanger 4	
Surface Tension	(dyne/cm)					
Thermal Conductivity	(W/m-K)	9.026e-002	2.472e-002	5.284e-002	3.800e-002	
Viscosity	(cP)	3.363e-002	1.884e-002	3.866e-003	2.741e-002	
Cv (Semi-Ideal)	(kJ/kgmol-C)	35.58	20.41	22.78	22.78	
Mass Cv (Semi-Ideal)	(kJ/kg-C)	1.368	0.7052	0.7518	0.7518	
Cv	(kJ/kgmol-C)	35.57	20.37	22.77	22.77	
Mass Cv	(kJ/kg-C)	1.368	0.7037	0.7512	0.7512	
Cv (Ent. Method)	(kJ/kgmol-C)	35.53	20.33		22.73	
Mass Cv (Ent. Method)	(kJ/kg-C)	1.366	0.7023		0.7499	
Cp/Cv (Ent. Method)		1.236	1.413		1.368	
Reid VP at 37.8 C	(kPa)					
True VP at 37.8 C	(kPa)	9.240e+004		1.211e+005	1.211e+005	
Liq. Vol. Flow - Sum(Std. Cond)	(m3/h)	0.2833	0.0000	0.0000	0.0000	

DYNAMICS

Vessel Parameters: Initialize from Product

Vessel Volume	(m3)		Level Calculator		Vertical cylinder
Vessel Diameter	(m)		Fraction Calculator		Use levels and nozzles
Vessel Height	(m)		Feed Delta P	(kPa)	0.0000
Liquid Level Percent	(%)	50.00	Vessel Pressure	(kPa)	101.3

Holdup: Vessel Levels

Phase	Level (m)	Percent (%)	Volume (m3)
Vapour			0.0000
Liquid			0.0000
Aqueous			0.0000

Holdup: Details

Phase	Accumulation (kgmol/h)	Moles (kgmol)	Volume (m3)
Vapour	0.0000	0.0000	0.0000
Liquid	0.0000	0.0000	0.0000
Aqueous	0.0000	0.0000	0.0000
Total	**0.0000**	**0.0000**	**0.0000**

NOTES

Valve: Control Valve

CONNECTIONS

Inlet Stream

STREAM NAME	FROM UNIT OPERATION	
To Control Valve	Tee	TEE-100

Outlet Stream

STREAM NAME	TO UNIT OPERATION
To Distribution	

PARAMETERS

Physical Properties

Pressure Drop:	2997 kPa		

User Variables

RATING

Sizing

Sizing Conditions

Inlet Pressure	3447 kPa	Molecular Weight	16.58	Current	
Valve Opening	50.00 %	Delta P	2997 kPa	Flow Rate	0.0000 kg/h

Valve Manufacturer and Valve Type

Manufacturer: Universal Gas Sizing	Type:

Valve Operating Characteristic and Sizing Method

Linear				Sizing Method:	Cv (standard) cal/min.sqrt(psi)
C1	25.00	Km	0.9000	Cv	Cg

Nozzle Parameters

Base Elevation Relative to Ground Level: 0.0000 m

		To Control Valve	To Distribution	
Diameter	(m)	5.000e-002	5.000e-002	
Elevation (Base)	(m)	0.0000	0.0000	
Elevation (Ground)	(m)	0.0000	0.0000	
Elevation (% of Height)	(%)			

CONDITIONS

Name		To Control Valve	To Distribution		
Vapour		1.0000	1.0000		
Temperature	(C)	104.4823	96.7417		
Pressure	(kPa)	3447.0000	450.0000		
Molar Flow	(kgmol/h)	0.0000	0.0000		
Mass Flow	(kg/h)	0.0000	0.0000		
Std Ideal Liq Vol Flow	(m3/h)	0.0000	0.0000		
Molar Enthalpy	(kJ/kgmol)	-7.038e+004	-7.038e+004		
Molar Entropy	(kJ/kgmol-C)	162.8	179.6		
Heat Flow	(kJ/h)	0.0000e-01	0.0000e-01		

PROPERTIES

Name		To Control Valve	To Distribution			
Molecular Weight		16.58	16.58			
Molar Density	(kgmol/m3)	1.116	0.1467			
Mass Density	(kg/m3)	18.50	2.433			
Act. Volume Flow	(m3/h)	0.0000	0.0000			
Mass Enthalpy	(kJ/kg)	-4244	-4244			
Mass Entropy	(kJ/kg-C)	9.820	10.83			
Heat Capacity	(kJ/kgmol-C)	41.42	39.31			
Mass Heat Capacity	(kJ/kg-C)	2.498	2.371			

Valve: Control Valve (continued)

PROPERTIES

Name	To Control Valve	To Distribution			
Lower Heating Value (kJ/kgmol)	7.833e+005	7.833e+005			
Mass Lower Heating Value (kJ/kg)	4.723e+004	4.723e+004			
Phase Fraction [Vol. Basis]					
Phase Fraction [Mass Basis]	4.941e-324	4.941e-324			
Partial Pressure of CO2 (kPa)	3.447	0.4500			
Cost Based on Flow (Cost/s)	0.0000	0.0000			
Act. Gas Flow (ACT_m3/h)	0.0000	0.0000			
Avg. Liq. Density (kgmol/m3)					
Specific Heat (kJ/kgmol-C)	41.42	39.31			
Std. Gas Flow (STD_m3/h)	0.0000	0.0000			
Std. Ideal Liq. Mass Density (kg/m3)	311.4	311.4			
Act. Liq. Flow (m3/s)					
Z Factor	0.9838	0.9973			
Watson K	18.77	18.77			
User Property					
Partial Pressure of H2S (kPa)	0.0000	0.0000			
Cp/(Cp - R)	1.251	1.268			
Cp/Cv	1.317	1.277			
Heat of Vap. (kJ/kgmol)	4192	8909			
Kinematic Viscosity (cSt)	0.7774	5.640			
Liq. Mass Density (Std. Cond) (kg/m3)					
Liq. Vol. Flow (Std. Cond) (m3/h)	0.0000	0.0000			
Liquid Fraction	0.0000	0.0000			
Molar Volume (m3/kgmol)	0.8961	6.816			
Mass Heat of Vap. (kJ/kg)	252.8	537.3			
Phase Fraction [Molar Basis]	1.0000	1.0000			
Surface Tension (dyne/cm)					
Thermal Conductivity (W/m-K)	4.741e-002	4.428e-002			
Viscosity (cP)	1.438e-002	1.372e-002			
Cv (Semi-Ideal) (kJ/kgmol-C)	33.10	30.99			
Mass Cv (Semi-Ideal) (kJ/kg-C)	1.996	1.869			
Cv (kJ/kgmol-C)	31.45	30.77			
Mass Cv (kJ/kg-C)	1.897	1.856			
Cv (Ent. Method) (kJ/kgmol-C)	31.22	30.76			
Mass Cv (Ent. Method) (kJ/kg-C)	1.883	1.855			
Cp/Cv (Ent. Method)	1.327	1.278			
Reid VP at 37.8 C (kPa)					
True VP at 37.8 C (kPa)					
Liq. Vol. Flow - Sum(Std. Cond) (m3/h)	0.0000	0.0000			

DYNAMICS

Dynamic Specifications

Total Delta P (kPa)	2997	Not Active
Pressure Flow Relation		Active

Dynamic Parameters

Valve Opening (%)	50.00		Mass Flow (kg/h)	0.0000	
Conductance (USGPM)			Friction Delta P (kPa)		

Pipe Model Parameters

Material	Cast Iron		Darcy Friction Factor		
Roughness (m)	2.590e-004		Pipe k (kg/hr/sqrt(kPa-kg/m3))	0.0000	
Pipe Length (m)	0.0000		Velocity (m/s)	0.0000	
Feed Diameter (m)	5.000e-002		Reynolds Number	0.0000	

Hold-Up Volume: 0.0000 m3

Valve: Control Valve (continued)

Phase	Accumulation (kgmol/h)	Moles (kgmol)	Volume (m3)
Vapour	0.0000	0.0000	0.0000
Liquid	0.0000	0.0000	0.0000
Aqueous	0.0000	0.0000	0.0000
Total	**0.0000**	**0.0000**	**0.0000**

Actuator Parameters

Parameters Mode: Instantaneous

Actuator Time Constant	(seconds)	1.000	Actuator Linear Rate	1.000e-002
Valve Stickiness Time Constant	(seconds)			

Activator Position

Fail Position: None

	Min (%)	Max (%)	Current (%)	Desired (%)	Offset (%)
Valve	0.00	100.00	50.00		0.00
Actuator	0.00	100.00	50.00	50.00	

MCFC

CONNECTIONS

Feed Stream

STREAM NAME	FROM UNIT OPERATION	
Feed1		
To Anode	Gibbs Reactor	Reformer
Cathode In		
Cathode In	Recycle	RCY-1

Product Stream

STREAM NAME	TO UNIT OPERATION	
Anode out		
Anode Out	Gibbs Reactor	Anode Gas Oxidizer
Cathode Out		
Cathode Out	Cooler	Exchanger5
Energy Out		
fuel cell heat		

CODE

```
Sub Initialize()
End Sub
Sub Execute()
End Sub
Sub StatusQuery()
End Sub
```

User Variables

Name	Variable Type	Value	Units	Enabled
Current Density	CurrentDensity	100000	uA/cm2	Yes
number of cells	Index	400		Yes
Electrolyte Thickness	Length	0.2000	m	Yes
Ambient Temperature	Temperature	25.00	C	Yes
Geometric Area	Index	9000		Yes
Open Circuit Voltage	User	0.8162		Yes
Cell Operating Voltage	User	0.2099		Yes
Electrical Efficiency	User	0.6019		Yes
Fuel Cell Work	User	0.1043		Yes
Fuel Cell Useful heat	User	-3.964e+006		Yes

Properties

Name		To Anode	Cathode In	Anode Out	Cathode Out	fuel cell heat
Vapour Fraction		1.0000	1.0000	1.0000	1.0000	
Temperature	(C)	650.1	650.0	650.1	650.0	
Pressure	(kPa)	101.3	101.3	101.3	101.3	
Actual Vol. Flow	(m3/h)	475.2	8195	667.7	6881	
Mass Enthalpy	(kJ/kg)	-7292	-168.0	-9159	20.05	
Mass Entropy	(kJ/kg-C)	15.71	5.903	8.442	5.914	
Molecular Weight		12.22	30.31	26.00	29.66	
Molar Density	(kgmol/m3)	1.320e-002	1.320e-002	1.320e-002	1.320e-002	
Mass Density	(kg/m3)	0.1613	0.4000	0.3432	0.3914	
Std Ideal Liq Mass Density	(kg/m3)	427.1	988.4	775.3	973.6	
Liq Mass Density @Std Cond	(kg/m3)			809.6		
Molar Heat Capacity	(kJ/kgmol-C)	35.75	34.44	43.90	33.94	

MCFC: MCFC (continued)

Properties

Mass Heat Capacity	(kJ/kg-C)	2.925	1.136	1.688	1.144	
Thermal Conductivity	(W/m-K)	0.1844	6.484e-002	9.026e-002	6.436e-002	
Viscosity	(cP)	2.672e-002	4.447e-002	3.363e-002	4.388e-002	
Surface Tension	(dyne/cm)					
Specific Heat	(kJ/kgmol-C)	35.75	34.44	43.90	33.94	
Z Factor		1.000	1.000	1.000	1.000	
Vap. Frac. (molar basis)		1.0000	1.0000	1.0000	1.0000	
Vap. Frac. (mass basis)		1.0000	1.0000	1.0000	1.0000	
Vap. Frac. (Volume Basis)		1.0000	1.0000	1.0000	1.0000	
Molar Volume	(m3/kgmol)	75.77	75.77	75.76	75.77	
Act.Gas Flow	(ACT_m3/h)	475.2	8195	667.7	6881	
Act.Liq.Flow	(m3/s)					
Std.Liq.Vol.Flow	(m3/h)			0.2831		
Std.Gas Flow	(STD_m3/h)	148.3	2557	208.4	2147	
Watson K		14.50	5.476	9.121	5.483	
Kinematic Viscosity	(cSt)	165.6	111.2	97.98	112.1	
Cp/Cv		1.303	1.318	1.234	1.325	
Lower Heating Value	(kJ/kgmol)	1.639e+005	5.886e-020	4.555e+004	7.010e-020	
Mass Lower Heating Value	(kJ/kg)	1.340e+004	1.942e-021	1752	2.364e-021	
Liquid Fraction		0.0000	0.0000	0.0000	0.0000	
Partial Pressure of CO2	(kPa)	8.170	3.376	38.21	1.261	
Avg.Liq.Density	(kgmol/m3)	34.94	32.61	29.82	32.83	
Heat Of Vap.	(kJ/kgmol)	3.090e+004	1.605e+004	5.887e+004	1.606e+004	
Mass Heat Of Vap.	(kJ/kg)	2528	529.4	2264	541.6	

NOTES

Gibbs Reactor: Pre-reformer

CONNECTIONS

Inlet Stream Connections

Stream Name	From Unit Operation	
To Prereformer	Heater	Exchanger2

Outlet Stream Connections

Stream Name	To Unit Operation	
To Mixer2	Mixer:	Mixer2
Bottoms		

Energy Stream Connections

Stream Name	From Unit Operation

PARAMETERS

Physical Parameters		Optional Heat Transfer:	Heating
Delta P	Vessel Volume	Duty	Energy Stream
0.0000 kPa		0.0000 kJ/h	

User Variables

REACTION DETAILS

MOLE FLOW SPECIFICATIONS

Components	Total Feed (kgmol/h)	Total Prod (kgmol/h)	Inerts	Frac Spec	Fixed Spec (kgmol/h)
Methane	1.042	0.7652	No		
Ethane	6.513e-003	4.065e-006	No		
Propane	2.171e-003	6.656e-011	No		
CO	0.0000	1.275e-002	No		
CO2	1.085e-003	0.2847	No		
Air	0.0000	2.901e-030	No		
Nitrogen	3.365e-002	3.365e-002	No		
Oxygen	0.0000	2.901e-030	No		
H2O	3.256	2.676	No		
Hydrogen	0.0000	1.162	No		

ATOM MATRIX DATA

	C	H	O	N		
Methane	1.000	4.000	0.0000	0.0000		
Ethane	2.000	6.000	0.0000	0.0000		
Propane	3.000	8.000	0.0000	0.0000		
CO	1.000	0.0000	1.000	0.0000		
CO2	1.000	0.0000	2.000	0.0000		
Air	0.0000	0.0000	2.000	0.0000		
Nitrogen	0.0000	0.0000	0.0000	2.000		
Oxygen	0.0000	0.0000	2.000	0.0000		
H2O	0.0000	2.000	1.000	0.0000		
Hydrogen	0.0000	2.000	0.0000	0.0000		

RATING

Sizing

Cylinder	Vertical	Reactor has a Boot: No
Volume	Diameter	Height

Nozzles

Base Elevation Relative to Ground Level	0.0000 m	Diameter	Height

Gibbs Reactor: Pre reformer (continued)

		To Prereformer	To Mixer2	Bottoms
Diameter	(m)	5.000e-002	5.000e-002	5.000e-002
Elevation (Base)	(m)	0.0000	0.0000	0.0000
Elevation (Ground)	(m)	0.0000	0.0000	0.0000
Elevation (% of Height)	(%)			

CONDITIONS

Name		To Prereformer	Bottoms	To Mixer2	
Vapour		1.0000	0.0000	1.0000	
Temperature	(C)	700.0000	429.7062	429.7062	
Pressure	(kPa)	101.3250	101.3250	101.3250	
Molar Flow	(kgmol/h)	4.3419	0.0000	4.9347	
Mass Flow	(kg/h)	76.6652	0.0000	76.6653	
Std Ideal Liq Vol Flow	(m3/h)	0.1166	0.0000	0.1396	
Molar Enthalpy	(kJ/kgmol)	-1.718e+005	-1.512e+005	-1.512e+005	
Molar Entropy	(kJ/kgmol-C)	228.0	203.3	203.3	
Heat Flow	(kJ/h)	-7.4605e+05	0.0000e-01	-7.4605e+05	

PROPERTIES

Name		To Prereformer	Bottoms	To Mixer2		
Molecular Weight		17.66	15.54	15.54		
Molar Density	(kgmol/m3)	1.252e-002	1.734e-002	1.734e-002		
Mass Density	(kg/m3)	0.2211	0.2695	0.2695		
Act. Volume Flow	(m3/h)	346.7	0.0000	284.5		
Mass Enthalpy	(kJ/kg)	-9731	-9731	-9731		
Mass Entropy	(kJ/kg-C)	12.91	13.08	13.08		
Heat Capacity	(kJ/kgmol-C)	48.34	39.61	39.61		
Mass Heat Capacity	(kJ/kg-C)	2.738	2.550	2.550		
Lower Heating Value	(kJ/kgmol)	1.958e+005	1.822e+005	1.822e+005		
Mass Lower Heating Value	(kJ/kg)	1.109e+004	1.173e+004	1.173e+004		
Phase Fraction [Vol. Basis]						
Phase Fraction [Mass Basis]		4.941e-324	2.122e-314	2.122e-314		
Partial Pressure of CO2	(kPa)	2.533e-002	0.0000	5.846		
Cost Based on Flow	(Cost/s)	0.0000	0.0000	0.0000		
Act. Gas Flow	(ACT_m3/h)	346.7		284.5		
Avg. Liq. Density	(kgmol/m3)	37.24		35.34		
Specific Heat	(kJ/kgmol-C)	48.34	39.61	39.61		
Std. Gas Flow	(STD_m3/h)	102.7	0.0000	116.7		
Std. Ideal Liq. Mass Density	(kg/m3)	657.6	549.0	549.0		
Act. Liq. Flow	(m3/s)		0.0000	0.0000		
Z Factor		0.9999				
Watson K		18.77	16.40	16.40		
User Property						
Partial Pressure of H2S	(kPa)	0.0000	0.0000	0.0000		
Cp/(Cp - R)		1.208	1.266	1.266		
Cp/Cv		1.208	1.266	1.266		
Heat of Vap.	(kJ/kgmol)	5.142e+004	4.959e+004	4.959e+004		
Kinematic Viscosity	(cSt)	133.2	8.816	84.39		
Liq. Mass Density (Std. Cond)	(kg/m3)	721.5	436.7	436.7		
Liq. Vol. Flow (Std. Cond)	(m3/h)	0.1063	0.0000	0.1753		
Liquid Fraction		0.0000	1.000	0.0000		
Molar Volume	(m3/kgmol)	79.85	57.66	57.66		
Mass Heat of Vap.	(kJ/kg)	2912	3192	3192		
Phase Fraction [Molar Basis]		1.0000	0.0000	1.0000		
Surface Tension	(dyne/cm)					
Thermal Conductivity	(W/m-K)	0.1021	0.1487	9.889e-002		
Viscosity	(cP)	2.945e-002	2.375e-003	2.274e-002		
Cv (Semi-Ideal)	(kJ/kgmol-C)	40.02	31.30	31.30		
Mass Cv (Semi-Ideal)	(kJ/kg-C)	2.267	2.015	2.015		
Cv	(kJ/kgmol-C)	40.01	31.28	31.28		

Gibbs Reactor: Pre reformer (continued)

PROPERTIES

Name		To Pre-reformer	Bottoms	To Mixer2		
Mass Cv	(kJ/kg-C)	2.266	2.013	2.013		
Cv (Ent. Method)	(kJ/kgmol-C)	39.97		31.23		
Mass Cv (Ent. Method)	(kJ/kg-C)	2.263		2.010		
Cp/Cv (Ent. Method)		1.209		1.268		
Reid VP at 37.8 C	(kPa)					
True VP at 37.8 C	(kPa)					
Liq. Vol. Flow - Sum(Std. Cond)	(m3/h)	0.1063	0.0000	0.1762		

DYNAMICS

Vessel Parameters: Initialize from Product

Vessel Volume	(m3)		Level Calculator		Vertical cylinder
Vessel Diameter	(m)		Fraction Calculator		Use levels and nozzles
Vessel Height	(m)		Feed Delta P	(kPa)	0.0000
Liquid Level Percent	(%)	50.00	Vessel Pressure	(kPa)	101.3

Holdup: Vessel Levels

Phase	Level (m)	Percent (%)	Volume (m3)
Vapour			0.0000
Liquid			0.0000
Aqueous			0.0000

Holdup: Details

Phase	Accumulation (kgmol/h)	Moles (kgmol)	Volume (m3)
Vapour	0.0000	0.0000	0.0000
Liquid	0.0000	0.0000	0.0000
Aqueous	0.0000	0.0000	0.0000
Total	**0.0000**	**0.0000**	**0.0000**

NOTES

Gibbs Reactor: Reformer

CONNECTIONS

Inlet Stream Connections

Stream Name	From Unit Operation	
To Reformer	Heater	Exchanger 3

Outlet Stream Connections

Stream Name	To Unit Operation	
To Anode	MCFC:	MCFC
Dummy Liquid		

Energy Stream Connections

Stream Name	From Unit Operation

PARAMETERS

Physical Parameters		Optional Heat Transfer:	Heating
Delta P	Vessel Volume	Duty	Energy Stream
0.0000 kPa		0.0000 kJ/h	

User Variables

REACTION DETAILS

MOLE FLOW SPECIFICATIONS

Components	Total Feed (kgmol/h)	Total Prod (kgmol/h)	Inerts	Frac Spec	Fixed Spec (kgmol/h)
Methane	0.7652	9.667e-002	No		
Ethane	4.065e-006	2.839e-007	No		
Propane	6.656e-011	2.279e-012	No		
CO	1.275e-002	0.4603	No		
CO2	0.2847	0.5057	No		
Air	2.901e-030	9.110e-023	No		
Nitrogen	3.365e-002	3.365e-002	No		
Oxygen	2.901e-030	9.110e-023	No		
H2O	2.676	1.787	No		
Hydrogen	1.162	3.389	No		

ATOM MATRIX DATA

	C	H	O	N		
Methane	1.000	4.000	0.0000	0.0000		
Ethane	2.000	6.000	0.0000	0.0000		
Propane	3.000	8.000	0.0000	0.0000		
CO	1.000	0.0000	1.000	0.0000		
CO2	1.000	0.0000	2.000	0.0000		
Air	0.0000	0.0000	2.000	0.0000		
Nitrogen	0.0000	0.0000	0.0000	2.000		
Oxygen	0.0000	0.0000	2.000	0.0000		
H2O	0.0000	2.000	1.000	0.0000		
Hydrogen	0.0000	2.000	0.0000	0.0000		

RATING

Sizing

Cylinder	Vertical	Reactor has a Boot: No
Volume	Diameter	Height

Nozzles

Base Elevation Relative to Ground Level	0.0000 m	Diameter	Height

Gibbs Reactor: Reformer (continued)

		To Reformer	To Anode	Dummy Liquid
Diameter	(m)	5.000e-002	5.000e-002	5.000e-002
Elevation (Base)	(m)	0.0000	0.0000	0.0000
Elevation (Ground)	(m)	0.0000	0.0000	0.0000
Elevation (% of Height)	(%)			

CONDITIONS

Name		To Reformer	Dummy Liquid	To Anode	
Vapour		1.0000	0.0000	1.0000	
Temperature	(C)	1262.0000	650.1032	650.1032	
Pressure	(kPa)	101.3250	101.3250	101.3250	
Molar Flow	(kgmol/h)	4.9347	0.0000	6.2718	
Mass Flow	(kg/h)	76.6653	0.0000	76.6659	
Std Ideal Liq Vol Flow	(m3/h)	0.1396	0.0000	0.1795	
Molar Enthalpy	(kJ/kgmol)	-1.133e+005	-8.914e+004	-8.914e+004	
Molar Entropy	(kJ/kgmol-C)	238.3	192.0	192.0	
Heat Flow	(kJ/h)	-5.5906e+05	0.0000e-01	-5.5906e+05	

PROPERTIES

Name		To Reformer	Dummy Liquid	To Anode		
Molecular Weight		15.54	12.22	12.22		
Molar Density	(kgmol/m3)	7.938e-003	1.320e-002	1.320e-002		
Mass Density	(kg/m3)	0.1233	0.1613	0.1613		
Act. Volume Flow	(m3/h)	621.7	0.0000	475.2		
Mass Enthalpy	(kJ/kg)	-7292	-7292	-7292		
Mass Entropy	(kJ/kg-C)	15.34	15.71	15.71		
Heat Capacity	(kJ/kgmol-C)	51.44	35.75	35.75		
Mass Heat Capacity	(kJ/kg-C)	3.311	2.925	2.925		
Lower Heating Value	(kJ/kgmol)	1.822e+005	1.639e+005	1.639e+005		
Mass Lower Heating Value	(kJ/kg)	1.173e+004	1.340e+004	1.340e+004		
Phase Fraction [Vol. Basis]						
Phase Fraction [Mass Basis]		4.941e-324	2.122e-314	2.122e-314		
Partial Pressure of CO2	(kPa)	5.846	0.0000	8.170		
Cost Based on Flow	(Cost/s)	0.0000	0.0000	0.0000		
Act. Gas Flow	(ACT_m3/h)	621.7		475.2		
Avg. Liq. Density	(kgmol/m3)	35.34		34.94		
Specific Heat	(kJ/kgmol-C)	51.44	35.75	35.75		
Std. Gas Flow	(STD_m3/h)	116.7	0.0000	148.3		
Std. Ideal Liq. Mass Density	(kg/m3)	549.0	427.1	427.1		
Act. Liq. Flow	(m3/s)		0.0000	0.0000		
Z Factor		1.000				
Watson K		16.40	14.50	14.50		
User Property						
Partial Pressure of H2S	(kPa)	0.0000	0.0000	0.0000		
Cp/(Cp - R)		1.193	1.303	1.303		
Cp/Cv		1.193	1.303	1.303		
Heat of Vap.	(kJ/kgmol)	4.959e+004	3.090e+004	3.090e+004		
Kinematic Viscosity	(cSt)	328.1	11.47	165.6		
Liq. Mass Density (Std. Cond)	(kg/m3)	437.4				
Liq. Vol. Flow (Std. Cond)	(m3/h)	0.1753	0.0000			
Liquid Fraction		0.0000	1.000	0.0000		
Molar Volume	(m3/kgmol)	126.0	75.77	75.77		
Mass Heat of Vap.	(kJ/kg)	3192	2528	2528		
Phase Fraction [Molar Basis]		1.0000	0.0000	1.0000		
Surface Tension	(dyne/cm)					
Thermal Conductivity	(W/m-K)	0.1872	6.922e-002	0.1844		
Viscosity	(cP)	4.046e-002	1.851e-003	2.672e-002		
Cv (Semi-Ideal)	(kJ/kgmol-C)	43.12	27.43	27.43		
Mass Cv (Semi-Ideal)	(kJ/kg-C)	2.776	2.244	2.244		
Cv	(kJ/kgmol-C)	43.12	27.43	27.43		

Gibbs Reactor: Reformer (continued)

PROPERTIES

Name		To Reformer	Dummy Liquid	To Anode		
Mass Cv	(kJ/kg-C)	2.776	2.244	2.244		
Cv (Ent. Method)	(kJ/kgmol-C)	43.08		27.39		
Mass Cv (Ent. Method)	(kJ/kg-C)	2.773		2.241		
Cp/Cv (Ent. Method)		1.194		1.305		
Reid VP at 37.8 C	(kPa)					
True VP at 37.8 C	(kPa)					
Liq. Vol. Flow - Sum(Std. Cond)	(m3/h)	0.1762	0.0000	0.0000		

DYNAMICS

Vessel Parameters: Initialize from Product

Vessel Volume	(m3)		Level Calculator		Vertical cylinder
Vessel Diameter	(m)		Fraction Calculator		Use levels and nozzles
Vessel Height	(m)		Feed Delta P	(kPa)	0.0000
Liquid Level Percent	(%)	50.00	Vessel Pressure	(kPa)	101.3

Holdup: Vessel Levels

Phase	Level (m)	Percent (%)	Volume (m3)
Vapour			0.0000
Liquid			0.0000
Aqueous			0.0000

Holdup: Details

Phase	Accumulation (kgmol/h)	Moles (kgmol)	Volume (m3)
Vapour	0.0000	0.0000	0.0000
Liquid	0.0000	0.0000	0.0000
Aqueous	0.0000	0.0000	0.0000
Total	**0.0000**	**0.0000**	**0.0000**

NOTES

Expander: Turbo Expander

CONNECTIONS

Inlet Stream

STREAM NAME	FROM UNIT OPERATION	
To Expander	Tee	TEE-100

Outlet Stream

STREAM NAME	TO UNIT OPERATION	
Low Pressure Pipeline	Tee	TEE-101

Energy Stream

STREAM NAME	TO UNIT OPERATION
Expander Duty	

PARAMETERS

Duty:	1.5085e+02 kW		Speed:	8.800e+004 rpm	
Adiabatic Eff.:	70.00		Polytropic Eff.:	64.48	
Adiabatic Head:	3.077e+004 m		Polytropic Head:	3.340e+004 m	
Adiabatic Fluid Head:	301.7 kJ/kg		Polytropic Fluid Head:	327.5 kJ/kg	
Polytropic Exp.	1.177	Isentropic Exp.	1.311	Poly Head Factor	1.003

User Variables

RATING

Curves

Expander Speed: 8.800e+004 rpm	Efficiency: Adiabatic	Curves Enabled: Yes

Curve Name	Activate

Speed:

Flow	Head	Efficiency (%)

Flow Limits

Surge Curve: Inactive

Speed	Flow	Speed	Flow	Speed	Flow

Stone Wall Curve: Inactive

Speed	Flow	Speed	Flow	Speed	Flow

Surge Flow Rate		Field Flow Rate	139.0 ACT_m3/h	Stone Wall Flow	Expander Volume 0.0000 m3

Nozzle Parameters

Base Elevation Relative to Ground Level 0.0000 m

		To Expander	Low Pressure Pipeline	
Diameter	(m)	5.000e-002	5.000e-002	
Elevation (Base)	(m)	0.0000	0.0000	
Elevation (Ground)	(m)	0.0000	0.0000	

Inertia

Rotational inertia (kg-m2)	6.000	Radius of gyration (m)	0.2000	Mass (kg)	150.0	Friction loss factor (kg-m2/s)	6.000e-003

CONDITIONS

Name		To Expander	Low Pressure Pipeline	Expander Duty	
Vapour		1.0000	1.0000		
Temperature	(C)	104.4823	3.0001		
Pressure	(kPa)	3447.0000	450.0000		
Molar Flow	(kgmol/h)	155.0694	155.0694		
Mass Flow	(kg/h)	2571.3934	2571.3934		
Std Ideal Liq Vol Flow	(m3/h)	8.2579	8.2579		

Expander: Turbo Expander (continued)

CONDITIONS

Molar Enthalpy	(kJ/kgmol)	-7.038e+004	-7.388e+004		
Molar Entropy	(kJ/kgmol-C)	162.8	168.7		
Heat Flow	(kJ/h)	-1.0913e+07	-1.1457e+07	5.4306e+05	

PROPERTIES

Name		To Expander	Low Pressure Pipeline			
Molecular Weight		16.58	16.58			
Molar Density	(kgmol/m3)	1.116	0.1980			
Mass Density	(kg/m3)	18.50	3.283			
Act. Volume Flow	(m3/h)	139.0	783.2			
Mass Enthalpy	(kJ/kg)	-4244	-4455			
Mass Entropy	(kJ/kg-C)	9.820	10.18			
Heat Capacity	(kJ/kgmol-C)	41.42	35.69			
Mass Heat Capacity	(kJ/kg-C)	2.498	2.152			
Lower Heating Value	(kJ/kgmol)	7.833e+005	7.833e+005			
Mass Lower Heating Value	(kJ/kg)	4.723e+004	4.723e+004			
Phase Fraction [Vol. Basis]						
Phase Fraction [Mass Basis]		4.941e-324	4.941e-324			
Partial Pressure of CO2	(kPa)	3.447	0.4500			
Cost Based on Flow	(Cost/s)	0.0000	0.0000			
Act. Gas Flow	(ACT_m3/h)	139.0	783.2			
Avg. Liq. Density	(kgmol/m3)	18.78	18.78			
Specific Heat	(kJ/kgmol-C)	41.42	35.69			
Std. Gas Flow	(STD_m3/h)	3667	3667			
Std. Ideal Liq. Mass Density	(kg/m3)	311.4	311.4			
Act. Liq. Flow	(m3/s)					
Z Factor		0.9838	0.9900			
Watson K		18.77	18.77			
User Property						
Partial Pressure of H2S	(kPa)	0.0000	0.0000			
Cp/(Cp - R)		1.251	1.304			
Cp/Cv		1.317	1.326			
Heat of Vap.	(kJ/kgmol)	4192	8909			
Kinematic Viscosity	(cSt)	0.7774	3.266			
Liq. Mass Density (Std. Cond)	(kg/m3)					
Liq. Vol. Flow (Std. Cond)	(m3/h)					
Liquid Fraction		0.0000	0.0000			
Molar Volume	(m3/kgmol)	0.8961	5.051			
Mass Heat of Vap.	(kJ/kg)	252.8	537.3			
Phase Fraction [Molar Basis]		1.0000	1.0000			
Surface Tension	(dyne/cm)					
Thermal Conductivity	(W/m-K)	4.741e-002	3.046e-002			
Viscosity	(cP)	1.438e-002	1.072e-002			
Cv (Semi-Ideal)	(kJ/kgmol-C)	33.10	27.37			
Mass Cv (Semi-Ideal)	(kJ/kg-C)	1.996	1.651			
Cv	(kJ/kgmol-C)	31.45	26.92			
Mass Cv	(kJ/kg-C)	1.897	1.623			
Cv (Ent. Method)	(kJ/kgmol-C)	31.22	26.91			
Mass Cv (Ent. Method)	(kJ/kg-C)	1.883	1.623			
Cp/Cv (Ent. Method)		1.327	1.326			
Reid VP at 37.8 C	(kPa)					
True VP at 37.8 C	(kPa)					
Liq. Vol. Flow - Sum(Std. Cond)	(m3/h)	0.0000	0.0000			

DYNAMICS

Dynamic Specifications

Duty	(kJ/h)	5.431e+005	Active	Head	(m)	3.077e+004	Not Active

Appendix B

Systems Specifications

FuelCell Energy

Ultra-Clean, Efficient, Reliable Power

DFC300

Key Features

- High Efficiency
- Low Environmental Impact
- Fuel Flexibility
- High Reliability
- Quiet Operation

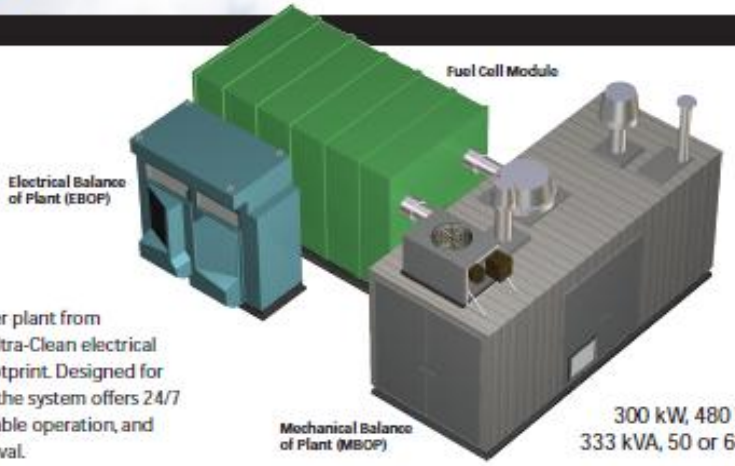

300 kW, 480 VAC,
333 kVA, 50 or 60 Hz

Advantages

The DFC®300™ stationary fuel cell power plant from FuelCell Energy provides high-quality, Ultra-Clean electrical power with 47% efficiency in a small footprint. Designed for commercial and industrial applications, the system offers 24/7 operation, easy transport, quiet and reliable operation, and easy site planning and regulatory approval.

Performance

Power Output	
Power @ Plant Rating	300 kW
Standard Output AC Voltage	480 V
Standard Frequency	60 Hz
Optional Output AC Voltages	460, 440, 420, 400, 380 V
Optional Output Frequency	50 Hz

Efficiency	
LHV	47 +/- 2 %

Available Heat	
Exhaust Temperature	700 +/- 50 °F
Exhaust Flow	3,950 lb/h
Allowable Backpressure	5 iwc
Heat Energy Available for Recovery (to 250°F) (to 120°F)	 480,000 Btu/h 808,000 Btu/h

Fuel Consumption	
Natural gas (at 930 Btu/ft³)	39 scfm
Heat rate, LHV	7,260 Btu/kWh

Water Consumption	
Average	0.9 gpm
Peak during WTS backflush	10 gpm

Water Discharge	
Average	0.45 gpm
Peak during WTS backflush	10 gpm

Pollutant Emissions	
NOx	0.01 lb/MWh
SOx	0.0001 lb/MWh
PM10	0.00002 lb/MWh

Greenhouse Gas Emissions	
CO_2	980 lb/MWh
CO_2 (with waste heat recovery)	520-680 lb/MWh

Specifications

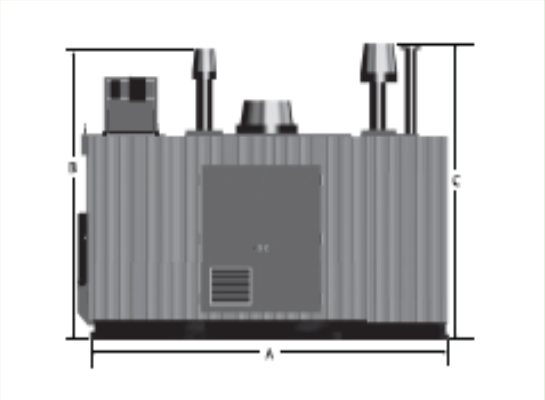

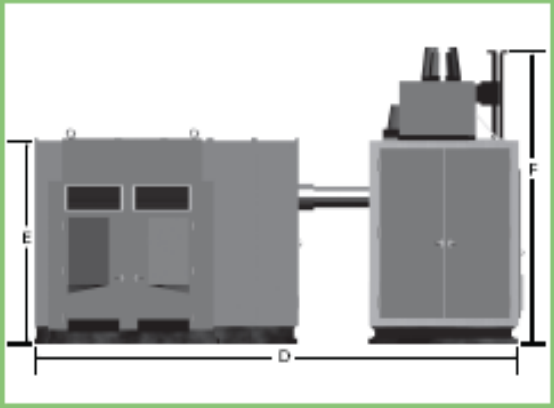

Dimensions

Front View

A	Overall Width	20.0 ft
B	Height of Air Intake Filter	15.1 ft
C	Height of Exhaust Stack (Required on units with no heat recovery)	14.5 ft

Side View

D	Overall Length	28.0 ft
E	Height of EBOP	11.8 ft
F	Height of Discharge Vent	14.5 ft

Weights

Mechanical Balance of Plant	27,000 lb
Electrical Balance of Plant	15,000 lb
Fuel Cell Module	35,000 lb

Noise Level

Standard	72 dB(A) at 10 feet
Optional	65 dB(A) at 10 feet

Experience & Capabilities

With more than 35 years of experience, FuelCell Energy is recognized as a world leader in the development, manufacture, and commercialization of fuel cells for stationary electric power generation. The result of years of research and the investment of more than $530 million, our patented, carbonate Direct FuelCell products have generated more than 200 million kilowatt hours of electrical energy to date at more than 50 locations worldwide.

FuelCell Energy's fleet of Direct FuelCell power plants are certified to or comply with a variety of commercial and industrial standards: ANSI/CSA America FC-1, UL 1741, CARB 2007, OSHA 29 CFR Part 1910, IEEE 1547, NFPA 70, NFPA 853, and California Rule 21.

Range of operation

TG		120	200	300	400
Inlet pressure max.	[bar]	60	60	60	60
	[psi]	870	870	870	870
Efficiencies max.	[%]	90	92	92	92
Cold production max.	[kW]	600	1700	3000	5000
	[HP]	804	2279	4023	6705
Flanges typical	[inches]	4/6	6/8	8/12	12/16

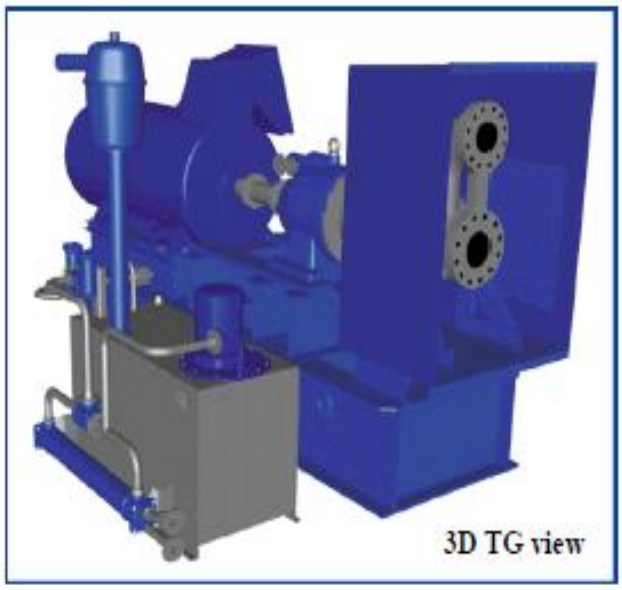

3D TG view

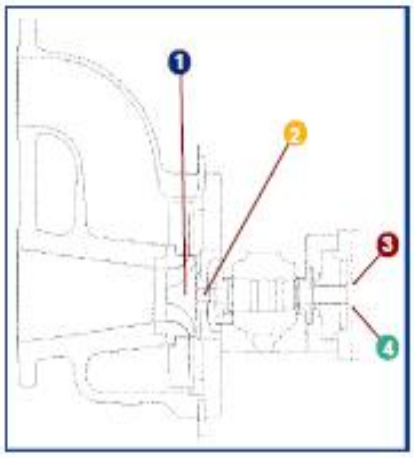

Cross-section of a TG type

1. High efficiency impeller.
2. Polygon shaft fixing.
3. High-speed coupling.
4. Epicyclical high speed, high efficiency gearbox. Rigid skid to ensure perfect alignment.

Dimensions

TG		120	200	300
A	[mm]	To be defined according to the power of the generator		
	[inch]			
B	[mm]	/	2500	2700
	[inch]		98.4	106.3
C	[mm]	/	2400	2600
	[inch]		94.5	102.3

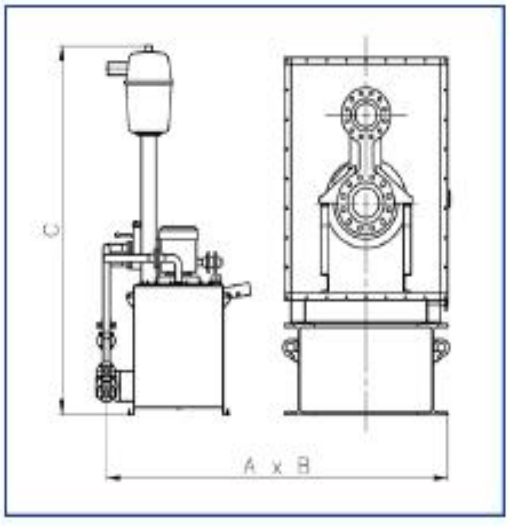

Appendix C

Derivations Calculations

Solution for the rate of WGS reaction, (R_2)

Solving for R_2,

From the material balance equations; equations (3.1), (3.2), (3.3), (3.4), (3.5), the equilibrium constant equation (3.9) can be re-rewritten in terms of known inlet compositions;

$$K_{WGS} = \frac{(N_{H2}^{i} + 3R_1 + R_2 - R_3) * (N_{CO2}^{i} + R_2 + R_3)}{(N_{H2O}^{i} - R_1 - R_2 + R_3) * (N_{CO}^{i} + R_1 - R_2)} \quad \text{A3.1}$$

Equation A3.1 can be expanded to equation A3.1and expressed as;

$$(K_{WGS} - 1)\, R_2^2 - (K_{WGS} N_{H2O}^{i} + 2 K_{WGS} R_1 + K_{WGS} N_{CO}^{i} + K_{WGS} R_3 + N_{H2}^{i} + 3R_1 + N_{CO2}^{i}) R_2 + (N_{CO}^{i} N_{H2O}^{i} K_{WGS} + N_{H2O}^{i} K_{WGS} R_1 - N_{CO}^{i} K_{WGS} R_1 - K_{WGS} R_1^2 + N_{CO}^{i} K_{WGS} R_3 + K_{WGS} R_1 R_2 - N_{H2}^{i} N_{CO2}^{i} - N_{H2}^{i} R_3 - 3N_{CO2}^{i} R_1 - 3R_1 R_3 + N_{CO2}^{i} R_3 + R_3^2) \quad \text{A3.2}$$

This is a second order polynomial solved using

R_2 was solved using the quadratic expression in equation A3.3

$$R_2 = \frac{-B \pm \sqrt{B^2 - 4AC}}{2A} \quad \text{(A3.3)}$$

The parameters A, B and C are expressed follows;

$A = \quad K_{WGS} - 1$	(A3.4)
$B = -\ (K_{WGS}\, N^i_{H2O} + 2\, K_{WGS}\, R_1 + K_{WGS}\, N^i_{CO} + K_{WGS}\, R_3 + N^i_{H2} + 3R_1 + N^i_{CO2})$	(A3.5)
$C = (K_{WGS}\, N^i_{CO} N^i_{H2O} + K_{WGS}\, N^i_{H2O} R_1 - K_{WGS}\, N^i_{CO} R_1 - K_{WGS} R_1^2 + K_{WGS} N^i_{CO} R_3 ..$ $\ldots + K_{WGS} R_1 R_3 - N^i_{H2}\, N^i_{CO2} - N^i_{H2} R_3 - 3N^i_{CO2} R_1 - 3R_1 R_3 + N^i_{CO2} R_3 + R_3^2)$	(A3.6)

Turbo Expander Design

In the current study, the performance of the turbo expander was simulated by UniSim based on specified inlet and outlet conditions of natural gas streams. It is however important to explain the mathematical model of the turbo expander.

The turbine steady flow energy equation is as given in equation (A3.7)

$$\dot{Q} - \dot{W}x = \dot{m}\,(h_2 - h_1) + \frac{1}{2}(C_2^2 - C_1^2) + g\,(Z_2 - Z_1) \qquad \text{(A3.7)}$$

The following assumptions hold for most expansion turbine design:

1. Flow process is adiabatic;
2. Negligible elevation difference between inlet and outlet stream.

Equation (A3.6) thus reduces to equation (A3.8)

$$\dot{W}_t = \dot{m}(h_{01} - h_{02}) \quad \text{(A3.8)}$$

h_o is the enthalpy at the stagnation state point related to the specific enthalpy as expressed in equation (A3.9)

$$h_0 = h + \frac{1}{2} C^2 \quad \text{(A3.9)}$$

The design of an expansion turbine is explained by the Mollier (Enthalpy-Entropy) and velocity diagrams as shown in Fig A3.1 and Fig A3.2 respectively.

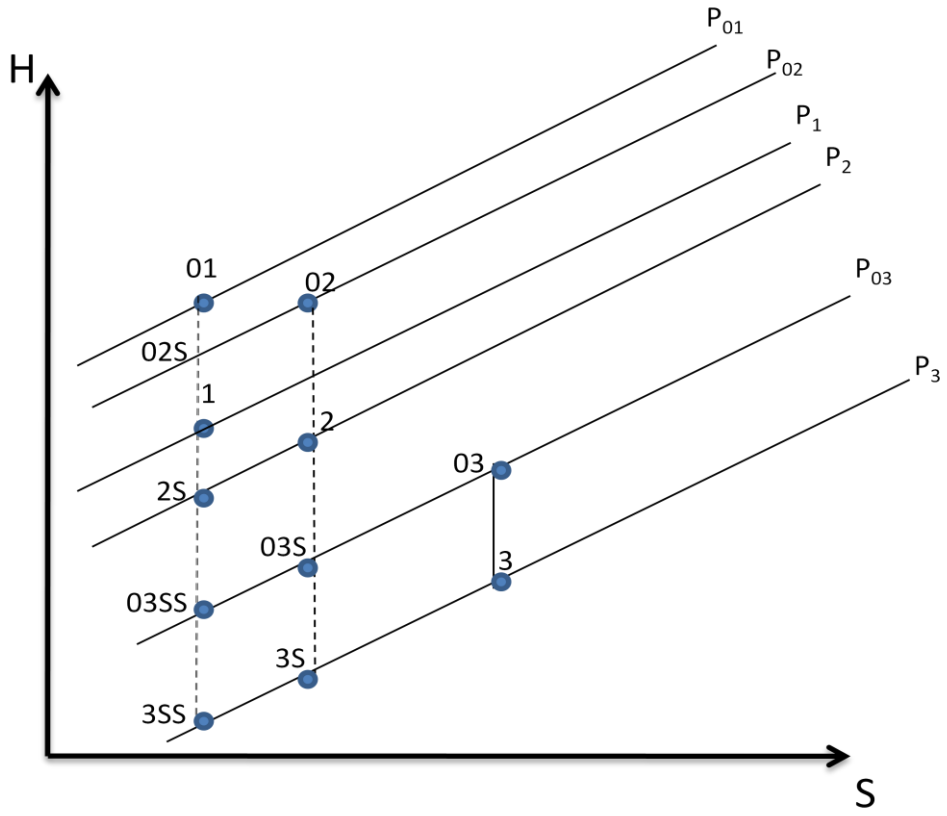

Figure A3.1 Mollier Enthalpy-Entropy Graph for a Turbine

The graph shows the expander stages as the natural gas enters through the stator that does not rotate hence performing zero work. Thus the stagnation enthalpy of stream entering and leaving the stator stage is equal in magnitude ($h_{01} = h_{02}$). Natural gas stream enters the rotor with pressure P_2 and enthalpy h_2. The rotor rotates, performing work and reduces the pressure of the natural gas stream to P_3. The mollier graph also shows isentropic and isobaric lines.

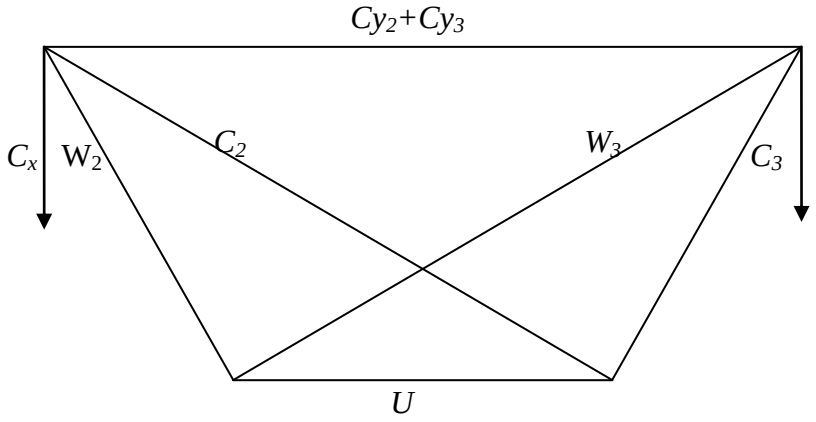

Figure A3.2 Axial Velocity Diagram

Figure (A3.2) defines the velocity diagram of an axial turbine. The inlet stream with pressure P_1 enters the turbo expander in the axial direction with velocity C_x. The tangential velocity at the stator and rotor are given as Cy_2 and Cy_3 respectively while U is the rotor speed. W_2 and W_3 are respectively the relative velocities at the rotor inlet and outlet.

The expansion turbine isentropic efficiency is defined as the ratio of mechanical energy supplied to the rotor in unit time and the maximum energy difference possible for the fluid in unit time. The isentropic efficiency is expressed mathematically as shown in equation (A3.10)

$$\eta_{te} = \frac{\Delta W_x}{\Delta W_{x(max)}} = \frac{h_{01} - h_{03}}{h_{01} - h_{03ss}} \qquad \text{(A3.10)}$$

Equation A3.8 is expressed in terms of the stagnation enthalpy. However, if the difference between the inlet and outlet kinetic energy of the expander is small, the efficiency can be expressed in terms of the state points; h_1, h_3 and h_{3s}.